UNIV. OF MICHIGAN
OCT 1 - 1955
CHEMISTRY LIBRARY

Journal of Research

of the

National Bureau of Standards

UNIV. OF MICHIGAN
OCT 1 - 1955
CHEMISTRY LIBRARY

SEPTEMBER 1955

VOLUME 55 NUMBER 3

U. S. DEPARTMENT OF COMMERCE
Sinclair Weeks, Secretary
NATIONAL BUREAU OF STANDARDS
A. V. Astin, Director

SEPTEMBER • 1955
VOLUME • 55
NUMBER • 3

JOURNAL OF RESEARCH
of the
NATIONAL BUREAU OF STANDARDS

PERIODICALS OF THE NATIONAL BUREAU OF STANDARDS
(Published monthly)

The National Bureau of Standards is engaged in fundamental and applied research in physics, chemistry, mathematics, and engineering. Projects are conducted in fifteen fields: electricity and electronics, optics and metrology, heat and power, atomic and radiation physics, chemistry, mechanics, organic and fibrous materials, metallurgy, mineral products, building technology, applied mathematics, data processing systems, cryogenic engineering, radio propagation, and radio standards. The Bureau has custody of the national standards of measurement and conducts research leading to the improvement of scientific and engineering standards and of techniques and methods of measurement. Testing methods and instruments are developed; physical constants and properties of materials are determined; and technical processes are investigated.

JOURNAL OF RESEARCH

The Journal presents research papers by authorities in the specialized fields of physics, mathematics, chemistry, and engineering. Complete details of the work are presented, including laboratory data, experimental procedures, and theoretical and mathematical analyses. Annual subscription: domestic, $4.00; $1.25 additional for foreign mailing

TECHNICAL NEWS BULLETIN

Summaries of current research at the National Bureau of Standards are published each month in the Technical News Bulletin. The articles are brief, with emphasis on the results of research, chosen on the basis of their scientific or technologic importance. Lists of all Bureau publications during the preceding month are given, including Research Papers, Handbooks, Applied Mathematics Series, Building Materials and Structures Reports, Miscellaneous Publications, and Circulars. Each issue contains 12 or more two-column pages; illustrated. Annual subscription: domestic, $1.00; 35 cents additional for foreign mailing.

BASIC RADIO PROPAGATION PREDICTIONS

The Predictions provide the information necessary for calculating the best frequencies for communication between any two points in the world at any time during the given month. The data are important to all users of long-range radio communications and navigation, including broadcasting, airline, steamship, and wireless services, as well as to investigators of radio propagation and ionosphere. Each issue, covering a period of one month, is released three months in advance and contains 16 large pages, including pertinent charts, drawings, and tables. Annual subscription: domestic, $1.00; 25 cents additional for foreign mailing.

Order all publications from the Superintendent of Documents
U. S. Government Printing Office, Washington 25, D. C.

The printing of this publication has been approved by the Director of the Bureau of the Budget, May 12, 1953.

Journal of Research of the National Bureau of Standards Vol. 55, No. 3, September 1955 Research Paper 2610

Heat Capacity of Some Butadiene-Styrene Copolymers from 0° to 330° K[1]

George T. Furukawa, Robert E. McCoskey, and Martin L. Reilly

The heat capacity of butadiene-styrene copolymer polymerized at 41° F (5° C) containing 22.61 weight percent of bound-styrene and of butadiene-styrene copolymer polymerized at 122° F (50° C) containing 42.98 weight percent of bound-styrene was determined in the range 15° to 330° K, and the data have been used to construct tables of smoothed values of heat capacity, enthalpy, and entropy. The glass-transformation temperature of the 41° F copolymer was estimated to be 213° K and that of the 122° F copolymer 237°K.

1. Introduction

The work presented in this paper is a part of the series of heat-capacity investigations being conducted at the National Bureau of Standards on rubber polymers and related substances. The results of earlier work with 41° F (5° C) and 122° F (50° C) butadiene-styrene copolymers [1] [2] containing 8.58 weight percent of bound-styrene and with 41° and 122° F polybutadienes [2] have shown that both polymerization temperature and composition influence the crystallizability and the glass-transformation temperature. The present two copolymers are of higher bound-styrene content than those previously studied [1]. The 41° F copolymer of 22.61 weight percentage of bound-styrene is of particular interest, inasmuch as it is similar to the "cold" rubber presently produced in large quantitites. The other copolymer prepared at 122° F with the butadiene-styrene charge ratio of 50:50 by weight contained 42.98 weight percent of bound-styrene. Heat-capacity measurements were made on the two copolymers from 15° to 330° K, and the data were used to obtain a table of smoothed values of heat capacity, enthalpy, and entropy from 0° to 330° K. The glass-transformation temperature of the 41° F copolymer was estimated to be 213° K and that of the 122° F copolymer to be 237° K. Neither copolymer exhibited any crystallization effects.

2. Apparatus and Method

The details of the calorimetric apparatus and methods used in this investigation can be found in previous reports dealing with 1,3-butadiene [3] and diphenyl ether [4]. The various heat treatments, to which the present copolymers were subjected, were similar to those of earlier investigations [1,2]. As the copolymers described herein did not crystallize, the prolonged annealing procedures in the crystallization temperature range were not involved. However, in several series of experiments, the copolymers were annealed just below the glass-transformation temperature; in other series, the copolymers were shock-cooled.

3. Samples

The copolymer sample identified as X–478 was obtained from the Copolymer Corporation, Baton Rouge, La. According to the information received from the manufacturer, this copolymer was emulsion polymerized at 41° F (5° C) with Dresinate-214 (potassium soap of disproportionated rosin) as the emulsifying agent. The initial butadiene-styrene charge ratio was 71:29 by weight, and the modifier of the polymerization reaction was Sulfole B–8 (tertiary dodecyl mercaptan). The activator was ferrous sulfate-potassium pyrophosphate, and the "short-stopping" agent was dinitrochlorobenzene. The reaction was "short-stopped" at about 60-percent conversion. No further information is known about this polymer.

The second copolymer sample was obtained through the University of Akron Government Laboratories [5] and was designated as GL–662 or 74PB1.[3] This copolymer was prepared at 122° F (50° C) by emulsion polymerization with an initial butadiene-styrene charge ratio of 50:50 by weight. The emulsifier was soap flakes (S. F.), and the modifier was dodecyl mercaptan (DDM). The polymerization reaction was activated by potassium persulfate and "short-stopped" by means of hydroquinone at 73.6-percent conversion.

The copolymers were purified by M. Tryon, of the Rubber Section of the Bureau, by a procedure previously outlined [1]. The analyses of the purified samples are summarized in table 1.[4] The styrene contents given in the table were computed from the carbon-hydrogen ratios corrected for mercaptan content (that is, Sulfole B–8 or dodecyl mercaptan).

[1] The work discussed herein was performed as a part of the research project sponsored by the Federal Facilities Corporation, Office of Synthetic Rubber, in connection with the Government Synthetic Rubber Program.

[2] Figures in brackets indicate the literature references at the end of this paper.

[3] Hereafter in this paper, the 41° F butadiene-styrene copolymer containing 22.61 weight percent bound-styrene will be identified as X–478 and the 122° F copolymer containing 42.98 weight percent bound-styrene as GL–662.

[4] The analyses were made by R. A. Paulson of the Analytical Chemistry Section of the Bureau.

TABLE 1. *Composition of the copolymers* [a]

	Percentage by weight	
	X–478	GL–662
Carbon	89.443	90.100
Hydrogen	10.4008	9.710
Sulfur	0.048	0.081
Oxygen	.15	.14
Ash	.098	.111
Styrene	22.61	42.98
Phenylbetanaphthylamine [b]	0.1	0.1

[a] Analysis by R. A. Paulson. [b] Added after the analysis.

The phenylbetanaphthylamine (stabilizer) was added after the analysis.

The samples, after being placed in the copper sample container, were further pumped on at high vacuum for several days to remove as much of the volatile impurities (moisture, air, and benzene) as possible. The mass of the X–478 copolymer investigated was 43.894 g and that of the GL–662 copolymer was 45.366 g.

4. Results

4.1. X–478 Copolymer

The heat-capacity measurements with the X–478 copolymer were carried out in a manner similar to those previously described [1,2]. In one series of experiments the measurements were made after shock-cooling the copolymer from room temperature to that of liquid nitrogen (78° C). In another series, the copolymer was cooled slowly over the same temperature range. The shock-cooling process took about 1 hour and the slow-cooling process from several days to a week or more, depending upon whether liquid nitrogen alone was used, or dry-ice and then liquid nitrogen were used successively. The heat treatments, the temperature range of measurements, and the various observations of temperature drifts are summarized in table 2. The observed heat capacities are given in table 3 and plotted in figure 1 to show the general nature of the results. When the copolymer was shock-cooled, upward temperature drifts were observed during heat-capacity measurements from about 170° to 215° K (runs 3 and 4). When slowly cooled, downward drifts were observed from about 207° to 216° K (run 5). The copolymer exhibited no crystallization effects. The glass-transformation temperature was estimated to be 213° K, the temperature at "half-height" in the upward sweep of the heat capacity.

The data were used to obtain the smoothed values of heat capacity, enthalpy, and entropy given in table 4. The details of the methods used in obtaining these quantities have been previously given [1,2]. In the temperature interval 195° to 225° K, where the heat capacity increased rapidly, the heat-capacity values of table 4 were obtained from a smooth curve drawn through the experimental results plotted on a large scale. From 225° to 330° K the heat capacity of this copolymer can be represented within 0.1 percent by the equation.

$$C = 1.396 + 2.63 \times 10^{-4} T + 4.688 \times 10^{-6} T^2$$

(abs j deg^{-1} g^{-1}).

Three experimental determinations of the enthalpy change were carried out for the temperature interval 195° to 225° K. In runs 3 and 4 the copolymer was previously shock-cooled. The observed changes in enthalpy for both runs were the same, 40.39 abs j g^{-1}. The enthalpy change observed in run 5, in

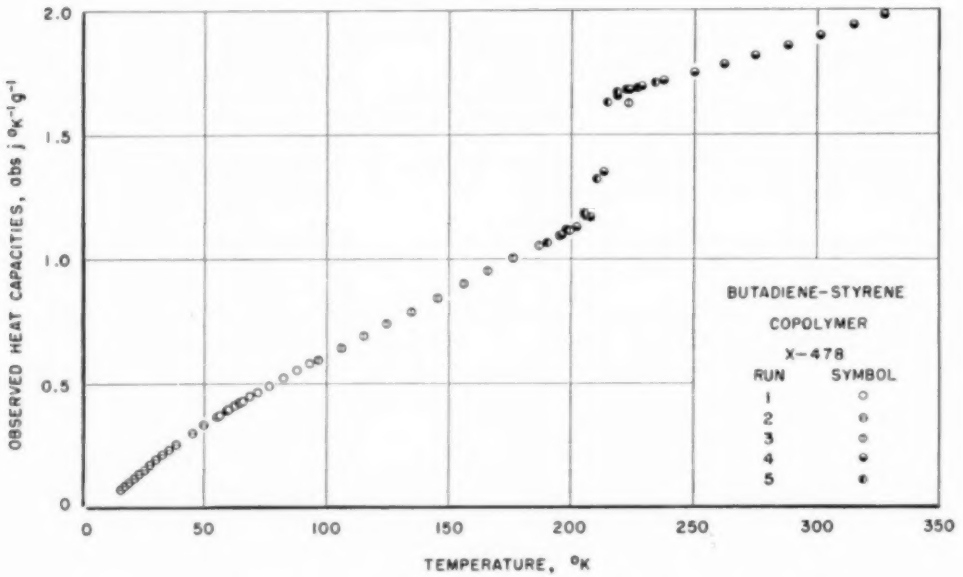

FIGURE 1. *Observed heat capacities of the butadiene-styrene copolymer X–478.*

TABLE 2. *Heat treatments and observations on the butadiene-styrene copolymer X–478*

(Temperatures are in °K; °K=°C+273.16°)

Run	Treatment of sample	Temperature range of measurements	Drift observations
1	Cooled slowly from room temperature to 90°; then rapidly to 54°.	54° to 95°	No drift.
2	After run 1 the sample was cooled rapidly from 95° to 15°.	15° to 66°	Do.
3	Cooled rapidly from room temperature to 83°.	83° to 234°	Upward drift from 170° to 211°.
4	Cooled rapidly from room temperature to 183° and heated to 193°	193° to 332°	Upward drift from 193° to 215°.
5	Cooled slowly from room temperature to 186° over 1 week.	186° to 238°	Downward drift from 207° to 216°.

TABLE 3. *Observed heat capacities of the butadiene-styrene copolymer X–478*

(°K=°C+273.16°)

T	C	T	C
Run 1		Run 3—Continued	
°K	*abs j deg⁻¹g⁻¹*	°K	*abs j deg⁻¹g⁻¹*
55.6399 [a]	0.3742	155.3546	0.8998
58.9542	.3947	165.4390	.9524
61.9540	.4133	175.7846	1.0037
65.1126	.4315	186.2819	1.0555
68.3386	.4495	193.9549	1.0906
71.4100	.4657	198.9514	1.1160
85.9445	.4906	206.2348	1.1705
81.8023	.5238	222.7774	1.6304
87.2943	.5546		
92.4913	.5808	Run 4	
Run 2		195.8999	1.0962
		201.6262	1.1309
15.6156	0.0744	207.2510	1.1664
17.2601	.0884	212.5443	1.3519
19.0338	.1027	218.0144	1.6000
21.0974	.1195	223.1011	1.6884
23.0131	.1361	228.1394	1.6999
24.9253	.1524	236.8196	1.7214
27.3024	.1724	249.3464	1.7534
29.9704	.1944	261.6749	1.7861
32.4460	.2140	274.3540	1.8202
35.1286	.2349	287.6538	1.8597
38.3874	.2589	300.7215	1.9000
44.9111	.3046	314.3536	1.9425
49.2922	.3334	326.9844	1.9825
54.5618	.3666		
59.3997	.3963	Run 5	
63.9250	.4238		
Run 3		189.8650	1.0677
		197.3133	1.1189
87.3050	0.5883	204.5483	1.1846
96.2926	.5982	209.9087	1.3222
105.4046	.6438	214.0593	1.6341
114.7106	.6918	217.9034	1.6770
124.1622	.7402	221.7021	1.6857
134.1576	.7919	226.1066	1.6958
144.6692	.8458	233.5882	1.7134

[a] The temperatures given are accurate to ±0.01 deg K. Figures beyond the second decimal are significant only insofar as small temperature differences are concerned.

TABLE 4. *Heat capacity, enthalpy, and entropy of butadiene-styrene copolymer X–478*

(°K=°C+273.16°)

T	C	$(H_T-H_{0°K})$	$(S_T-S_{0°K})$
°K	*abs j deg⁻¹g⁻¹*	*abs j g⁻¹*	*abs j deg⁻¹g⁻¹*
0	0	0	0
5	0.0034	0.0043	0.0011
10	.0259	.0071	.0090
15	.0674	.2967	.0270
20	.1091	.7374	.0522
25	.1530	1.393	.0812
30	.1947	2.263	.1128
35	.2339	3.335	.1458
40	.2706	4.598	.1795
45	.3052	6.038	.2133
50	.3380	7.647	.2472
55	.3694	9.416	.2809
60	.4000	11.34	.3144
65	.4304	13.42	.3476
70	.4584	15.64	.3806
75	.4853	18.00	.4131
80	.5137	20.49	.4453
85	.5419	23.13	.4773
90	.5685	25.91	.5091
95	.5930	28.82	.5405
100	.6171	31.84	.5715
105	.6421	34.99	.6022
110	.6676	38.26	.6327
115	.6932	41.66	.6629
120	.7188	45.19	.6930
125	.7445	48.85	.7229
130	.7703	52.64	.7526
135	.7960	56.56	.7821
140	.8217	60.60	.8115
145	.8474	64.77	.8408
150	.8731	69.07	.8700
155	.8987	73.50	.8990
160	.9242	78.06	.9280
165	.9497	82.74	.9568
170	.9750	87.56	.9856
175	1.000	92.49	1.014
180	1.025	97.56	1.043
185	.049	102.7	1.071
190	1.074	108.0	1.099
195	1.096	113.5	1.128
200	1.12	----------	----------
205	1.17	----------	----------
210	1.25	----------	----------
215	1.65	----------	----------
220	1.68	----------	----------
225	1.693	155.4	1.326
230	1.705	163.9	1.364
235	1.717	172.5	1.400
240	1.729	181.1	1.437
245	1.742	189.8	1.472
250	1.755	198.5	1.508
255	1.768	207.3	1.543
260	1.782	216.2	1.577
265	1.795	225.1	1.611
270	1.808	234.1	1.645
273.16	1.817	239.8	1.666
275	1.822	243.2	1.678
280	1.837	252.4	1.711
285	1.852	261.6	1.744
290	1.867	270.9	1.776
295	1.882	280.2	1.808
298.16	1.892	286.2	1.828
300	1.898	289.7	1.840
305	1.913	299.2	1.871
310	1.929	308.8	1.903
315	1.944	318.5	1.934
320	1.960	328.3	1.964
325	1.976	338.1	1.995
330	1.992	348.0	2.025

which the copolymer was previously cooled slowly, was 41.95 abs j g^{-1}. The latter value was used in constructing the enthalpy values of table 4. The difference, 1.56 abs j g^{-1}, indicates qualitatively the extent of relaxation effects associated with glass transformation under the experimental conditions as outlined. The enthalpy values given above were obtained by summing various experimental input energies in the region of glass transformation and by correcting to the even temperature interval. The

small input energies in this range also served to establish the general shape and position of glass transformation.

The entropy change (0.198 abs j deg^{-1} g^{-1}) for the temperature interval 195° to 225° K was obtained by summing various $\Delta H/T_m$'s of run 5, where ΔH is the input energy and T_m the mean temperature of the heating interval.

4.2. GL–662 Copolymer

The experimental details and the results with the GL–662 copolymer are given in tables 5 and 6 and shown in figure 2. This copolymer responded to heat treatments in a fashion similar to the X–478 copolymer. When shock-cooled, upward temperature drifts were observed from about 198° to 240° K (run 1). Also, when slowly cooled, downward drifts in temperature were observed from about 230° to 240° K (run 3). As with the X–478 copolymer, no crystallization effects were found in this copolymer.

TABLE 5. *Heat treatments and observations on the butadiene-styrene copolymer GL–662*

(Temperatures are in °K; °K = °C + 273.16°)

Run	Treatment of sample	Temperature range of measurements	Drift observations
1	Cooled rapidly from room temperature to 78°.	78° to 240°	Upward drift from 198° to 240°.
2	Cooled overnight from 240° to 223°.	223° to 335°	Downward drift from 231° to 240°.
3	Cooled slowly from room temperature to 218° over 3 days.	218° to 252°	Downward drift from 232° to 242°.
4	Cooled slowly from room temperature to 278° overnight.	278° to 296°	No drift.
5	Cooled slowly from room temperature to 78° over 2 days and then cooled to 15°.	15° to 89°	Do.

The glass-transformation temperature was estimated to be 237° K.

The smoothed values of heat capacity, enthalpy, and entropy given in table 7 were obtained by procedures similar to those used with the X–478 copolymer. From 255° to 330° K the heat capacity can be

TABLE 6. *Observed heat capacities of the butadiene-styrene copolymer GL–662*

(°K = °C + 273.16°)

T	C	T	C
Run 1		Run 3	
°K	abs j deg^{-1} g^{-1}	°K	abs j deg^{-1} g^{-1}
[a] 81.7380	0.4849	222.3920	1.152
89.4599	.5220	229.2360	1.209
96.6180	.5534	233.2240	1.272
104.9560	.5906	235.7802	1.355
114.3959	.6335	238.2239	1.477
123.2797	.6742	240.5432	1.584
131.7172	.7125	243.3349	1.650
139.8044	.7502	248.2819	1.677
148.2216	.7868	Run 4	
157.5082	.8284		
166.9044	.8712	280.9400	1.768
175.9899	.9120	287.1780	1.786
184.7992	.9522	293.3646	1.805
193.6374	.9940	Run 5	
202.7465	1.036		
211.6238	1.076	16.3153	0.0794
220.2657	1.124	18.3333	.0956
228.6698	1.167	20.4590	.1115
236.7170	1.202	22.6254	.1290
Run 2		24.8051	.1464
		26.9764	.1632
226.8692	1.181	29.4574	.1822
235.3946	1.375	32.4430	.2043
242.0276	1.640	35.8330	.2284
246.4884	1.659	39.9171	.2555
253.0864	1.6?8	44.6071	.2849
263.9458	1.718	49.2670	.3130
276.8888	1.756	54.6340	.3437
288.8206	1.792	60.3004	.3753
301.2004	1.831	65.7303	.4041
313.3714	1.871	71.2582	.4314
323.5662	1.904	76.3689	.4572
331.2600	1.930	81.5713	.4840
		86.8869	.5109

[a] The temperatures given are accurate to ±0.01 deg. K. Figures beyond the second decimal are significant only insofar as small temperature differences are concerned.

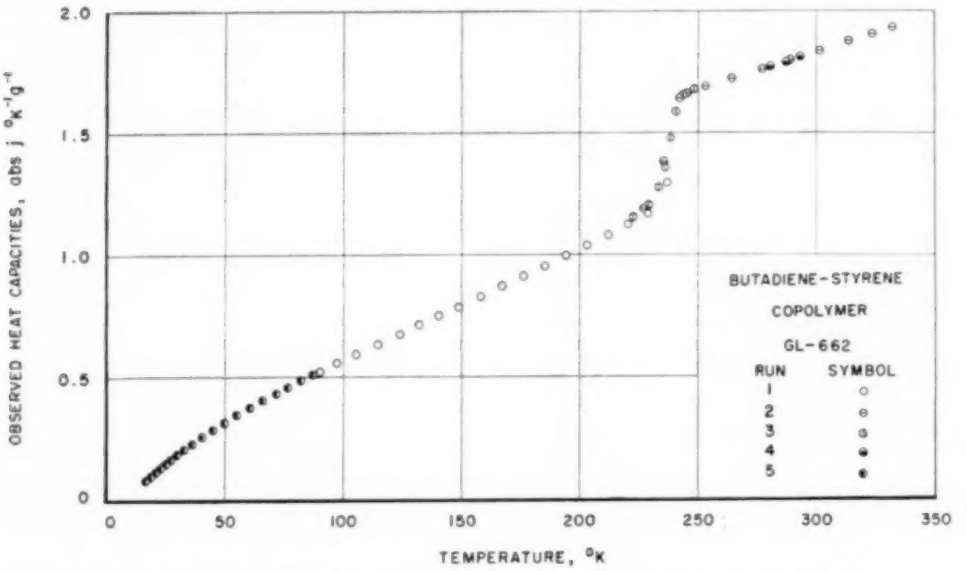

FIGURE 2. *Observed heat capacities of the butadiene-styrene copolymer GL–662.*

TABLE 7. *Heat capacity, enthalpy, and entropy of butadiene-styrene copolymer GL–662*

(°K = °C + 273.16°)

T	C	$(H_T - H_{0°K})$	$(S_T - S_{0°K})$
°K	*abs j deg⁻¹ g⁻¹*	*abs j g⁻¹*	*abs j deg⁻¹ g⁻¹*
0	0	0	0
5	0.0034	0.0043	0.0011
10	.0259	.0666	.0089
15	.0674	.2067	.0270
20	.1085	.4467	.0521
25	.1486	1.050	.0807
30	.1865	1.929	.1111
35	.2223	2.952	.1426
40	.2561	4.148	.1745
45	.2880	5.509	.2065
50	.3182	7.026	.2384
55	.3468	8.689	.2701
60	.3741	10.49	.3014
65	.4002	12.43	.3324
70	.4253	14.49	.3630
75	.4497	16.68	.3932
80	.4737	18.99	.4230
85	.4976	21.42	.4524
90	.5215	23.96	.4815
95	.5453	26.63	.5104
100	.5688	29.42	.5389
105	.5917	32.32	.5672
110	.6143	35.33	.5953
115	.6367	38.46	.6231
120	.6591	41.70	.6507
125	.6815	45.05	.6780
130	.7040	48.52	.7052
135	.7266	52.09	.7322
140	.7492	55.78	.7590
145	.7712	59.58	.7857
150	.7944	63.50	.8122
155	.8170	67.52	.8386
160	.8396	71.67	.8649
165	.8622	75.92	.8911
170	.8849	80.29	.9172
175	.9077	84.77	.9432
180	.9306	89.36	.9691
185	.9535	94.08	.9949
190	.9765	98.90	1.021
195	.9995	103.8	1.046
200	1.022	108.9	1.072
205	1.046	114.1	1.097
210	1.069	119.4	1.123
215	1.093	124.8	1.148
220	1.122	130.3	1.174
225	1.16	.....	.....
230	1.22	.....	.....
235	1.36	.....	.....
240	1.57	.....	.....
245	1.65	.....	.....
250	1.67	.....	.....
255	1.694	180.5	1.384
260	1.708	189.0	1.417
265	1.722	197.6	1.450
270	1.736	206.2	1.482
273.16	1.745	211.8	1.502
275	1.750	215.0	1.514
280	1.765	223.7	1.546
285	1.780	232.6	1.577
290	1.796	241.5	1.608
295	1.812	250.6	1.639
298.16	1.822	256.4	1.659
300	1.828	259.7	1.670
305	1.845	268.8	1.700
310	1.861	278.1	1.730
315	1.877	287.4	1.760
320	1.893	296.9	1.790
325	1.909	306.4	1.819
330	1.925	316.0	1.848

represented to within 0.1 percent by the quadratic equation

$$C = 1.322 + 1.83 \times 10^{-4} T + 5.000 \times 10^{-6} T^2$$

(abs j deg^{-1} g^{-1}).

In the temperature interval 220° to 255° K two determinations (runs 2 and 3) of the enthalpy were made. In run 2 (refer to table 5), the copolymer had been previously shock-cooled from room temperature, heated to 240° K, and cooled again slowly. In run 3 the copolymer was cooled slowly from room temperature. The close agreement in the enthalpy changes (50.24 and 50.21 abs j g^{-1}, respectively) of runs 2 and 3 indicates that within the limits described in this paper the rate of cooling above the glass-transformation temperature has no appreciable effect on the enthalpy change between 220° and 255° K. The mean of the two values was used in constructing table 7.

4.3. Reliability of the Results

Except near the glass-transformation temperature, the results of the heat-capacity measurements in general do not scatter by more than 0.2 to 0.3 percent. In the region of the glass-transformation temperature, however, the values of heat capacity differ by as much as 1 percent. As no attempt was made to reach complete thermal equilibrium in this region of temperature drifts, the results will differ slightly from the values that would be obtained if thermal equilibrium had been reached. Previous experience [1,2] with polymers showed that temperature drifts occurred even several hours after heating. Any reasonable change in the time intervals used would certainly not alter the general nature of the results.

Upon consideration of various sources of errors, such as reproducibility of the physical state of the polymers, energy input, heat leak, and thermometry, the authors believe that the heat-capacity values given in tables 4 and 7, except near the glass-transformation temperature, are accurate to 0.3 percent. The enthalpy and entropy values, derived from the heat-capacity values, are probably accurate to 0.3 to 0.4 percent.

5. Discussion

Below the temperature region of glass transformation certain degrees of freedom of the polymer molecules, because of the increased relaxation times, do not have sufficient time during an ordinary course of heat-capacity experiments to come into thermodynamic equilibrium [6]. The heat capacities of the copolymers described in this paper decreased by about 30 percent on cooling through the glass-transformation temperature interval because of the "freezing-in" of these degrees of freedom. This rapid decrease in heat capacity extended over a temperature interval of about 5 to 10 deg. Previous heat-capacity investigations [1, 2] have shown similar percentage decrease in the heat capacity at the glass-transformation temperature.

In the region of the glass-transformation temperature some of the polymer molecules undergo slow transitions among the energy states of the degrees of freedom referred to in the previous paragraph.

These slow transitions are observed during heat-capacity experiments as temperature drifts, the direction depending upon whether the transitions involve liberation or absorption of energy. The relaxation time increases with decrease in temperature, and finally at sufficiently low temperatures these degrees of freedom become completely "frozen-in." When a polymer is shock-cooled from room temperature to 80° K, a large portion of the polymer molecules that would have undergone transition to lower states of energy if cooled slowly through the glass-transformation temperature remains "suspended" in states of higher energy. When the polymer is later raised to temperatures near the glass-transformation region, the polymer molecules transform from the higher states of energy to the lower, causing upward temperature drifts. When slowly cooled, the polymer molecules are given more time to transform into energy states closer to equilibrium. Subsequently, when the temperature is raised, a certain range is reached at which the equilibrium requires the molecules to transform into states of higher energy, causing downward temperature drifts. When the copolymers described in this paper were shock-cooled, upward temperature drifts started at about 40 to 45 deg below the glass-transformation temperature (see tables 2 and 5); when the copolymers were slowly cooled, downward temperature drifts were observed starting at about 6 to 7 deg below the glass-transformation temperature. The occurrence of the upward temperature drifts at much lower temperature than of the downward temperature drifts is believed to be consistent with the requirement of lower activation energy for a system in a higher energy state to transform into that of lower energy state. It is expected, on the basis of the observed results, that no temperature drifts would occur if the cooling process were sufficiently slow so that all calorimetrically detectable transformations associated with the polymer molecules took place and if the heating rate were as slow or slower than the cooling rate. Measurements of the heat capacity are generally made at a heating rate of about ¼ to 1 deg/min, which is considerably faster than the cooling rate and the time necessary for complete transformation of the polymer molecules to higher energy states. Consequently, during the waiting period for temperature equilibrium, there are observed downward temperature drifts as the polymer molecules slowly adjust to the distribution of energy states consistent with the temperature.

Überreiter [7] and Tuckett [8] have shown that in butadiene-styrene copolymers the bound styrene hinders free rotation of polymer segments and that the increase in bound-styrene content raises the glass-transformation temperature. The results presented in this paper and those previously obtained on butadiene-styrene copolymers are consistent with their findings.

From above the glass-transformation temperature to the upper temperature limit of the measurements given in this paper, the heat capacity of the copolymers can be represented by a simple quadratic equation, of the form $C=a+bT+cT^2$, within 0.1 percent or better. The heat capacity of Hycar O. R.–15 [9], GR–S [10], and the butadiene-styrene copolymer containing 8.58 weight percent of bound-styrene [1] can also be represented by a similar type of equation in the region above the glass-transformation temperature.

6. References

[1] G. T. Furukawa, R. E. McCoskey, and G. J. King, J. Research NBS **50,** 357 (1953) RP2425.
[2] G. T. Furukawa and R. E. McCoskey, J. Research NBS **51,** 321 (1953) RP2460.
[3] R. B. Scott, C. H. Meyers, R. D. Rands, Jr., F. G. Brickwedde, and N. Bekkedahl, J. Research NBS **35,** 39 (1945) RP1661.
[4] G. T. Furukawa, D. C. Ginnings, R. E. McCoskey, and R. A. Nelson, J. Research NBS **46,** 195 (1951) RP2191.
[5] R. W. Laundrie (private communication from Government laboratories).
[6] W. Kauzmann, Chem. Revs. **43,** 219 (1948).
[7] K. Überreiter, Kolloid-Z. **102,** 272 (1943).
[8] R. F. Tuckett, Trans. Faraday Soc. **38,** 310 (1942).
[9] N. Bekkedahl and R. B. Scott, J. Research NBS **29,** 87 (1942) RP1487.
[10] R. D. Rands, Jr., W. J. Ferguson, and J. L. Prather, J. Research NBS **33,** 63 (1944) RP1595.

Washington, March 4, 1955.

Journal of Research of the National Bureau of Standards Vol. 55, No. 3, September 1955 Research Paper 2611

Setting Reaction of Zinc Oxide and Eugenol[1]

Henry I. Copeland, Jr.,[2] Gerhard M. Brauer, W. T. Sweeney, and A. F. Forziati

Zinc oxide-eugenol mixtures have been used in dentistry for a number of years. The setting mechanism of these mixtures was investigated. X-ray diffraction data and electron photomicrographs give evidence that a crystalline compound is formed. Analysis and molecular-weight determinations show that this compound corresponds to the empirical formula $(C_{10}H_{11}O_2)_2Zn$, zinc eugenolate. Infrared data, as well as the nonreactivity of meta and para substituted phenols as compared to the ortho isomers, suggest that the zinc eugenolate is a chelate. The hardened mass consists of zinc oxide embedded in a matrix of long sheath-like crystals of zinc eugenolate. The excess eugenol is sorbed by both the zinc eugenolate and the zinc oxide.

1. Introduction

Zinc oxide-eugenol materials have been developed for utilization in a number of dental applications. They are most widely employed as palliative and antibacterial agents in the treatment of carious lesions [1].[3] With modifiers, these materials are used as impression pastes and as surgical cements.

Generally, the use of zinc oxide and eugenol depends on their tendency to form a hardened coherent mass when mixed. Unexplained variations in the behavior of the mixtures are important to the clinician who uses these materials to treat dental conditions. Of special concern are variations in setting rate, hardness, and strength of the set mass.

The mechanism of the setting process of zinc oxide and eugenol is unknown. Factors that have been reported to produce variations in the physical behavior are the type of zinc oxide used, the amount of water present (both in the zinc oxide and atmosphere), and the ambient temperature. The following theories have been advanced in regard to the setting process: 1. The setting process is a purely physical one in which the constituents retain their individuality [2]; 2. a chemical reaction occurs and a compound resembling zinc phenolate is formed [3]; and 3. the setting process is a combination of physical and chemical reactions [3].

The object of this investigation was to study the setting of zinc oxide and eugenol mixtures in order to more nearly define physical and chemical processes involved.

2. Experimental Procedures

2.1. Materials

The zinc oxide (reagent grade) used had a particle size of around 3000 A in diameter and contained less than 2 percent of water. It was white. An experimental type of zinc oxide (Merck Hyperfine) was also used. According to the manufacturer's specifications it had a particle size of 125 to 250 A in diameter and contained approximately 5 percent of water. This zinc oxide was reddish in color.

The eugenol was USP grade. All other chemicals used were reagent grade.

2.2. Setting of Mixtures

Mixes of zinc oxide (reagent grade) were made with guaiacol, methylguaiacol, eugenol, phenol, veratrole, safrol, anethole, *m*-methoxyphenol, and thymol. The mixtures were made with a stellite spatula on a glass slab at room temperature. It was necessary to melt the phenol and thymol prior to mixing. The maximum amount of zinc oxide that could be wetted by the liquids was incorporated.

Setting time was determined by means of a penetrometer. A modification of the ASTM Penetration Test for Bituminous Materials was used with a 100-g load for 5 sec and $\frac{1}{16}$-in. needle. The tests were made at room temperature, and the material was considered set when the needle could no longer penetrate the material or three successive penetrations at 30-sec intervals gave identical values.

Samples of the zinc oxides were dehydrated by heating at 110° C for 24 hr. The dehydrated zinc oxides were mixed with eugenol in the same manner.

2.3. Temperature Change During Setting

The change in temperature caused by the reaction was determined by means of a calibrated iron-constantan thermocouple connected to a recording potentiometer. Zinc oxide (Hyperfine)-eugenol mixtures were used in this experiment.

2.4. Analysis for Reaction Products

Mixtures of 0.5-mole zinc oxide (reagent grade) and 0.1-mole eugenol were prepared. The hardened mass was pulverized by grinding in a mortar to a fine powder. The particles were extracted with chloroform for 30 hr in a Soxblet extractor. The residue left in the filter thimble was vacuum-dried and weighed. The chloroform was distilled off from the

[1] The data in this publication were presented in a thesis by Henry I. Copeland, Jr., in partial fulfillment of the requirements of the Graduate School of Georgetown University, Washington, D. C., for the degree of Master of Science.
This paper was presented to the International Association for Dental Research, Chicago, March 1955; and to the Medicinal Division, American Chemical Society, Cincinnati, April 1955.

[2] Guest worker at the National Bureau of Standards, and member of the Dental Corps, U. S. Air Force.

[3] Figures in brackets indicate the literature references at the end of this paper.

extract and the residue distilled over at 87° to 101° C and 2-mm Hg pressure.

Equimolar mixtures of zinc oxide (Hyperfine) and eugenol were prepared and extracted as above. The residue in the filter thimble was dried to constant weight at 110° C and 1- to 2-mm Hg pressure. The extract was filtered through a weighed Gooch crucible and the residue purified by washing with three 10-ml portions each of chloroform, methanol, and ether and dried to constant weight. This residue was a white crystalline material, which was examined by X-ray diffraction. The elementary analysis, molecular weight, dissociation temperature, crystal form, refractive index, fluorescence, and density of this residue were determined.

The low-boiling solvents used for extraction and washing were distilled off from the filtrate, and the weight, refractive index, and boiling point of the remaining liquid were determined.

The experiments were repeated, using methanol, benzene, and chlorinated hydrocarbons other than chloroform as the extraction solvent.

2.5. Measurement of X-ray Diffraction

The X-ray diffraction measurements were made by the Section on Constitution and Microstructure at the Bureau. The instrument used was a diffractometer utilizing a Geiger counter and a recording potentiometer. All measurements were made through 90 deg. Patterns were obtained of zinc oxide (reagent grade), zinc oxide (Hyperfine), eugenol, mixtures of eugenol with each of the two zinc oxides, and a mixture of zinc oxide (Hyperfine) with guaiacol. Patterns were also obtained of the purified reaction product and a zinc oxide-water mixture.

2.6. Elementary Analysis [4]

The purified reaction product was analyzed for carbon, hydrogen, and zinc content, using microtechniques. The dry combustion method was used for the carbon and hydrogen determinations, whereas the zinc was determined as the sulfate by digestion in the presence of sulfuric acid.

2.7. Infrared Studies [5]

Zinc 8-quinolinolate was prepared according to Zetzsche [4]. Zinc guaiacolate was obtained on mixing guaiacol with zinc oxide. The unreacted guaiacol was removed by repeated washing with cold chloroform. The infrared absorption spectra of 8-quinolinol, zinc 8-quinolinolate, eugenol, zinc eugenolate, guaiacol, and zinc guaiacolate were measured. The solid samples were incorporated in potassium bromide pellets. All samples were examined with a Perkins-Elmer, model 21 spectrophotometer.

[4] Elementary analyses were performed by R. A. Paulson.
Infrared absorption spectra were made by J. E. Stewart and G. Wyman.

2.8. Electron Micrographs [6]

Electron micrographs of the Hyperfine zinc oxide-eugenol mixture and the purified reaction product were made at 10,000- and 4,000-diameter magnifications, respectively.

2.9. Water Sorption Study

Dried zinc eugenolate samples were placed in a desiccator over a saturated potassium nitrate solution (93.3-percent relative humidity at 30° C). The samples were removed from the desiccators at various time intervals and weighed. This procedure was repeated until constant weight was obtained.

3. Results and Discussion

The mixtures of zinc oxide (reagent grade) with eugenol (I), guaiacol (II), or methyl guaiacol (III) set into a hardened mass.

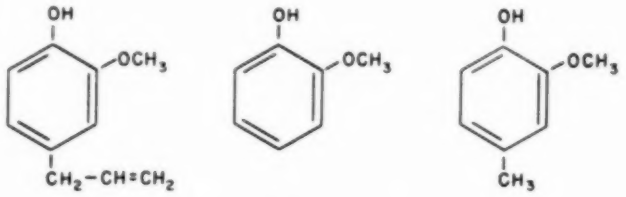

These aromatic oils have a methoxy group ortho to a phenolic hydroxy group. Guaiacol has no substituent group in the para position. Methylguaiacol has a methyl group as a para substituent. Eugenol has a para-beta allyl group.

Mixtures of zinc oxide with phenol itself (IV), veratrole (V), safrol (VI), anethole (VII), thymol (VIII), and *m*-methoxyphenol (IX) did not harden.

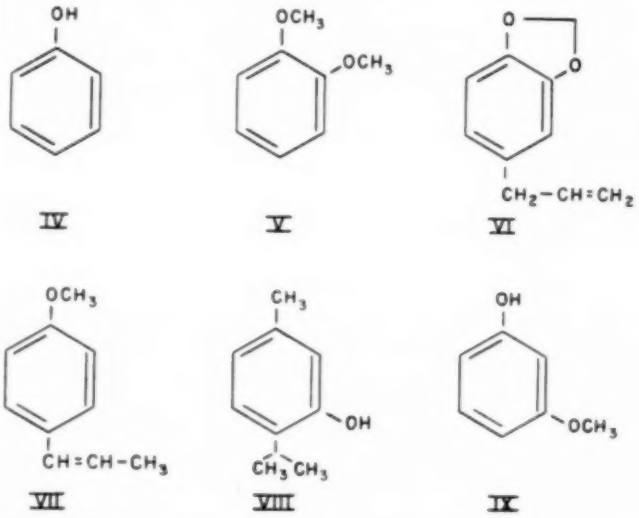

[6] Electron micrographs were made with F. A. Heckman.

These compounds do not have a methoxy group ortho to a hydroxy group.

From the above considerations, it appears that the para groups are not involved in the setting reaction, and the ortho methoxy group is essential for setting to take place.

The dehydrated zinc oxides did not form a hardened mass when mixed with eugenol. The untreated reagent grade zinc oxide (less than 2 percent of water) required more than 24 hr to set when mixed with eugenol. The Hyperfine zinc oxide-eugenol mixture set in less than 15 min. This zinc oxide had the greater water content (5 percent according to manufacturer) and also had a much larger surface area. In all experiments, the setting rate of either of the zinc oxides mixed with eugenol was more rapid in warm and humid weather than when the relative humidity was low.

The hardening process was found to be exothermic in nature. Rapidly setting mixtures gave a harder product and a greater temperature rise.

On extraction with chloroform the reagent-grade zinc oxide-eugenol mixture yielded approximately 80 percent of eugenol. The residue in the filter thimble showed a 10-percent increase in weight over the original weight of the zinc oxide, and analysis indicated that some eugenol was still in the residue. An insoluble film deposited in the extractor flask suggested some chemical change had taken place.

Because the zinc oxide (Hyperfine)-eugenol mixture had demonstrated faster setting and increased exothermic activity, the extractions were repeated, using this mixture. The following tabulation shows typical results:

BEFORE SETTING		
Zinc oxide (containing 1.3% of water).	9.60 g	0.117 mole
Weight of dry zinc oxide	9.48 g	
Eugenol	19.26 g	0.117 mole
Material in mixture	28.74 g	
AFTER SETTING		
Residue on extraction	15.5480 g	
Residue in extract (other than eugenol).	1.1909 g	
Eugenol recovered	11.6676 g	65.2 %
Material accounted for	28.4065 g	98.9 %

After the chloroform was removed from the extract, the residue soon formed an oily paste. This paste was composed of a white crystalline material and eugenol.

X-ray diffraction measurements were made to determine changes in crystal structure that might have occurred during setting. Both reagent-grade zinc oxide and the Hyperfine zinc oxide gave the characteristic pattern indicating principal spacings of approximately 2.9, 2.6, and 2.5 A. The small particle size of the Hyperfine zinc oxide caused broadening of the bases of the peaks in its pattern. There were no other differences in the diffraction pattern. Eugenol showed no peaks, being noncrystalline.

The mixture of reagent-grade zinc oxide with eugenol showed peaks indicating the presence of a new crystal form with spacings of approximately 17.0, 8.8, and 7.0 A. The zinc oxide (Hyperfine) mixed with eugenol demonstrated the presence of the same crystal form with approximately the same spacings. The peaks were much higher in the pattern of the latter mixture, which indicated the presence of a much greater quantity of the new crystal form. Zinc oxide mixed with guaiacol demonstrated the presence of a new crystal form with spacings of 12.0, 9.3, and 8.7 A. A zinc oxide-water mixture gave only the characteristic zinc oxide pattern.

The diffraction pattern of the purified reaction product showed only the presence of the new crystal form, although as little as 2 percent of zinc oxide could have been detected by the diffractometer used.

Representative X-ray diffraction patterns are shown in figures 1 and 2. The peaks between 30 and 90 deg have been identified as belonging to zinc oxide [5]. The peaks occurring between 6 and 26 deg are the result of chemical reaction. The reaction product is identified as zinc eugenolate in pattern 1 of figure 2.

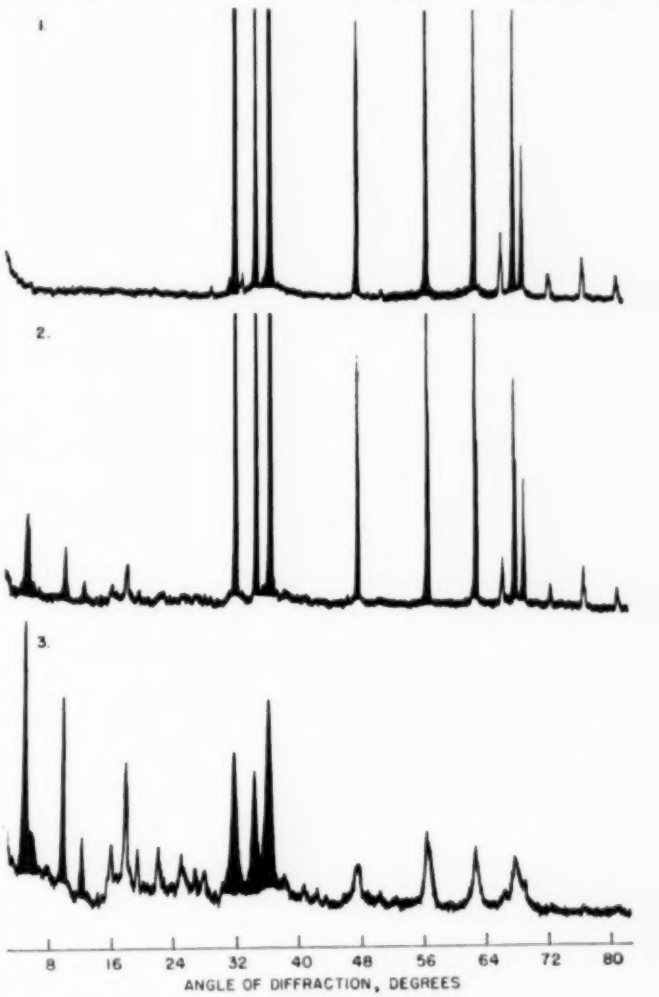

FIGURE 1. *X-ray diffraction patterns.*

1, ZnO (reagent); 2, ZnO (reagent)–Eug. mixture; 3, ZnO (Hpf.)–Eug. mixture.

351356—55—2

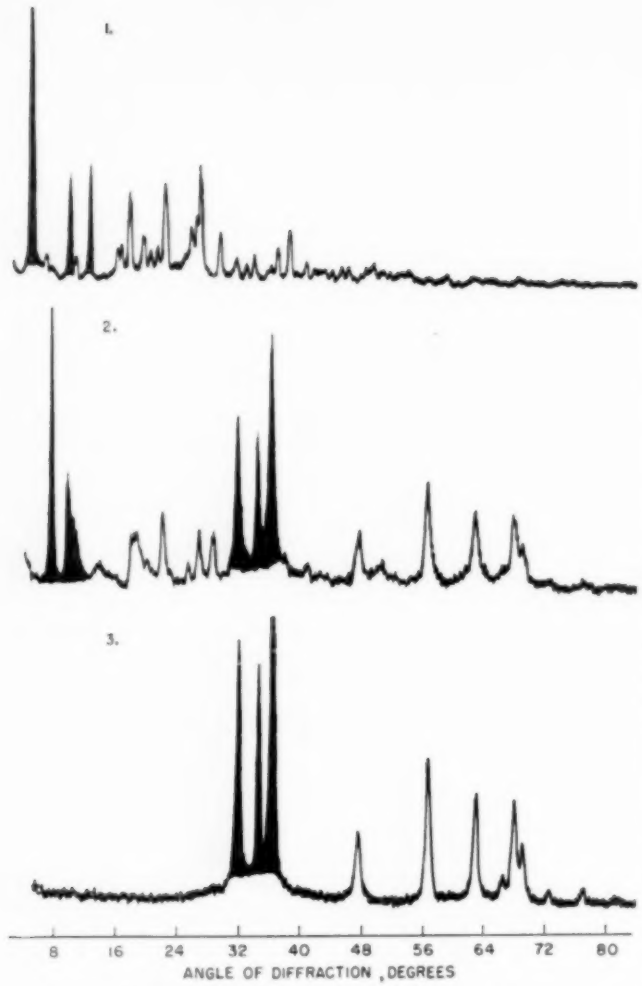

FIGURE 2. *X-ray diffraction patterns.*

1, Zinc eugenolate; 2, ZnO–Guaiacol mixture; 3, ZnO–Water mixture.

The analysis of the compound formed by the reaction of zinc oxide and eugenol is given in table 1. As a compound resembling zinc phenolate had been suggested [3] as a possible reaction product, the composition of zinc eugenolate was calculated from the empirical formula and compared with the values obtained for the new crystalline compound. The comparison indicated that the formula for the compound would be that of zinc eugenolate, $[(C_{10}H_{11}O_2)_2Zn]_n$.

The molecular weight was determined cryoscopically in acetamide (molar freezing point depression K_f equals 36.3° C). The molecular weight was found to be 435. The calculated molecular weight when n equals 1 is 391. This indicated that the empirical formula for zinc eugenolate is $(C_{10}H_{11}O_2)_2Zn$.

TABLE 1. *Analysis of reaction product*

Element	Calculated	Found
	%	%
Carbon	61.34	* 59.6
Hydrogen	5.61	5.7
Zinc	16.72	* 17.1
Oxygen (by difference)	16.33	* 17.6

* The low carbon, as well as the high zinc and oxygen percentages, would be explained by the presence of a small amount of zinc oxide in the purified product.

Some physical properties of the zinc eugenolate are given in table 2.

Zinc eugenolate was found to be insoluble in all common organic solvents, including anisole, mesityl oxide, α-chloronaphthalene, dioxanone, *N*, *N*-diethyl carbamate, ethylene carbonate, diethylphosphite, dimethylamidophosphate, tributylamine, and dimethyl formamide.

Infrared absorption spectra were studied in an attempt to gain more information on the molecular configuration of zinc eugenolate. Zinc 8-quinolinolate was used for comparison because an X-ray analysis of its structure had been reported [6]. For further comparison, guaiacol and the zinc oxide-guaiacol reaction product were used.

TABLE 2. *Some physical properties of zinc eugenolate*

Dissociation temperature	mp	245° C
Crystal form [a] (by petrographic analysis)		Monoclinic
Refractive index (N_D^{25})		1.69
Density	g/ml	1.6
Fluorescence [b] (excited by 3650 A radiation)		White
Solubility		[c]

[a] Figure 3 and 4, respectively, show zinc eugenolate crystals and electron micrographs of a zinc oxide-eugenol mixture.

[b] The presence of zinc eugenolate may be readily detected by means of the characteristic white fluorescence emitted by this compound when excited by ultraviolet radiation. When similarly excited, zinc oxide and eugenol fluoresce bright yellow and dark brown, respectively. A mixture of zinc oxide and eugenol fluoresces deep red.

[c] Very slightly soluble hot chloroform; soluble in ammonium hydroxide, pyridine, hot acetamide, and hot butyrolactone.

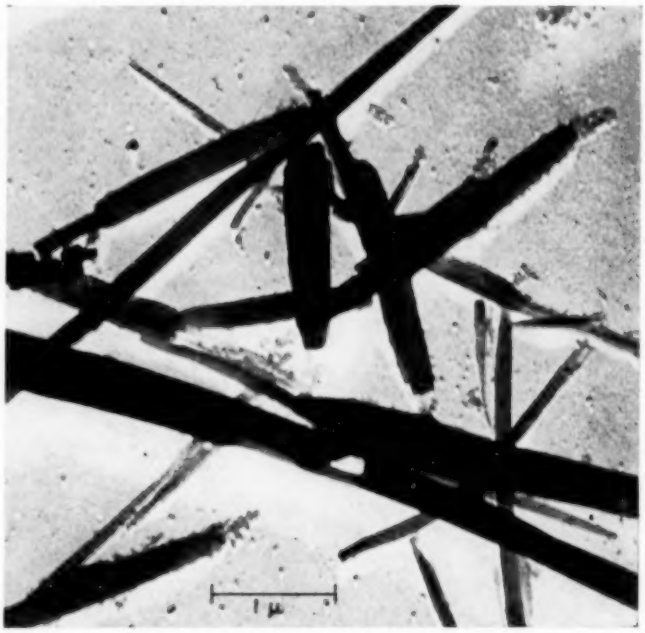

FIGURE 3. *Electron micrograph of zinc eugenolate, palladium shadowed 4:1, showing the crystal habit typical of the extracted reaction product.*

The small, rounded particles seen in the background and on the surfaces of the large, crystalline formations are probably zinc oxide.

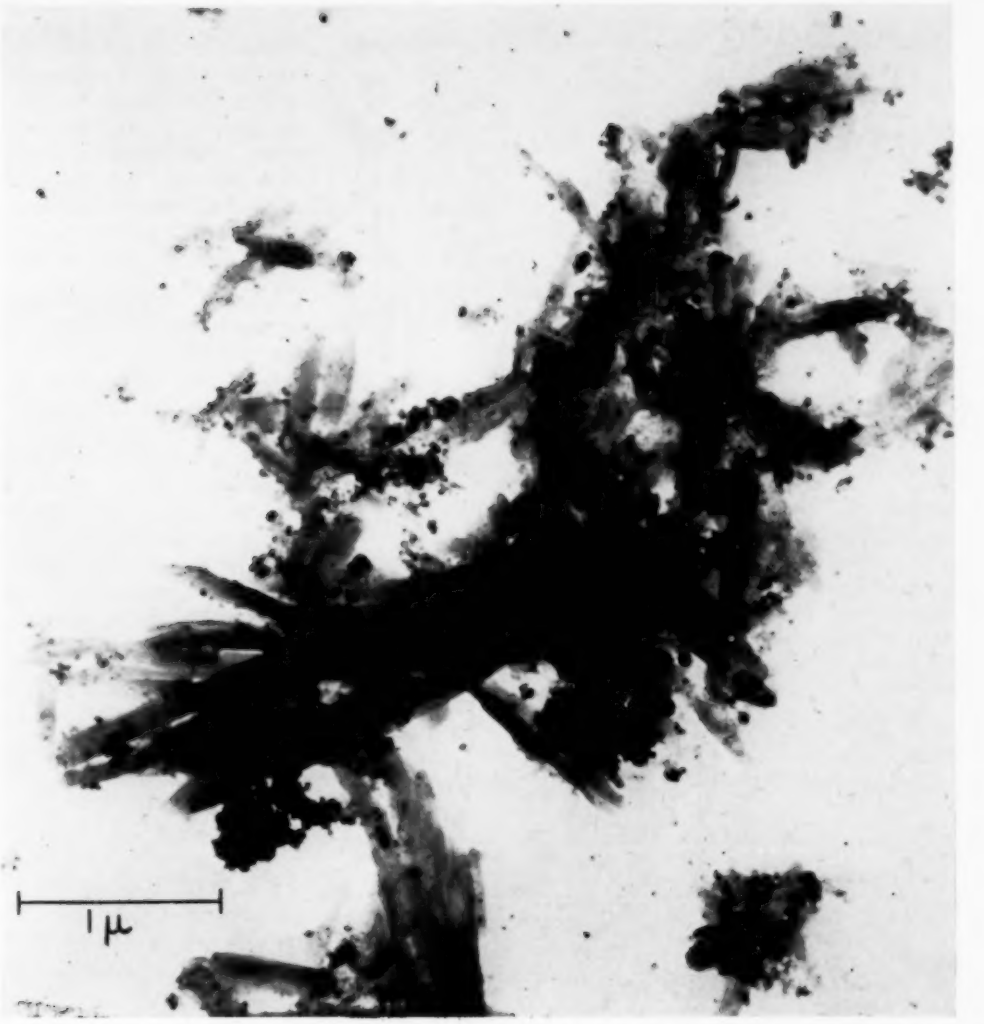

FIGURE 4. *Electron micrograph of a zinc oxide-eugenol mixture showing the small, rounded particles of zinc oxide and the thin, elongated crystals of zinc eugenolate.*

The sheaf-like aggregation is typical of the unextracted hardened mass.

Interesting changes in infrared absorption occurred, as shown in figure 5. In the 7.1- to 7.4-μ area the absorption due to the hydroxy aromatic group of 8-quinolinol, eugenol, and guaiacol was not evident in their zinc derivatives. The disappearance of this band is due to the replacement of the phenolic hydrogen by zinc. At 7.5-μ absorption was observed in all three zinc compounds, whereas none was in the original hydroxy aromatics. This absorption has been attributed to the appearance of bond-bending strain.

An absorption band at 6.08 μ due to the vinyl group was in both eugenol and its zinc derivative spectra. This was evidence that the para substituent did not take part in the reaction. Absorption in the 8.1-μ region due to the methoxy group is present in both the original hydroxy aromatics and their zinc derivatives. However, there is a slight shift (not more than 0.1 μ) in the wavelength at which the absorption occurs.

The apparent inability of the setting reaction to take place in the absence of the *o*-methoxy group, the insolubility of the reaction product, and the infrared absorption changes suggest that zinc eugenolate is related to the metallo-pyrocatechol complexes or chelates [7].

Zinc is a bivalent element with a common coordination number of four. As such, zinc is a metal likely to form a chelate. Eugenol, guaiacol, and methylguaiacol have a replaceable hydrogen and a nearby donor in the oxygen of the *o*-methoxy group. The chelate formed would have a proportion of two eugenol molecules to one zinc. It may be represented as follows:

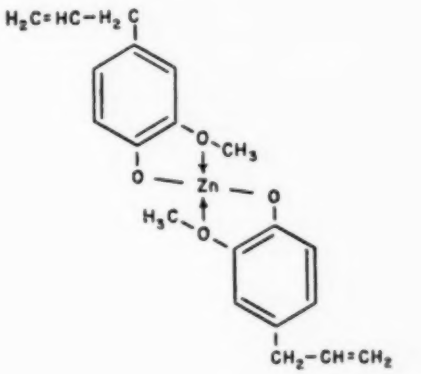

The compound did not sorb an appreciable amount of water on storage in a high-humidity (93.3%)

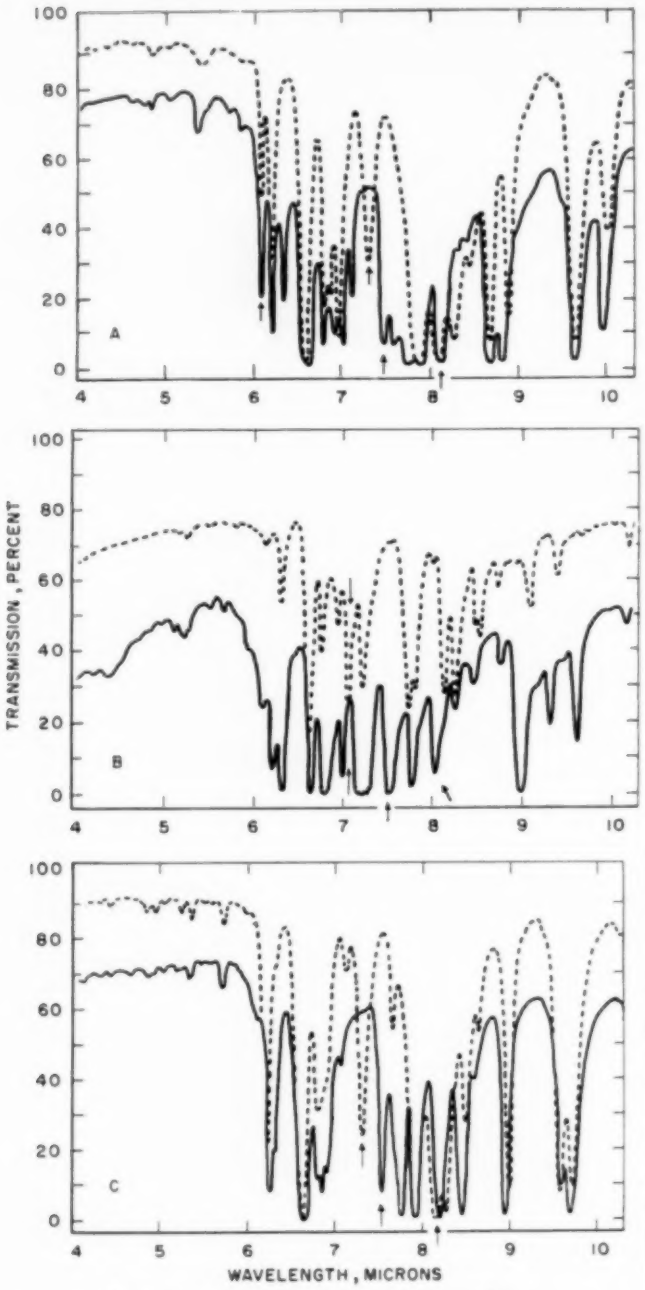

FIGURE 5. *Infrared absorption spectra.*

In each case the broken line is the hydroxy aromatic and the solid lin is the zinc derivative. A, Eugenol and zinc eugenolate; B, 8-quinolinol and zinc quinolinolate; C, guaiacol and zinc guaiacolate.

atmosphere for 10 days. Therefore, the formation of a hydrate at room temperature is not likely to occur.

The set mass resulting from an equimolar mixture of zinc oxide and eugenol contains zinc oxide, zinc eugenolate, and eugenol. The recovery of eugenol from the extraction procedures shows the presence of excess eugenol. A comparison of data from the extraction procedures and X-ray diffraction pattern 3 of figure 1 indicates that only a portion of the zinc eugenolate formed was recovered by the extraction procedures, and both methods show the presence of a considerable amount of unreacted zinc oxide. The sheath-like zinc eugenolate crystals formed act as a matrix for the zinc oxide. Excess eugenol is sorbed by the zinc eugenolate and likely sorbed by the zinc oxide. Sorption of eugenol by zinc eugenolate is demonstrated by paste formation when zinc eugenolate crystals are dispersed in eugenol.

4. Summary

1. The setting of mixtures of zinc oxide and eugenol involves both physical and chemical processes.

2. X-ray diffraction data and electron photomicrographs give evidence that a crystalline compound is formed by the chemical reaction.

3. Chemical analysis and molecular weight determinations show that this crystalline compound corresponds to the empirical formula $(C_{10}H_{11}O_2)_2Zn$, zinc eugenolate.

4. Infrared absorption data suggest that zinc eugenolate is a chelate compound with the following structure:

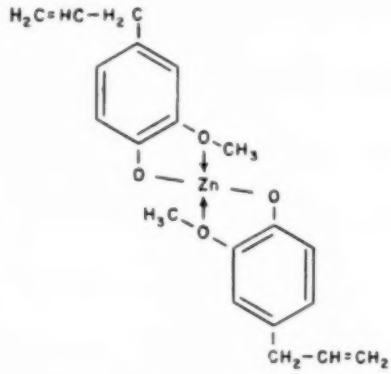

5. The set mass resulting from mixes of zinc oxide and eugenol consists of zinc oxide embedded in a matrix of long, sheath-like crystals of zinc eugenolate. The excess eugenol is likely sorbed by both the zinc eugenolate and the zinc oxide.

The authors especially acknowledge the generous assistance given by H. Swanson and G. Ugrinic of the Microstructure Section, National Bureau of Standards, in performing X-ray diffraction measurements.

The authors thank J. B. Conn of Merck and Co., Inc., for supplying the Hyperfine zinc oxide.

5. References

[1] H. J. Turkheim, Brit. Dental J. **45,** 1 (1953).
[2] E. Forster, Stomatologia **27,** 217 (1929).
[3] W. Harvey and N. J. Petch, Brit. Dental J. **80,** 1, 35 (1946).
[4] F. Zetzsche, H. Silbermann, and G. Vieli, Helv. Chim. Acta **8,** 596 (1925).
[5] H. E. Swanson and R. Fuyat, NBS Circular 539, vol. II (1953).
[6] L. Merrit, Jr., Anal. Chem. **25,** 718 (1953).
[7] A. E. Martell and M. Calvin, Chemistry of Metal Chelates (Prentice-Hall Inc., New York, N. Y., 1952).

WASHINGTON, April 1, 1955.

Journal of Research of the National Bureau of Standards Vol. 55, No. 3, September 1955 Research Paper 2612

Development of a Photoresist for Etching Designs in Glass

Chester I. Pope and Raymond Davis

The preparation of a light-sensitive coating from phenol-formaldehyde resin is described. The light-sensitive coating may be used as a resist or mask in etching scales or reticule patterns in glass. A new etching solution was developed for use with this resist, and it is also recommended for fine line etching with wax resists.

1. Introduction

Etched glass scales and reticules are commonly produced by using a wax resist as a mask. A thin layer of wax coated on the glass is engraved or ruled in such a manner that the design or pattern is accurately positioned and the glass is uncovered in the engraved areas. The design is etched into the glass with hydrofluoric acid. After removing the resist, the etched areas are usually filled with an opaque pigment to increase the contrast and legibility. The workers in this field have a need for a light-sensitive coating, or resist, so that duplicate etchings may be made by contact printing, as in photography.

The problem of finding a suitable substance for making a light-sensitive resist is difficult because the glass must be etched with hydrofluoric acid, which attacks all of the known light-sensitive coatings. The coatings invariably crack, undercut, decompose, or become permeable to the etching solution before the etching is complete. Procedures using an undercoat, such as silver or a varnish, under the light-sensitive resist did not prove satisfactory.

Phenol-formaldehyde resin was known to be quite resistant to the action of hydrofluoric acid, and it seemed possible that a thin layer coated on glass might serve as a resist for hydrofluoric-acid etching after development of the image. Doelker [1][1] patented a process in which a phenol-formaldehyde resin, sensitized with ammonium dichromate, was recommended as an etching resist for zinc plates. Beebe, Murray, and Herlinger [2] patented the use of light-sensitive phenol-formaldehyde resin for photographic processes. They sensitized the resin with iodine, iodoform, etc., and, after exposure, developed the coating in a solution of about equal parts of alcohol and water. The resin made according to their directions was quite soft, remained tacky too long after coating for contact printing, and was low in light sensitivity. In the course of the present investigation it was found that the softness and tackiness of the resin was due in part to the presence of methyl alcohol in the formaldehyde solution used in the synthesis of the resin. The addition of methyl alcohol to trioxymethylene and phenol, in a concentration corresponding to that generally found in 40-percent formaldehyde solutions, yielded a soft, tacky resin. Therefore, trioxymethylene was used instead of the 40-percent aqueous solution of formaldehyde for the production of the phenol-formaldehyde resin in this work. Also the alcohol-water developer used by Beebe, Murray, and Herlinger [2] was not a satisfactory developer for the resin on glass. A resorcinol-formaldehyde resin was also made and was found useful as an additive in the phenol-formaldehyde resin.

[1] Figures in brackets indicate the literature references at the end of this paper.

2. Synthesis of the Phenol-formaldehyde Resin and the Resorcinol-formaldehyde Resin

2.1. Synthesis of the Phenol-formaldehyde (State–A) Resin

Baekeland [3, 4, 5] divided the phenol-formaldehyde reaction during resinification into three stages, A, B, and C, which are characterized by the appearance and solubility of the resin. The A-stage, or initial product, is a low molecular weight condensation product soluble in acetone; the B-stage, or intermediate condensation product, is swelled by acetone but not soluble in it; and the C-stage, or final condensation product, is infusible and completely insoluble in acetone. The resin used for the photoresist is that formed in the A-stage and is condensed to the state where it is just soluble in 95-percent ethyl alcohol. The resin is a thermosetting phenolic, which slowly passes into the B-stage on drying at room temperature.

Sodium acetate, a weak alkaline salt, proved to be the best catalyst for the condensation of the phenol and formaldehyde. It yielded a resin that had the greatest light sensitivity and which was readily developable by an organic solution. Other salts tested as catalysts were potassium acetate, lithium acetate, calcium acetate, barium acetate, and sodium formate. These salts produced resins that were low in light sensitivity and could not be as easily developed as the resin formed with sodium acetate. Acids such as hydrochloric acid act as strong catalysts and produce a resin that is not as light sensitive as that produced by the weak alkaline catalyst, sodium acetate, and the condensation

reaction is difficult to control because the resin passes rapidly from the A-stage to the B-stage.

Investigation of the condensation reaction showed that the ratio of 1 mole of phenol, 3 moles of trioxymethylene, 6 moles of water, and 0.3 mole of sodium acetate ($CH_3COONa.3H_2O$), produced a satisfactory light-sensitive resin that was not too soft. Decreasing the sodium acetate gave a softer resin, which is less light sensitive.

The following formula and procedure were worked out for synthesizing the light-sensitive resin:

Phenol	282 g
Water	324 ml
Sodium acetate ($CH_3COONa.3H_2O$)	122 g
Trioxymethylene (paraformaldehyde)	270 g

The phenol and trioxymethylene were USP grade, and the sodium acetate was reagent quality, meeting ACS specifications. Distilled water was used in the synthesis and tap water in washing the resin.

The apparatus consisted of a 3,000-ml round-bottomed flask fitted with a reflux condenser by means of a ground-glass joint and mounted on a ring stand. The apparatus should be located in a chemical hood. The chemicals were added to the flask in the order listed in the formula followed by the addition of boiling ships made from an unglazed porcelain plate. The mixture was heated through an asbestos pad with a Bunsen burner to a gentle boil. The ring stand was rocked gently and frequently to prevent superheating until the boiling began. The boiling was continued throughout the period of the reaction, and the time required was 2½ to 3½ hr. The temperature of the boiling solution during the reaction and before precipitation was 105° C. Toward the end of the condensation reaction the solution became cloudy. It became opaque to transmitted light about 20 min before two definite phases developed, accompanied by foaming. After the two phases appeared, a gentle and frequent rocking of the ring stand was helpful in preventing the resin, which slowly precipitates from the boiling mixture, from sticking to the flask. After the two phases appeared, the boiling was continued about 5 min, and the hot reaction mixture was immediately poured into cool water while being rapidly stirred, thus completing the precipitation of the resin from the hot reaction mixture. The resin was washed and kneaded in about five changes of water and tested for degree of condensation. This test was made by taking about 10 g of the resin batch, heating it on the steam bath in a small porcelain dish while stirring with a glass rod, and noting the time for the resin to pass into the B-stage. This time was observed visually when the resin became rubbery, stringy, or lumpy and was the point at which all or most of the resin became insoluble in 95-percent ethyl alcohol. If the resin has condensed close enough to the B-stage, the small sample of resin should become insoluble in 95-percent ethyl alcohol after being heated for 10 min on the steam bath. If the time was much greater than 10 min, the precipitated resin batch was heated on the steam bath in a large porcelain dish and stirred constantly with a glass rod, and the time of the heating was estimated from the time required for the small sample to become insoluble in 95-percent ethyl alcohol. With experience, the operator will find no difficulty in determining the end-point of the condensation. As a safeguard against carrying the condensation of the precipitated resin too far on the steam bath, the resin batch may be cooled with water at intervals and a small sample tested for degree of condensation as described above. The resin passes rapidly from A-stage to B-stage at a temperature of 100° C., and if the resin shows any signs of stringiness, or a tendency to be rubbery and lumpy, it should be cooled immediately by stirring in cool water. The resin is usable even if a few insoluble particles appear in the alcohol solution, but it should be discarded if essentially insoluble in alcohol. The highest degree of light sensitivity and developability were obtained by condensing the resin as close to the B-stage as possible, without the resin becoming insoluble in 95-percent ethyl alcohol.

After the resin had been condensed to the desired state and cooled, as much of the water as possible was pressed out and the resin dissolved immediately in 700 ml of methyl ethyl ketone (2-butanone) of a good commercial grade, free from acid or any substance that would react with iodoform. Then 500 g of anhydrous sodium sulfate was added and the resin solution allowed to stand for several days, with occasional shaking. After filtering the resin solution it was ready for sensitizing and use. The amount of resin, determined from the water-free solutions of different batches, gave yields of 220 to 300 g. The resin solutions contained from 22.5 to 30 g of resin per 100 ml of solution. The concentration of the resin in the filtered solution was determined by noting the volume, evaporating 10 ml of the solution to dryness in a tared 50-ml beaker, and weighing.

For use as a light-sensitive resist coating, the concentration of the resin was adjusted to 20 g of resin per 100 ml of solution and sensitized by adding 1 g of iodoform for each 10 g of resin. The iodoform used was Eastman Kodak Cat. No. P–341. Just before use, the sensitized resin solution was filtered through a coarse fritted-disk filtering funnel without pressure. Sensitized resin solutions have been usable after storage for 2 years in a refrigerator. Unsensitized resin solutions stored in the dark at room temperature were still usable after 3 years. The phenol-formaldehyde resin required about 2 to 3 times more exposure to actinic light than the well-known cold top enamel to render the coating insoluble in the developer solution.

A second formula containing ethylene glycol as part of the solvent was developed for the synthesis of the resin. The resin made by this last formula was generally sufficiently condensed when precipitated so that no further treatment was necessary on the steam bath. However, it should be tested for degree of condensation, as described above, before dissolving it in the methyl ethyl ketone. The resin has the same sensitivity as that made by the first formula but contains a trace of ethylene glycol.

Ethylene glycol, because of its hydroscopic nature, caused a slight decrease in the light sensitivity of the resin coating at high relative humidities. The effect was nil at a relative humidity of 50 percent or less.

The following alternative formula was worked out for synthesizing the phenol-formaldehyde resin:

Phenol	282 g
Ethylene glycol	186 g
Water	270 ml
Sodium acetate ($CH_3COONa \cdot 3H_2O$)	122 g
Trioxymethylene (paraformaldehyde)	270 g

The ethylene glycol was of reagent grade. The apparatus and procedure for producing the resin were the same as described for the previous formula. The time required for the reaction was 2 to 3 hr. The temperature of the boiling solution during the reaction and before precipitation was 107.5° C. The reaction mixture remained clear until very close to the end of the reaction. The solution became cloudy, and the boiling was continued about 3 min after it had become opaque to transmitted light. The resin was immediately precipitated from the hot reaction mixture by pouring into cool water with rapid stirring. The resin was treated in the same manner as that obtained from the first formula.

2.2. Synthesis of the Resorcinol-formaldehyde Resin

The resorcinol-formaldehyde resin, because of its reactivity and chemical similarity to the phenol-formaldehyde resin, should improve the sensitivity and resist properties of the phenol-formaldehyde resin, and this was found to be true. A resin, soluble in 95-percent ethyl alcohol, was produced from the condensation of resorcinol and formaldehyde. Although this resin was light sensitive, it was not possible to develop the image satisfactorily. It is somewhat more resistant to hydrofluoric acid than the phenol-formaldehyde resin. The addition of 5-percent of the resin, based on the weight of the phenol-formaldehyde resin, increased the sensitivity about 25 percent, increased the intensity of the dyeing of the image during development, and improved its resist properties slightly.

The following formula and procedure were used in synthesizing the alcohol-soluble resorcinol-formaldehyde resin:

Resorcinol	55 g
Water	75 ml
Sodium sulfate, anhydrous	12.5 g
Formaldehyde solution, 40%	41 ml

The resorcinol was Eastman Kodak Cat. No. P–222, and the sodium sulfate was reagent quality, meeting ACS specifications. The formaldehyde was USP grade. Distilled water was used both in the synthesis and in washing the precipitate. The chemicals were added to a 250-ml Erlenmeyer flask and brought into solution. The reaction mixture was stored without agitation in a constant-temperature room at 22 ±1° C. The solution was clear after 24 hr, but after 40 hr a precipitate began to settle out. At the end of 140 hr the reaction mixture was diluted to 1,500 ml, and then 100 g of anhydrous sodium sulfate was added. The sodium sulfate salts out the resin during the reaction and also on dilution before filtering. The precipitated resin was removed with suction by means of a Buchner filtering funnel. The precipitate was thoroughly washed, air-dried overnight, and finally dried in the dark in a desiccator over anhydrous calcium chloride. When the reaction time was extended much beyond 140 hr the resin became insoluble in 95-percent ethyl alcohol.

The rate of the condensation reaction increased with increase in temperature, accompanied by an increase in the yield of an alcohol-insoluble resin. At 100° C the reaction was very rapid, and the resin was completely insoluble in ethyl alcohol. It was difficult to obtain a good yield of the alcohol-soluble resorcinol-formaldehyde resin when the reaction was carried out at a temperature much above 25° C.

The dried resin, when stored in a dry brown bottle in the dark at room temperature, was still soluble in 95-percent ethyl alcohol after 2 years. The resin, when dissolved in methyl ethyl ketone over anhydrous sodium sulfate at a concentration of about 20 g per 100 ml of solution, was still usable after 3 years of storage at room temperature.

3. Development of the Exposed Resin Coating

After suitable exposure in contact with a master positive, the unexposed areas of the resin coating were dissolved out (developed), and the exposed areas were dyed simultaneously by means of an organic solution developed for use on this resin coating. The developer solution was made up as follows:

Ethyl alcohol, 95%	1,000 ml
Normal butyl alcohol, bp 117 to 117.8° C	1,000 ml
Methyl ethyl ketone, bp 79 to 80.5° C	200 ml
Methyl violet	2 g
Basic fuchsin (aniline red, magenta)	2 g

Before use the solution was filtered through a coarse frittered-disk filtering funnel.

The ethyl alcohol, normal butyl alcohol, and methyl ethyl ketone were of reagent grade and were used without distillation or drying. The developer solution contained about 3 percent of water. The mixture of methyl violet and basic fuchsin dyed the resin coating a heavy blue-purple and was found to be the best combination of dyes tested. Methyl violet dyed the resin coating blue-green; basic fuchsin, red; and malachite green, green. Another developer solution was also made up without the dye for use in removing the excess dye that collected on the surface during the developing procedure. The exposed resin coating was developed by immersing the coated specimen in the developer-dye solution for 30 to 40 sec with gentle agitation and rinsing it 2 or 3 times in developer solutions that contained no dye. Although the development took place in 30 to 40 sec at room temperature, there were no adverse effects on the resin coating if the developing time was extended for as long as 2 min.

4. Etching Solution

After developing and drying, the resistance of the resin coating to hydrofluoric acid was increased by baking it in an oven between 100 to 135° C for 1 to 3 hr. Concentrated hydrofluoric acid (48%) attacked the phenol-formaldehyde resin coating. The problem was to find a solvent for the hydrofluoric acid that would delay its attack on the resin coating and prevent the formation of insoluble salts during the etching. Experimentally the answer was found in using hydrofluoric acid in aqueous solution with phosphoric acid. Also, phosphoric acid assisted the hydrofluoric acid in etching the glass [6]. The phosphoric acid retarded the attack of the hydrofluoric acid on the developed resin and gave a clear etch when sufficient water was added. The following formula was developed:

Ortho phosphoric acid, 85%	100 ml
Water	50 ml
Hydrofluoric acid, 48%	25 ml

The phosphoric and hydrofluoric acids were of reagent quality, meeting ACS specifications. The etching solution was easy to make up as no noticeable heating took place when the chemicals were mixed. The etching solution may be used as soon as it is made up, and, if stored in a wax pot fitted with a tight cover, it will keep for several months. If the developed phenol-formaldehyde resin coating is not too thin (not less than 0.00004 in. thick), and has been baked, it will withstand the etching solution for periods up to 15 sec at room temperature. A 5-sec etch is recommended for fine line work where the etch is to be filled chemically. A deep etch may be obtained by etching several times for 3 to 4 sec, washing and drying at 100° C for about 30 min between each etch. At the end of the etch, the glass specimen was immersed immediately in a 20-percent solution of sodium hydroxide solution to neutralize the hydrofluoric acid and to remove the resin coating.

5. Conclusion

Many organic substances are sensitive to or hardened by actinic light, but it is generally a difficult problem to find a developer solution that will dissolve out the unexposed areas of the resin and not attack the exposed areas. The developer solution dissolved the unexposed light-sensitive resin quickly and yet did not attack the exposed resin, even if the development was extended several times beyond the normal developing time. Iodoform was found to be a very good sensitizer. The addition of 5 percent of the resorcinol-formaldehyde resin, based on the weight of the phenol-formaldehyde resin, improved the sensitivity and resist properties of the phenol-formaldehyde resin, although its presence was not necessary to make the phenol-formaldehyde resin function as a resist for etching glass.

The light-sensitive resist made with the phenol-formaldehyde resin will not withstand the action of concentrated hydrofluoric acid (48%). However, the etching solution containing hydrofluoric acid and phosphoric acid may be used for etching times up to 15 sec. An etching time of 5 sec was used to produce fine lines (10 microns wide). Even though the light-sensitive resist will not withstand a long etching time, deep lines may be obtained with the hydrofluoric acid-phosphoric acid etching solution by etching the glass several times for 3 or 4 sec, washing, and drying between each etch.

For the details on the use of the phenol-formaldehyde light-sensitive resist, see National Bureau of Standards Circular 565 [7] Techniques for Ruling and Etching Precise Scales in Glass and Their Reproduction by Photoetching with a New Light-sensitive Resist.

6. References

[1] E. Doelker, British Patent 183,817 (1923).

[2] M. C. Beebe, A. Murray, and H. V. Herlinger, U. S. Patent 1,587,270 (1926).

[3] L. H. Baekeland, Ind. Eng. Chem. **1**, 149 (1909).

[4] R. L. Wakeman, The chemistry of commercial plastics, p. 115 (Reinhold Publishing Corp., New York, N. Y., 1947).

[5] C. Ellis, The chemistry of synthetic resins, vol. 1, pp. 295, 342 (Reinhold Publishing Corp., New York, N. Y., 1935).

[6] B. Schweig, Principles and methods of etching and embossing, Glass, 143 (April 1938).

[7] Raymond Davis and Chester I. Pope, NBS Circular 565 (in press).

Washington, April 5, 1955.

Journal of Research of the National Bureau of Standards Vol. 55, No. 3, September 1955 Research Paper 2613

Preferred Orientation in Stark Rubber

C. J. Newton, L. Mandelkern, and D. E. Roberts

The method of pole-figure analysis of preferred orientation is outlined and is applied to the problem of X-ray diffraction from stark rubber. A single nonrotating texture is deduced. The texture indicates that the chain-molecule axis is tilted about 22° from the plane of the rubber sheet and that a (101) plane normal lies approximately parallel to the sheet.

1. Introduction

Natural rubber is occasionally found to be hard and inelastic when received or stored in temperate climates. This type of rubber has been designated as "stark rubber", and it is known that its unusual physical properties are due to the development of appreciable amounts of crystallinity. When stark rubber is heated, the observed melting temperature is appreciably higher than that usually assigned to natural rubber. It has been shown recently [1] [1] that these higher melting temperatures are a consequence of the fact that the crystallites are not randomly arranged relative to one another in stark rubber. These conclusions were based on the X-ray diffraction patterns for several different samples wherein the intensities around the circumferences of diffraction haloes were found to be nonuniform.

If a thin piece of polycrystalline material composed of a very large number of randomly oriented crystallites is placed in a finely collimated X-ray beam, it will cause some of the rays to be diffracted and to form on a photographic film placed normal to the undeviated beam several concentric rings, or haloes, which vary in intensity one from another, but which are uniformly dense each around its own circumference. If the polycrystalline material is made into the form of a fiber and is strained axially, the crystallites will usually no longer be randomly oriented. Each diffraction halo will no longer be uniform but will show broadening and darkening at certain positions, and in extreme cases will break up into a pattern of discrete spots. This is caused by the tendency of the crystallites to approach a "fiber texture", wherein each would ideally have a common crystallographic direction parallel to the axis of the fiber, with radial orientations still random. The X-ray diffraction pattern in such an ideal case would be identical with that from a single crystal of the same material rotating about the fiber direction. Orientations in drawn metal wires and in stretched organic fibers often approach this ideal closely enough that their diffraction patterns may be interpreted by methods similar to those used with rotating single crystal patterns.

When this type of diffraction pattern is observed, the lengths of the spots or areas are related to the angular deviation between the molecular axis direction in the crystallites and the axis of the fiber. A measure of the distribution of orientations can then be obtained from the variation of the intensity along the arcs [2, 3].

Although the X-ray diffraction haloes from various stark-rubber samples were nonuniform around their circumferences, the patterns did not approach those of fiber-type diagrams. Hence, to describe the preferred orientations of the crystallites in stark rubber, it was necessary to employ a more general method of analysis, the use of the pole figure. Pole-figure analysis, which is explained below, is regularly used in the study of preferred orientation in sheets of metal; but, so far as the authors are aware, it has not heretofore been carried out with a semicrystalline polymer, although a discussion of idealized pole figures for various types of preferred orientation in cellulose has been presented by W. A. Sisson [4, 5].

2. Pole-Figure Analysis

2.1. Stereographic Projection

The pole figure is the conventional method of portraying the angular clustering of certain poles or crystallographic directions with respect to the geometry of the specimen. The means of portrayal is the stereographic projection, which is a two-dimensional representation of the angular relationships between elements of direction in three dimensions. It is based upon the spherical projection, as outlined below.

Let the object to be described, such as the unit cell of a crystal, be placed at the center of a sphere. Lines now drawn from the center, perpendicular to the faces of the cell, will intersect the surface of the sphere when extended. These intersections, or "poles", on the sphere constitute the spherical projection of the unit cell. Angular measurements and symmetry relationships observed among the poles on the sphere reflect the same relationships to be found among the faces of the cell, or the elements of any other entity so projected.

The mapping of the pattern on the sphere onto a plane may be done in several ways. The method we are interested in is the stereographic projection. To visualize this projection, first pass a plane tangent to the reference sphere; this will be known as the plane of projection. Draw a diameter from the point of

[1] Figures in brackets indicate the literature references at the end of this paper.

tangency to the opposite side of the sphere. This locates the point of projection, a point on the surface of the sphere diametrically opposite the point of tangency of the plane of projection. Lines are now drawn from the point of projection through the poles on the surface of the reference sphere and extended until they intersect the plane of projection. These intersections result in a pattern on the plane that makes up the stereographic projection. This construction is illustrated in figure 1.

Poles on that half of the reference sphere opposite the point of projection will project inside the basic circle formed by the projection of the equator of the sphere. Poles on the other hemisphere would project outside the basic circle, but by convention they are usually placed on a second pattern formed by interchanging the point of tangency of the plane and the point of projection, with the points then falling inside the basic circle. If desired, the projections of the two hemispheres may then be superimposed, with some mode of distinction between points if necessary.

The measurement of angles between poles on a stereographic projection is accomplished with the aid of a projection of lines of latitude and longitude from the reference sphere. The chart usually employed for this purpose is known as a Wulff net. Standard projections of crystal plane normals, crystallographic zones, or zone axes are also often used in orientation problems. The general procedure, in brief, is to find suitable rotations about the central point and the meridian on the net that will bring the stereographic projection under examination into coincidence with the standard projection. Details of theory and application of the stereographic projection may be found in *Structure of Metals* by C. S. Barrett [6].

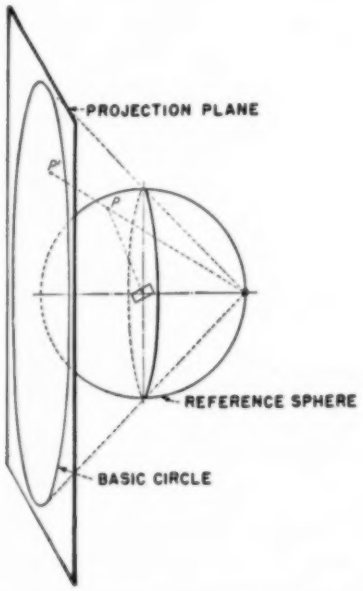

FIGURE 1. *Construction of stereographic projection.*
(After C. S. Barrett)

2.2. Pole Figure

A pole figure is a graphical representation on a stereographic projection of the clustering of poles relative to the geometry of the specimen. It is developed from the variation in intensity of a certain order of X-ray diffraction at various angles in space around a polycrystalline specimen. The intensity at any point on a diffraction halo is closely related to the number of crystallites oriented in such a manner in the volume of the specimen illuminated by X-rays that they contribute to the diffraction in the direction specified. The pole (i. e., normal) of a crystallographic plane diffracting an X-ray beam bisects the angle between the incident beam and the diffracted beam and lies in the plane they determine. Hence, information read from the diffraction pattern in terms of intensity (corrected if necessary for absorption) may be plotted on a pole figure in such a manner as to represent the increase or decrease over randomness of crystallite orientation in that particular direction.

By reading the intensity at reasonably close increments around a diffraction halo and by systematically varying the angle of incidence of the direct beam upon the specimen, one may plot the distribution of poles for all directions on a pole figure for one family of crystal lattice planes. Then, by combining the pole figures of several orders of diffraction, it may be possible to conclude that there is a single or multiple fiber texture or some other type of preferred orientation system.

3. Application to Stark Rubber

3.1. Experimental Procedure

The specimen was approximately a 1-mm cube, cut with one edge perpendicular to the surface of a sheet of Hevea rubber designated as sample III in the previous investigation [1]. Reference should be made to this earlier paper for details concerning the preparation and history of the sample. The sheet was microscopically heterogeneous and porous, and the surfaces were extremely rough. The specimen was fixed with water-soluble glue to the end of a thin glass capillary and placed in a collimated beam of X-rays. The X-rays were generated in a copper target tube operated at 30 kv and 26 ma. The radiation was filtered by a nickel foil, leaving a predominant radiation maximum of copper Kα, with a wavelength of 1.5405 A. An X-ray film was placed 10 cm beyond the specimen to record the diffraction haloes.

Seven patterns were made at 15-deg increments of rotation about one cube axis of the specimen. The specimen was then removed, remounted with another cube axis vertical, and the procedure was repeated, after which the third axis was mounted vertical, and again seven exposures were made. In all, 21 patterns were made with stepwise changes in orientation of the specimen with respect to the X-ray beam. In this manner sufficient data for all directions, assuming twofold symmetry, were obtained for the

pole figures. The patterns were exposed and processed under as nearly constant conditions as practical, so that the densitometer readings, which were then made around each of the three lowest-angle haloes, were comparable from one film to another. A recording microphotometer was used to determine the relative optical densities of the haloes of each film. A special holder was constructed so that the diameter of the film could be scanned; then the film was rotated 10 deg in its plane, and another diameter was scanned. This was repeated until the film had been rotated 180 deg. The density distribution for each halo then could be read from the recorder tracings.

The Bragg angle, θ, for each of the three haloes was calculated from the film to specimen distance and the radius of the halo on the film. From this angle and the wavelength, λ, of the X-rays, one calculated the interplanar spacing d_θ, by Bragg's Law:

$$d_\theta = \frac{\lambda/2}{\sin\theta}.$$

Indices were assigned to the haloes by matching observed spacings, d_θ, with claculated spacings, d_{hkl}, arrived at by considering the crystalline rubber to belong to the monoclinic system with lattice parameters $a=12.46$A, $b=8.89$A, $c=8.10$A, and $\beta=92$ deg, as reported by C. W. Bunn [7]. The spacing is calculated from

$$\frac{1}{d_{hkl}^2} = \frac{h^2}{a^2\sin^2\beta} + \frac{k^2}{b^2} + \frac{l^2}{c^2\sin^2\beta} - \frac{2hl\cos\beta}{ac\sin\beta}$$

where h, k, and l are the order indices of the diffraction produced by the family of atomic planes in question.

The results for the three strongest low-angle haloes were

Obs. θ	Sin θ	Obs. d_θ in A	Calc. d_{hkl} in A	hkl
7.0°	0.1219	6.32	6.23	(200)
8.9°	.1541	5.00	4.86 (201) } not resolved 5.02 (20$\bar{1}$) }	
10.5°	.1822	4.23	4.19	(120)

It should be noted that, though the spacing when h and l are of like signs is different from that calculated when h and l are of unlike signs, the diffractions from such slightly different planes may not be resolved. Some uncertainty arises in this matching procedure because of the inherent lack of experimental precision in determining small angles of X-ray diffraction and the presence in a monoclinic structure of numerous spacings whose diffraction maxima are separated by small angular differences. The tables of indices, with calculated and observed intensities, reported by Bunn were of particular value at this point in the problem.

3.2. Pole-Figure Construction

As a preliminary to plotting the intensities of a given halo as a pole figure, it is advantageous to make up a set of plotting charts for the diffraction, characterized by its Bragg angle. These plotting guides show, for each setting of the specimen, the traces of the circles on which the poles pertaining to the halo will lie. As the construction of these charts is rather complex, it will not be described here; for details the reader is referred to the excellent article by B. F. Decker [8].

With the aid of the standard charts, the densitometer data for each halo was plotted separately in terms of three magnitudes of intensity. The reliability of the figures so constructed was somewhat reduced because of the lack of very strong variations of intensity around a given halo. It did seem clear, however, that there was a real lack of randomness in the orientations of the diffracting crystallites. Each of the three diffracting haloes showed some changes of intensity, and these changes for each one yielded data that, when plotted in a pole figure for the halo, showed a single region of angular concentration of normals to the plane diffracting.

It was next necessary to construct a standard projection of the monoclinic unit cell of rubber, showing the positions of the normals to the diffracting planes, and certain others, relative to the axes of the crystal. This projection, which may be seen in figure 2, was made by laying out the known configuration of the axes according to Bunn, and by calculating the angular positions of the required plane normals with respect to these axes and plotting them accordingly. In order to see if there existed any mutual relationship of the three pole-figure maxima that would define a single texture in the sheet of rubber, the three individual pole figures were

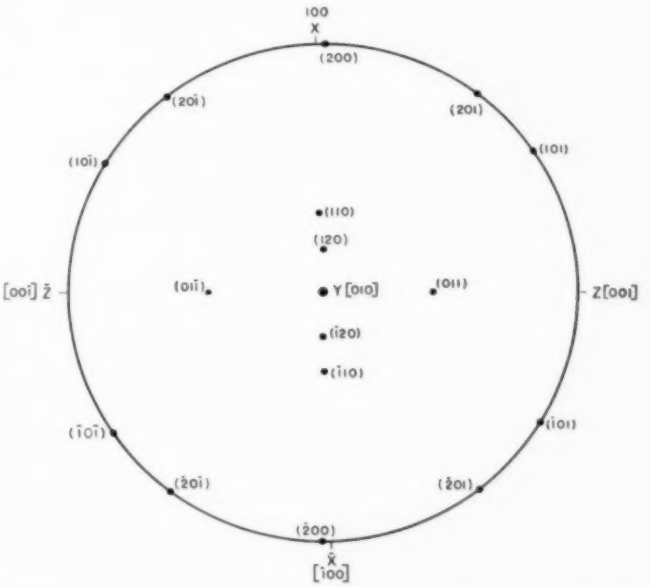

FIGURE 2. *Standard stereographic projection of unit crystalline cell of monoclinic rubber.*

combined on a single stereographic projection for comparison with the standard projection of the unit cell.

3.3. Interpretation of Pole Figures

At first examination, the detection or even the existence of a single texture to explain the observed orientations seemed highly unlikely. As stated before, the lack of sharp intensity variations prevented a high degree of positiveness here. Moreover, each of the three haloes on diffraction rings showed a single pole concentration, whereas the standard projection showed multiple poles for the diffracting planes giving rise to the middle and outer rings. Upon close inspection, however, it was found that the spread of each of the regions of secondary intensity on the projection was wide enough to take in its pair of poles, and the single maximum in each case could be explained as the region of their greatest overlap.

If this interpretation of the data is permissible, it does appear that all of the maxima may arise from a single nonrotational texture, characterized by a preference of the z-axis (to which the chain molecule is parallel) of the crystallites to cluster about a texture axis, making an angle of about 22° with the plane of the sheet. This is shown on the stereographic projection in figure 3. Two qualifications of this specification are to be understood, however: one, the degree of preferred orientation is not very great, only a fraction of the crystallites tending to line up; and, two, the orientation specified for the unit cell is no more than the weighted average orientation, which is subject to the lack of precision, amounting to about ±15° in any direction on the projection, inherent in the low-contrast diffraction readings.

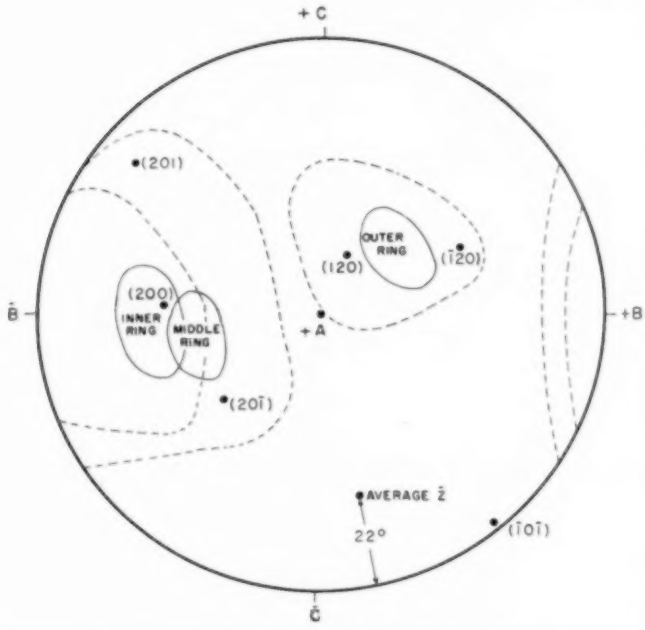

FIGURE 3. *Combined pole figures for stark rubber specimen.*

+A represents normal to sheet.

It may be of interest to observe that the normal to the (101) crystallographic plane showed a preference to lie parallel to the plane of the sheet of rubber. The authors have not determined whether or not this plane or its normal has any special structural significance in the unit cell. It is interesting to point out, however, that A. Brown [9] found with polyethylene at low extensions (less than 200%) that the (011) plane normal was preferred in the stretch direction; and W. A. Sisson [5] working with cellulose found, in addition to the major orientating tendency with respect to the cellulose-chain axis, a minor or selective tendency with reference to the (101) plane. It may be that the apparent alinement of the pseudo-dodecahedral plane normal in the stark-rubber sheet is an analogous phenomenon. Strictly speaking, the above interpretation applies only to the small X-ray specimen. There is of course the possibility that, due to the heterogeneity of the original sample, the interpretation with respect to the geometry of the sheet may not be typical of the sample as a whole.

4. Summary

It has been shown that the crystallites in stark rubber are not randomly oriented; and, by means of pole figures, the preferred orientation of the particular specimen under study has been herewith presented. A study of the figure reveals that a (101) plane normal lies in the original plane of the rubber sheet, a condition that may be related to observations made with other polymers. The pole-figure method of analysis, of long standing in metallurgical studies, would appear to deserve wider employment in orientation problems of polymers, especially in those cases in which the diffraction patterns do not approach those of fibers.

5. References

[1] D. E. Roberts and L. Mandelkern, The nature of stark rubber, J. Research NBS **54,** 167 (1955) RP2578.

[2] C. W. Bunn (R. Hill, Ed.) Fibers from synthetic polymers, p. 263 (Elsevier Publishing Co., Amsterdam, 1953).

[3] P. H. Herman, The physics and chemistry of cellulose fibers, p. 296 (Elsevier Publishing Co., Amsterdam, 1949).

[4] W. A. Sisson (E. Ott, Ed.) Cellulose and cellulose deviations, p. 231 (Interscience Publishers, Inc., New York, N.Y., 1946).

[5] W. A. Sisson, X-ray studies of crystallite orientation in cellulose fibers II, J. Phys. Chem. **40,** 343 (1936).

[6] C. S. Barrett, Structure of metals, 2d ed., p. 28 (McGraw-Hill Book Company, Inc., New York, N. Y., 1952).

[7] C. W. Bunn, Molecular structure and rubber-like elasticity, Proc. Roy. Soc. (London) [A] **180,** 40 (1942).

[8] B. F. Decker, Preferred orientations in rolled metals: Construction of pole figures, Am. Soc. Testing Materials, Proc. **43,** 785 (1943).

[9] A. Brown, X-ray diffraction studies of the stretching and relaxation of polyethylene, J. Appl. Phys. **20,** 552 (1949).

WASHINGTON, March 24, 1955.

Journal of Research of the National Bureau of Standards Vol. 55, No. 3, September 1955 Research Paper 2614

Thermodynamic Properties of Some Gaseous Halogen Compounds

William H. Evans, Thomas R. Munson,[1] and Donald D. Wagman

Tables of values of the heat of formation, $\Delta Hf°$; free energy of formation, $\Delta Ff°$; logarithm of the equilibrium constant of formation, $\log_{10}Kf$; free-energy function, $(F°-H°_0)/T$; heat-content function, $(H°-H°_0)/T$; entropy, $S°$; heat content, $(H°-H°_0)$, and heat capacity, $C°_p$, are given from 0° K to high temperatures for the following gaseous substances: F, F_2, F_2O, Cl, Cl_2, ClO_2, Cl_2O, ClF, ClF_3, Br, Br_2, BrF, BrF_5, BrCl, I, I_2, IF, IF_5, IF_7, ICl and IBr. The data used in preparing the tables are discussed in detail.

1. Introduction

As part of the general program of the National Bureau of Standards on the collection, analysis, and compilation of data on the chemical thermodynamic properties of substances [1, 2] [2], the available information relating to the heats and free energies of formation and the thermodynamic functions of a number of gaseous halogen and oxyhalogen molecules has been assembled and reviewed. Tables of selected values of the heat of formation, $\Delta Hf°$; free energy of formation, $\Delta Ff°$; logarithm of the equilibrium constant of formation, $\log_{10}Kf$; free-energy function, $(F°-H°_0)/T$; heat-content function, $(H°-H°_0)/T$; entropy, $S°$; heat content, $(H°-H°_0)$; and heat capacity, $C°_p$, are given from 0° K to high temperatures for the gaseous substances F, F_2, F_2O, Cl, Cl_2, ClO_2, ClF, ClF_3, Br, Br_2, BrF, BrF_5, BrCl, I, I_2, IF, IF_5, IF_7, ICl, and IBr. Some of the values reported here have been published [1], but no analysis of the data used to obtain the values was given. The present report not only includes a discussion of the sources and treatment of the data but also makes use of the available molecular and spectroscopic data to extend the tables to include values for high temperatures. It is this high-temperature region that is of great interest and importance to many engineers, chemists, and physicists working in the fields of reaction kinetics, fuels, propellants, and explosives.

2. Units and Standard States

The calorie used in these calculations is the thermochemical calorie, defined as 4.1840 abs j. The other constants used are those given by Wagman et al. [2]. The ice point, 0° C, is taken as 273.16° K [3]. The chemical atomic weights used are [4] O, 16; F, 19.00; Cl, 35.457; Br, 79.916; I, 126.91. The standard state chosen for all gases is the ideal gas at 1-atm pressure. As is customary, nuclear spin and isotopic mixing effects are omitted; all values are for the naturally occurring isotopic mixture.

3. Calculations of the Thermodynamic Functions

3.1. Monatomic Gases

The translational contributions to the thermodynamic functions of the monatomic gases F, Cl, Br, and I were calculated by use of the equations given by Wagman et al. [2] (corrected for the new definition of the thermochemical calorie). The additional contributions due to electronic excitation were evaluated by direct summation [5]. The energy levels and multiplicities used were taken from Moore [6].

3.2. Diatomic Gases

The translational contributions to the thermodynamic functions for the diatomic molecules other than F_2 and ClF were evaluated with the same equations used for the monatomic gases [2]. The rotational and vibrational constants given in table 1 were used to calculate the thermodynamic functions for a rigid rotator [2] with moment of inertia I, equal to $h/[8\pi^2 cB_e(1-\alpha_e/2)]$, and an independent harmonic oscillator [8] with a fundamental frequency $(\omega_e-2x_e\omega_e)$.[3] These constants have been adjusted to the usual isotopic mixture, using the product rule; isotopic masses were taken from Collins, Nier, and Johnson [9] (Cl), and Bainbridge and Nier [10] (Br).

Corrections for rotational stretching, vibrational anharmonicity, and rotational-vibrational interaction were calculated at 250°, 300°, 500°, 1,000°, and 1,500° K (and 2,000°, 2,500°, and 3,000° K for Cl_2, Br_2, and I_2), using equations [5] based on the treatment of the general diatomic molecule given by Mayer and Mayer [11]. Values at intermediate temperatures were obtained by graphical interpolation. Table 2 shows the magnitude of these corrections at 1,500° K.

[1] Present address: The Vitro Laboratories, West Orange, N. J.

[2] Figures in brackets indicate the literature references at the end of this paper.

[3] The spectroscopic notation is that used by Herzberg [14].

TABLE 1. *Molecular constants used in calculating the thermodynamic functions for the diatomic halogen molecules*

	P_e	α_e	ω_e	$x_e\omega_e$	$10^9 D_e$
	cm^{-1}	cm^{-1}	cm^{-1}	cm^{-1}	cm^{-1}
F_2	0.8901 [12,13]	0.0146 [7]	919.0 [12,13]	13.6 [7]	334. [7]
Cl_2	0.2404 [14]	0.00166 [14]	561.0 [14]	3.94 [14]	[a] 17.66
ClF	0.514012 [15]	0.0043272 [15]	784.43 [16,17]	6.20 [16,17]	86.9 [15]
Br_2	0.08092 [14]	0.000275 [14]	323.2 [14]	1.07 [14]	2.03 [14]
BrF	0.356319 [18]	0.005206 [18]	673 [19,20]	4. [19,20]	[a] 40.0
BrCl	0.150797 [21]	0.0007597 [21]	443.1 [22,23]	1.8 [22]	[a] 6.99
I_2	0.037364 [24]	0.0001206 [24]	214.248 [24]	[b] 0.6074 [24]	[a] 0.455
IF	[d] 0.2799	[c] 0.00763	[c] 612. [19]	[c] 4. [19]	[a] 23.42
ICl	0.112984 [25]	0.0005275 [25]	382.18 [14]	1.450 [14]	5.19 [14]
IBr	[d] 0.05634	[c] 0.000193	267.4 [14]	0.77 [14]	[a] 1.00

[a] Calculated from the relationship $D_e=(4P_e^3/\omega_e^2)$ [27].
[b] $y_e\omega_e=0.00130$; $z_e\omega_e=0.00000525$.
[c] Recalculated from Durie's data [19].
[d] Calculated from the constants of the other halogen molecules, using Schomaker and Stevenson's relation [26].
[e] Calculated from the relationship $\alpha_e=\frac{6B_e^2}{\omega_e}\left[\left(\frac{x_e\omega_e}{B_e}\right)^{1/2}-1\right]$ [27]

The thermodynamic functions of F_2 and ClF were taken from unpublished calculations made by the Heat and Power Division of the Bureau [7]. These were calculated in essentially the way outlined above.

TABLE 2. *Corrections added to the thermodynamic functions obtained by the rigid rotator-harmonic oscillator approximation at 1,500° K, cal deg mole*

	$-(F^\circ-H_0^\circ)/T$	$(H^\circ-H_0^\circ)/T$	C_p°
F_2	0.0696	0.1083	0.247
Cl_2	.0628	.0860	.182
ClF	.0487	.0709	.156
Br_2	.0629	.0762	.155
BrF	.0646	.0894	.190
BrCl	.0567	.0722	.149
I_2	.0867	.0991	.200
IF	.0563	.0780	.166
ICl	.0625	.0776	.159
IBr	.0710	.0833	.169

3.3. Polyatomic Gases

The thermodynamic functions for the polyatomic molecules, except ClO_2, were calculated by using the rigid rotator-harmonic oscillator approximation [2,8]. The molecular data used, summarized in table 3, are as follows:

F_2O (table 9). The infrared spectrum has been measured by Bernstein and Powling [28]; Jones, Kirby-Smith, Woltz, and Nielsen [29]; Hettner, Pohlman, and Schumacher [30]; and Sutherland and Penney [31]. From their data the three nondegenerate fundamental frequencies were taken as 461, 828, and 929 cm^{-1}. The structural parameters necessary to calculate the moments of inertia were calculated by Bernstein and Powling [28] from a combination of their infrared data and various electron diffraction data;[4] they obtained a F–O–F angle of 101.5 ±1.5° and a F–O distance of 1.38 A. The symmetry of the molecule is C_{2v}. The product $I_AI_BI_C$ from these data is 88.65×10^{-117} g^3 cm^6.

TABLE 3. *Molecular constants used in calculating the thermodynamic functions for the polyatomic halogen and oxyhalogen molecules*

Molecule	Frequencies	Moments of inertia
	cm^{-1}	$10^{-39} g\ cm^2$
F_2O	461; 828; 929	7.211; 1.424; 8.635
ClO_2 [a]	450.1; 958.0; 1128.2	8.411; 1.749; 10.160
Cl_2O	320; 684; 971	23.028; 2.032; 25.060
ClF_3	247; 318; 426; 508; 710; 750	6.1129; 18.1803; 24.3148
BrF_3	244 [b]; 315; 365; 415 [b]; 481; 536; 572; 626 [b]; 683.	33.77; 28.16; 28.16
IF_5	192 [b]; 275; 317; 375 [b]; 572; 605; 645 [b]; 693; 710.	39.53; 33.03; 33.03
IF_7	250 [b]; 313 [b]; 350 [b]; 360 [b]; 426 [b]; 511 [b]; 547 [b]; 635; 638; 670; 678.	52.82; 47.54; 47.54

[a] Anharmonicity terms also available.
[b] Doubly degenerate frequencies.

ClO_2 (table 12). Nielsen and Woltz [33], by combining their infrared data with that of Bailey and Cassie [34], Hedberg [35], Coon [36, 37], and Coon and Ortiz [38], and with the Raman data of Kujumzelis [39], were able to obtain the harmonic fundamentals and the anharmonic constants for the ground state. Dunitz and Hedberg [40] and Coon [41] have measured the Cl—O distance as 1.487 A and the O—Cl—O angle as 115.5°. The symmetry is C_{2v}. The product $I_AI_BI_C$ is then 149.46×10^{-117} g^3 cm^6.

These data were used to compute the thermodynamic functions for a rigid rotator-anharmonic oscillator by the method of Stockmayer, Kavanagh, and Mickley [42]. At 1,500° K the corrections to the harmonic oscillator approximation were 0.043, 0.080, and 0.174 cal/deg mole for $-(F^\circ-H_0^\circ)/T$, $(H^\circ-H_0^\circ)/T$, and C_p°, respectively.

Cl_2O (table 13). The infrared spectrum has been studied by Hedberg [35], Bailey and Cassie [43], Pohlman and Schumacher [44], and Sutherland and Penney [31]. From their data the three nondegenerate frequencies were taken as 320, 684, and 971 cm^{-1}. Dunitz and Hedberg [40] obtained the molecular structure from electron diffraction measurements. The symmetry is C_{2v}. Their values lead to a product $I_AI_BI_C$ of $1{,}173\times10^{-117}$ g^3 cm^6.

ClF_3 (table 15). Jones, Parkinson, and Murray [45] have measured the Raman spectrum of the liquid and the infrared spectrum of the gas; Schäfer and Wicke [46] have also measured the Raman spectrum of the liquid. Unfortunately their assignments were based upon a pyramidal C_{3v} structure. Recently, Smith [47], from microwave measurements, and Burbank and Bensey [125], from X-ray diffraction measurements on the solid, have

[4] After these calculations had been completed, Ibers and Schomaker [32] reported new electron diffraction data. They selected as the "best" values, based upon their own and upon other data, a F–O distance of 1.418 A and a F–O–F angle of 103.2°. Use of these values would increase the values of $-(F^\circ-H_0^\circ)/T$ and S° in table 9 by 0.16 cal/deg mole, and make the values of ΔFf° more negative by (0.167/1000) kcal/mole.

shown that the structure is a planar distorted "T" with C_{2v} symmetry. Such a molecule has six nondegenerate fundamental frequencies, all of which are both infrared and Raman active. On the basis of the C_{v2} symmetry a selection of the apparent fundamental frequencies was made from the spectral data: 247, 318, 426, 508, 710, and 750 cm^{-1}. The microwave data of Smith [47] give a product $I_AI_BI_C$ of $2702.2\times10^{-117}g^3$ cm^6.

BrF_5 (table 19). The Raman spectrum of BrF_5 has been measured by Stephenson and Jones [48]; with the aid of the infrared data of Burke and Jones [49], they have assigned the fundamental frequencies based upon a C_{4v} structure. In the absence of experimental data on the structure of BrF_5 it was assumed that the bromine atom is located at the center of mass and that the Br—F distance is 1.69 A. This distance is based on Pauling's tetrahedral radii [50] and a value for F of 0.55 A, based on CF_4. (See Allen and Sutton [51].) The product $I_AI_BI_C$ is then $26.78\times10^{-114}g^3$ cm^6.

IF_5 (table 24). Lord, Lynch, Schumb, and Slowinski [52] have measured the Raman and infrared spectra and assigned the fundamental frequencies on the basis of a C_{4v} structure. The I—F distance used, 1.83 A, was obtained in the same way as the Br—F distance in BrF_5. The product $I_AI_BI_C$ is then $43.13\times10^{-114}g^3$ cm^6.

IF_7 (table 25). The Raman and infrared spectra were measured by Lord, Lynch, Schumb, and Slowinski [52]; they have assigned the fundamentals on the basis of a pentagonal bipyramidal D_{5h} structure. Slutsky and Bauer [53] report provisional electron diffraction data that lead to 1.93 A for the two I—F bonds along the principal rotation axis and 1.83 A for the radial bonds. These give a product $I_AI_BI_C$ of $131.62\times10^{-114}g^3$ cm^6.

4. Calculation of the Heats and Free Energies of Formation

The heats of formation of gaseous O_2, F_2, Cl_2, Br_2, and I_2 are taken as zero (reference state); *for bromine and iodine this differs from the liquid and solid states customarily used at 25° C* [1]. Auxiliary data, except where noted otherwise, have been taken from Rossini et al. [1].

F (g). The dissociation energy of F_2 (g) has been the subject of much discussion in recent years. (See the reviews by Nathans [54], Evans, Warhurst, and Whittle [55], and Herzberg [14].) From the recent experimental measurements, summarized in table 4, we have selected the heat of dissociation of F_2 as 36.7 ± 1.0 kcal.[5]
This gives

$$\tfrac{1}{2}\ F_2\ (g)=F\ (g)$$

$$\Delta H_0^\circ=18.4\pm0.5\ \text{kcal.}$$

F_2O (g). Von Wartenberg and Klinkott [61] have measured the heat of reaction of fluorine oxide with an aqueous solution of potassium iodide containing hydrofluoric acid to give a solution of potassium triiodide and potassium fluoride; they obtained $\Delta H_{291}=-176.6$ kcal/mole. When combined with the necessary auxiliary heats of formation their data give $\Delta Hf^\circ_{298.16}$ F_2O (g)$=6.0$ kcal/mole. They also measured the heat of reaction of fluorine oxide with aqueous potassium hydroxide to form oxygen gas and aqueous potassium fluoride, and obtained $\Delta H_{291}=-135.8$ kcal/mole. This gives $\Delta Hf^\circ_{298.16}$ F_2O (g)$=7.1$ kcal/mole. In a third experiment they measured the heat of reaction of fluorine oxide with aqueous hydrobromic acid to form a solution of bromine and hydrofluoric acid, obtaining $\Delta H_{291}=-134.4$ kcal/mole. If corrections are applied for the heats of solution of HBr and HF in aqueous hydrobromic acid (see Ruff and Menzel [62]), this value gives $\Delta Hf^\circ_{298.16}$ F_2O (g)$=9.7$ kcal/mole. The average was selected as the "best" value:

$$F_2\ (g)+1/2\ O_2\ (g)=F_2O\ (g)$$

$$\Delta H^\circ_{298.16}=7.6\ \pm2.0\ \text{kcal.}$$

Cl (g). Gaydon [63] calculated from various spectral data $D_0^\circ=19{,}969$ cm^{-1}, or 57.08 kcal. This gives

$$1/2\ Cl_2\ (g)=Cl\ (g)$$

$$\Delta H_0^\circ=28.54\ \pm0.05\ \text{kcal.}$$

[5] All uncertainties, unless otherwise indicated, represent our estimate of the over-all uncertainty.

TABLE 4. *Dissociation energy of* F_2

Observer	Method	Temperature range	Number of experiments	H_0 [a]
		°K		*kcal*
Wicke and Friz [56]	H_2+F_2 explosion	Approx. 1,000	5	36.36±1.34
Gilles and Margrave [57]	Gas density	815 to 869	3	32.07±0.76
Doescher [58]	do	760 to 1,115	24	36.75±0.03
Wise [59]	Effusion	508 to 676	9	38.36±0.28
Barrow and Caunt [60]	Dissociation of alkali halides.			[b] 36.6±3.5

[a] Probable error of the mean.
[b] Over-all uncertainty as given by authors.

Attempts have been made to measure the dissociation of Cl_2 at high temperatures. Because of the difficulties of working at the high temperatures necessary to obtain measurable pressure changes, the results are not too concordant. Von Wartenberg and Henglein [64, 65] obtained gas-density data in the range 955° to 1,151° K, which lead to $D_0^\circ = 53.0$ kcal. Wohl [66], from measurements of the pressure rise during explosions of H_2-Cl_2 gas mixtures, calculated $D_0^\circ = 59.1$ kcal. Trautz and Geissler [67] measured gas densities between 1,425° and 1,537° K; their data give $D_0^\circ = 49.9$ kcal. These last measurements were questioned by von Wartenberg and Weigel [68], who obtained data at 1,478° K that give $D_0^\circ = 56.4$ kcal. Except for the value from Trautz and Geissler, the results agree with the spectroscopic value within their estimated uncertainties of ±2 to 3 kcal.

ClO_2 (g). Wallace and Goodeve [69] measured the heat of explosion of chlorine dioxide gas into the elements; their data give $\Delta Hf^\circ_{298.16}$ ClO_2 (g) = 26.3 kcal. Booth and Bowen [70] also studied this decomposition and obtained $\Delta Hf^\circ_{298.16}$ ClO_2 (g) = 23.5 kcal. Mayer [71], from spectroscopic measurements of predissociation, obtained $\Delta H_0^\circ = 3.6$ kcal for the reaction ClO_2 (g) = Cl (g) + O_2 (g). This gives $\Delta H^\circ_{298.16}$ ClO_2 (g) = 24.4 kcal. Finkelnburg and Schumacher [72] measured spectroscopically the ionization dissociation energy of ClO_2 (g) to ClO (g) and O^+ (g) as 111 kcal. If this is combined with the dissociation energy of ClO (g) given by Parker and Wright [73], $D_0^\circ = 60.7$ kcal, then $\Delta Hf^\circ_{298.16}$ ClO_2 (g) = 18.7 kcal is obtained. However, Finkelnburg and Schumacher state that their value for the dissociation energy is probably high by 5 or 6 kcal because of predissociation; this correction would give a value of about 24.5 kcal for $\Delta Hf^\circ_{298.16}$ ClO_2 (g). A value based primarily on the heats of explosion was selected:

$$1/2\ Cl_2\ (g) + O_2\ (g) = ClO_2\ (g)$$

$$\Delta H^\circ_{298.16} = 25.0 \pm 1.5 \text{ kcal.}$$

Cl_2O (g). Jakowkin [74] measured the solubility of chlorine gas in water and the hydrolysis equilibrium of aqueous chlorine to give aqueous hydrochloric and hypochlorous acids. Goldschmidt [75] studied the hydrolysis equilibrium of Cl_2O (aq) to give hypochlorous acid, and the equilibrium distribution of Cl_2O between water and carbon tetrachloride; his data have been recalculated by Roth [76]. Yost and Felt [77] measured the solubility of Cl_2O (g) in carbon tetrachloride. These data give the following series of free-energy equations:

$2\ Cl_2\ (g) = 2\ Cl_2\ (aq)$	$\Delta F^\circ_{273.16} = 2.050$ kcal
$2\ Cl_2\ (aq) + 2\ H_2O\ (liq) = 2\ HCl\ (aq) + 2\ HClO\ (aq)$	$\Delta F^\circ_{273.16} = 9.510$
$2\ HClO\ (aq) = Cl_2O\ (aq) + H_2O\ (liq)$	$\Delta F^\circ_{273.16} = 3.063$
$Cl_2O\ (aq) = Cl_2O\ (in\ CCl_4)$	$\Delta F^\circ_{273.16} = -0.433$
$Cl_2O\ (in\ CCl_4) = Cl_2O\ (g)$	$\Delta F^\circ_{273.16} = 1.344$
$2\ HCl\ (aq) = H_2\ (g) + Cl_2\ (g)$	$\Delta F^\circ_{273.16} = 64.072$
$H_2\ (g) + 1/2\ O_2\ (g) = H_2O\ (liq)$	$\Delta F^\circ_{273.15} = -57.657$
$Cl_2\ (g) + 1/2\ O_2\ (g) = Cl_2O\ (g)$	$\Delta F^\circ_{273.16} = 21.95$ kcal

From the thermodynamic functions $\Delta S^\circ_{273.16} = -14.06$ cal/deg mole for this reaction. Combining these gives $\Delta Hf^\circ_{273.16}$ Cl_2O (g) = 18.10 kcal; corrected to 298.16° K, this becomes 18.08 kcal.

Thomsen [78] measured the heat of hydrolysis of Cl_2O (g) to HClO (aq) as $\Delta H_{291} = -9.44$ kcal, which becomes −9.51 kcal at 298.16° K. He also measured the heat of the reaction of chlorine gas with aqueous sodium hydroxide to give an aqueous solution of sodium chloride and sodium hypochlorite, and the heats of neutralization of hydrochloric and hypochlorous acids with aqueous sodium hydroxide. Combining these data gives $\Delta Hf^\circ_{298.15}$ Cl_2O (g) = 18.3 kcal.

Wallace and Goodeve [69] obtained the heat of explosion of Cl_2O (g); their data give $\Delta Hf^\circ_{298.16}$ Cl_2O (g) = 21.4 kcal. Günther and Wekua [79] also measured the heat of explosion; their data give $\Delta Hf^\circ_{298.16}$ Cl_2O (g) = 24.7 kcal.

For the "best" value we have taken

$$Cl_2\ (g) + 1/2\ O_2\ (g) = Cl_2O\ (g)$$

$$\Delta H^\circ_{298.16} = 18.1 \pm 0.3 \text{ kcal.}$$

ClF (g). Wicke and Friz [56, 80] measured the heat evolved in the adiabatic explosion of Cl_2-F_2 mixtures; their results give ΔHf°_0 ClF (g) = −11.7

kcal. Schmitz and Schumacher [81] measured the heat of the reaction NaCl (c)+ClF (g)=NaF (c)+Cl_2 (g) at 18° C. Their value of ΔH, −24.5 kcal, gives ΔHf_0° ClF (g)=−13.3 kcal. They also measured the heat of the reaction 1/2 F_2 (g)+NaCl (c)=NaF (c)+1/2 Cl_2 (g); if this heat, ΔH=−39.5 kcal, is combined with that given above for the reaction of ClF, then ΔHf_0° ClF (g)=−15.0 kcal. Schmitz and Schumacher [82], Schumacher, Schmitz, and Brodersen [83], and Warhaftig [84] obtained the dissociation limit of ClF (g) from spectroscopic measurements. Two combinations of dissociation products are possible: $Cl(^2P_{1/2})+F(^2P_{3/2})$ or $Cl(^2P_{3/2})+F(^2P_{1/2})$. After reducing the measured dissociation energies to the atomic ground states, using energies from Moore [6], the values in table 5 are obtained. These data give ΔHf_0° ClF (g)=−12.0 or −13.4 kcal. The data for IBr (g) and ICl (g) (see below) show that in these molecules the lighter atom is in the excited $^2P_{1/2}$ state; by analogy the fluorine should be in the excited state. This choice also agrees somewhat better with the data for ClF_3 (g). (See also, the discussion by Slutsky and Bauer [53].) The "best" value appears to be

$$1/2\ Cl_2\ (g)+1/2\ F_2\ (g)=ClF\ (g)$$

$$\Delta H_0^\circ=-13.4\pm0.5\ \text{kcal.}$$

TABLE 5. *Dissociation energy of* ClF

Observer	D_0°, kcal, if products of dissociation are—	
	$Cl(^2P_{1/2})+F(^2P_{3/2})$	$Cl(^2P_{3/2})+F(^2P_{1/2})$
Schmitz and Schumacher [82]	59.00	60.37
Schumacher, Schmitz, and Brodersen [83]	58.97	60.34
Warhaftig [84]	58.96	60.33

Ruff and Laass [85] measured the heat of reduction of ClF (g) by hydrogen. The data they report are self-consistent, but give a much too negative value of −27.6 kcal for ΔHf_0° ClF (g).

ClF_3 (g). Schmitz and Schumacher [86] reported three measurements of the equilibrium constant for the reaction ClF_3 (g)=ClF (g)+F_2 (g); their data give ΔH_0°=24.50 kcal for this reaction. Schäfer and Wicke [46] reported 13 measurements of the same equilibrium; their results as read from a graph give ΔH_0°=24.6 kcal. The value ΔH_0°=24.5 kcal was selected for this reaction. Two possible values of ΔHf_0° ClF (g) may be combined with this value of ΔH_0° to calculate the heat of formation of ClF_3. If ΔHf_0° ClF (g) is taken as −12.0 kcal, ΔHf_0° ClF_3 (g)=−36.5 kcal; if ΔHf_0° ClF (g) is −13.4 kcal, the value for ClF_3 becomes −37.9 kcal.

Schmitz and Schumacher [81] also obtained, at 18° C, for the reaction ClF_3 (g)+3 NaCl (c)=3 NaF (c)+2 Cl_2 (g), ΔH=−76.5 kcal. A number of different values of ΔHf_0° ClF_3 (g) can be calculated from this value, depending upon the auxiliary data used. If the heats of formation of NaCl and NaF are taken as the selected "best" values [1], ΔHf_0° ClF_3 (g)=−35.9 kcal. A second value can be obtained by using Schmitz and Schumacher's [81] data for the reaction, at 18° C, 1/2 F_2 (g)+NaCl (c)=1/2 Cl_2 (g)+NaF (c), ΔH=−39.5 kcal, and the selected heat of formation of NaCl. From these data we calculate ΔHf_0° ClF_3 (g)=−41.9 kcal. The third and fourth values are obtained by combining Schmitz and Schumacher's [81] data for the reaction ClF (g)+NaCl (c)=NaF (c)+Cl_2 (g), ΔH=−24.5 kcal at 18° C, with the data for the similar reaction with ClF_3 given above, to get ClF_3 (g)+Cl_2 (g)=3 ClF (g), ΔH=−3.0 kcal. Depending upon the value chosen for ΔHf_0° ClF (g), −12.0 or −13.4 kcal, this gives ΔHf_0° ClF_3 (g)=−32.1 or −36.3 kcal, respectively.

The value most consistent with all of the data summarized above, and also with the data for ClF, seems to be that from the equilibrium measurements. We have selected as the "best" value

$$1/2\ Cl_2\ (g)+3/2\ F_2\ (g)=ClF_3\ (g)$$

$$\Delta H_0^\circ=-37.9\pm1.0\ \text{kcal.}$$

Br (g). Herzberg [14] and Gaydon [63] give the dissociation energy D_0° (Br_2) as 1.971 ev, or 45.456 kcal. This was used to obtain the selected value

$$1/2\ Br_2\ (g)=Br\ (g)$$

$$\Delta H_0^\circ=22.73\pm0.05\ \text{kcal.}$$

Vapor-density measurements have been made at high temperatures by von Wartenberg and Henglein [64, 65] (833° to 1,003° K), Perman and Atkinson [87, 88] (1,175° to 1,330° K), Cramer [87] (1,056° to 1,558° K), and Bodenstein and Schmidt [126] (1,495° K). Their data give, respectively, 46.33, 44.92, 46.04, and 45.20 kcal for D_0° (Br_2), in agreement with the spectroscopic value within the estimated uncertainty of ±1.0 kcal. DeVries and Rodebush [90] have also reported data in the range 923° to 1,173° K; their data give values of D_0°, approximately 5 kcal more positive, which show a pronounced trend with temperature.

BrF (g). Durie [19] has obtained the spectroscopic dissociation limit of BrF as 21,190 cm^{-1}. As in the case of ClF, there are two possible sets of dissociation products: $Br(^2P_{1/2})+F(^2P_{3/2})$ or $Br(^2P_{3/2})+F(^2P_{1/2})$. Correcting the observed dissociation limit to the ground states of the atoms gives two values for D_0°(BrF); if fluorine is the excited atom ($F(^2P_{1/2})$), D_0°=59.42 kcal; if bromine is excited, D_0°=50.04 kcal. By analogy with ClF and IF (see below) the "best" value seems to be the higher one: this gives

$$1/2\ Br_2\ (g)+1/2\ F_2\ (g)=BrF\ (g)$$

$$\Delta H_0^\circ=-18.3\pm0.5\ \text{kcal.}$$

BrF_5 (g). Experimental data leading to a heat of formation for BrF_5(g) are not available. Slutsky and Bauer [53] have estimated average bond energies that give

$$1/2\ Br_2\ (g)+5/2\ F_2\ (g)=BrF_5\ (g)$$

$$\Delta H_0^\circ=-122\pm10\ \text{kcal.}$$

BrCl (g). The equilibrium $2\ BrCl(g)=Br_2(g)+Cl_2(g)$ has been studied by several investigators; their results are summarized in table 6. The average of all, except Jost's, gives

$$1/2\ Br_2\ (g)+1/2\ Cl_2\ (g)=BrCl\ (g)$$

$$\Delta H_0^\circ=-0.20\pm0.05\ \text{kcal.}$$

TABLE 6. *Heat of dissociation of* BrCl (g)

Observer	ΔH_0°
	kcal
Mattraw, Pachucki, and Hawkins [22]	0.150
Braune and Victor [92]	.105
Vesper and Rollefson [93]	.245
Gray and Style [94]	.233
Beeson and Yost [95]	.265
Jost [96]	.378

I (g). Gaydon [63] and Herzberg [14] give the dissociation limit of I_2 to $I(^2P_{1/2})+I(^2P_{3/2})$ as 20,037 cm^{-1}. When corrected to the ground state this becomes 12,434 cm^{-1}, or 35.543 kcal, for D_0° (I_2). High-temperature gas-density measurements have been made by Braune and Ramstetter [87] (915° to 1,385° K), Starck and Bodenstein [98] (1,073° to 1,473° K), DeVries and Rodebush [90] (732° to 898° K), Bodenstein and Schmidt [126] (1,495° K), and Perlman and Rollefson [99] (872° to 1,274° K). Their data give values of D_0° (I_2) of 35.95, 35.49, 35.68, 35.17, and 35.534 kcal, respectively. We have taken 35.538 kcal as the "best" value for D_0° (I_2); this is the average of the values from the very careful work of Perlman and Rollefson and from the spectroscopic data. Consequently,

$$1/2\ I_2\ (g)=I\ (g)$$

$$\Delta H_0^\circ=17.77\pm0.03\ \text{kcal}$$

IF (g). Durie [19] has obtained the dissociation limit of IF as 23,570 cm^{-1}. As in the case of the other interhalogen compounds, two sets of dissociation products are possible: $I(^2P_{1/2})+F(^2P_{3/2})$ or $I(^2P_{3/2})+F(^2P_{1/2})$. When corrected to the normal atoms, this limit gives D_0° (IF) as 45.64 or 66.22 kcal, respectively. Durie and Gaydon [91], arguing from the much higher stability of IF_5, as compared with IF, favored the lower value. However, Slutsky and Bauer [53] have pointed out a numerical error in their calculations, which removes the chief support for the low value, and presented additional evidence favoring the high value. The data for ICl (g) and IBr (g) also support this value. At present the "best" value seems to be the higher one. This gives

$$1/2\ I_2\ (g)+1/2\ F_2\ (g)=IF\ (g)$$

$$\Delta H_0^\circ=-30.0\pm0.5\ \text{kcal.}$$

IF_5 (g). Woolf [100] measured the heat of hydrolysis of liquid IF_5:

$$IF_5\ (liq)+3\ H_2O\ (liq)=5\ HF\ (250\ H_2O)+HIO_3\ (1{,}250\ H_2O)$$

$$\Delta H_{291}=-22.05\ \text{kcal.}$$

Correcting this to 298° K gives $\Delta H_{298.16}=-23.55$ kcal. From this, $\Delta Hf^\circ_{298.16}$ IF_5 (liq) $=-212.3$ kcal. Woolf also measured the alkaline heat of hydrolysis:

$$IF_5\ (liq)+6\ KOH\ (220\ H_2O)=$$

$$5\ KF\ (250\ H_2O)+KIO_3\ (1{,}250\ H_2O)+3\ H_2O\ (liq)$$

$$\Delta H_{291}=-118.9\ \text{kcal;}$$

at 298° K this becomes −118.7 kcal. From this, $\Delta Hf^\circ_{298.16}$ IF_5 (liq) $=-212.5$ kcal. The average, -212.4 ± 1.5 kcal, was taken as the "best" value.

The heat of vaporization of IF_5 (liq) at 10° C is 10.12 kcal [1]; correction to 25° C makes this 9.85 kcal. When added to the value for the liquid this gives

$$1/2\ I_2\ (g)+5/2\ F_2\ (g)=IF_5\ (g)$$

$$\Delta H^\circ_{298.16}=-202.6\pm1.6\ \text{kcal.}$$

IF_7 (g). Bernstein and Katz [101] have measured the dissociation equilibrium of IF_7 (g) between 450° and 550° K. Their data give

$$IF_7\ (g)=IF_5\ (g)+F_2\ (g)$$

$$\Delta H_0^\circ=28.0\pm0.5\ \text{kcal}$$

$$\Delta H^\circ_{298.16}=29.1\pm0.5\ \text{kcal.}$$

Combining this with $\Delta Hf^\circ_{298.16}$ IF_5 (g) gives

$$1/2\ I_2\ (g)+7/2\ F_2\ (g)=IF_7\ (g)$$

$$\Delta H^\circ_{298.16}=-231.7\pm1.8\ \text{kcal.}$$

ICl (g). Brown and Gibson [102] obtained the dissociation limits of ICl going to both $I(^2P_{3/2})+Cl(^2P_{3/2})$ and $I(^2P_{3/2})+Cl(^2P_{1/2})$. Their data give D_0° (ICl) as 49.64 and 49.65 kcal, respectively; from these ΔHf_0° ICl (g) is −3.33 and −3.34 kcal. McMorris and Yost [103] measured the dissociation equilibrium of ICl (g); their data give ΔHf_0° ICl (g) $=-3.32$ kcal. The average was taken as the "best" value:

$$1/2\ I_2\ (g)+1/2\ Cl_2\ (g)=ICl\ (g)$$

$$\Delta H_0^\circ=-3.33\pm0.05\ \text{kcal.}$$

IBr (*g*). McMorris and Yost [104] measured the dissociation equilibrium of IBr (g); their data give $\Delta Hf_0^\circ = -1.42$ kcal. Brown [105] obtained the dissociation limits of IBr going to $I(^2P_{3/2})+Br(^2P_{1/2})$ and to $I(^2P_{3/2})+Br(^2P_{3/2})$; both limits give D_0° (IBr) = 41.91 kcal and ΔHf_0° IBr (g) $= -1.41$ kcal.

$$1/2\ I_2\ (g)+1/2\ Br_2\ (g)=IBr\ (g)$$

$$\Delta H_0^\circ = -1.41 \pm 0.06 \text{ kcal.}$$

Bodenstein and Schmidt [126] obtained ΔHf_0° IBr (g) $= -1.48$ kcal from gas-density measurements at 1,495° K; Müller [127] calculated −1.73 kcal from his kinetic studies. The agreement between the equilibrium data and the spectroscopic dissociation limits, in which the lighter atom is in the excited state in the normal dissociation process, furnishes additional support for the selection of the dissociation products assumed for ClF, BrF, and IF.

5. Discussion

The thermodynamic functions calculated, as outlined in section 3, are given in tables 7 to 27. The uncertainties in the functions are estimated to be not more than about 20 in the last figure given; the heat contents, $H^\circ - H_0^\circ$, however, as quantities derived directly from the heat-content functions, may retain one additional significant figure.

Tables 7 to 27 also include values of the heat of formation, ΔHf°, free energy of formation, ΔFf°, and logarithm of the equilibrium constant of formation, log Kf, as a function of temperature. These were calculated from the relations

$$\Delta Hf^\circ = \Delta Hf_0^\circ + \Delta(H^\circ - H_0^\circ)$$

$$\Delta Ff^\circ = \Delta Hf_0^\circ + T\Delta[(F^\circ - H_0^\circ)/T]$$

$$\log_{10} Kf = -\Delta Ff^\circ / 4.57567\,T.$$

The values of ΔHf_0° used were those selected in section 4; where $\Delta H_{298.16}^\circ$ has been selected, this was corrected to ΔHf_0° for the calculations. The values of ΔHf° and ΔFf° are often given to more significant figures than the basic value at 0° K or 298.16° K to retain differences that are more precise than the basic value. As a derived quantity, log Kf is given to one more decimal place than is ΔFf°.

Cole, Farber, and Elverum [106], Murphy and Vance [107], and Butkov and Rozenbaum [108] have calculated the thermodynamic functions for F (g); our calculations agree closely with those of Cole, Farber, and Elverum, and of Murphy and Vance, when allowance is made for the different values used for the fundamental constants. They have also calculated the thermodynamic functions for F_2 (g). Because of different choices for molecular and fundamental constants, none of these calculations agrees exactly with the present one. Recently Hu, White, and Johnston [109] have calculated the entropy of F_2 (g) at 85.02° K from low-temperature heat-capacity data and heats of transition, fusion, and vaporization; their value, 39.58 ± 0.16 cal/deg mole, agrees very closely with one calculated from the data used in the present calculation, 39.57 ± 0.03 cal/deg mole.

Potter [110] has calculated thermodynamic functions for F_2O (g), using a different frequency assignment. His values differ from ours and have a different temperature dependence.

Giauque and Overstreet [111] have calculated the free-energy function for Cl (g), using fundamental constants from the International Critical Tables; when revised to the constants used in this paper their values agree with ours. Giauque and Overstreet also calculated the free-energy functions for Cl_2 (g) by a semidirect summation method. Their values, as corrected to new constants [113] by Sherman and Giauque [112], agree with the present results. Giauque and Powell [114] calculated the entropy of Cl_2 (g) from low-temperature calorimetric data to be 51.56 ± 0.10 cal/deg mole at 239.05° K; the present calculations give 51.54 ± 0.03 cal/deg mole.

Thermodynamic functions for ClF (g) were calculated by Schäfer and Wicke [46], using the rigid rotator-harmonic oscillator approximation, and by Potter [110] (revised by Cole and Elverum [115] for new fundamental constants). When converted to the same fundamental constants used here, the latter calculations agree with the present ones.

Previous calculations of the thermodynamic functions for ClF_3 (g) by Schäfer and Wicke [46] and Scheer [116] were based upon structural parameters and frequency assignments for the incorrect pyramidal structures.

Grisard, Bernhardt, and Oliver [117] measured the heat capacity of solid and liquid ClF_3 from 14° to 278° K and the vapor pressure of the liquid from 226° to 303° K. The calculation of the entropy of the gas from these data is complicated by the presence of the dimer $(ClF_3)_2$ in the vapor. The data of Schmitz and Schumacher [123] on the monomer-dimer equilibrium were used to obtain the partial pressure of the monomer for each reported total pressure. From a log P—$1/T$ plot of these partial pressures the normal boiling point of monomeric ClF_3 was obtained as 285.74° K. Calculation of the heat of vaporization from the vapor pressure data by use of the Clapeyron equation requires the molar volumes of the gas and liquid. The volume of the gas was obtained from the Berthelot equation of state, using the critical constants estimated by Grisard, Bernhardt, and Oliver. The liquid volume was taken from the data of Banks and Rudge [124]. With dP/dT obtained from the slope of the monomer vapor-pressure curve, these data gave 6,490 cal/mole for the heat of vaporization of ClF_3 at its boiling point and an entropy of vaporization of 22.71 cal/deg mole.

The entropy of liquid ClF_3, 43.74 cal/deg mole, was obtained by correcting the value given by Grisard, Bernhardt, and Oliver at 284.91° K to the boiling point 285.74° K. The entrophy change in going from the real to the ideal gas was calculated

from the Berthelot equation to be 0.11 cal/deg mole.

The entropy of ClF_3 as an ideal gas at 285.74° K and 1 atm calculated from these data is 66.56 cal/deg mole. The value calculated statistically is 67.38 cal/deg mole. The reason for the difference is not known at present. The vibrational frequency assignment used is not certain and may be in error; however, it seems to be consistent with all the available spectroscopic data. (cf. Weber and Ferigle [118].) On the other hand, Burbank and Bensey [125] have obtained some evidence that there is a random arrangement within the crystal that would lead to a residual entropy in the solid at 0° K.

Gordon and Barnes [119] and Zeise [120] have calculated the functions for Br_2 (g). The more precise calculations of Gordon and Barnes, when converted to the new fundamental constants, agree with the present ones within 0.005 cal/deg mole.

The thermodynamic functions for BrF (g) and BrCl (g) have been calculated by Cole and Elverum [115]. Different choices of molecular constants, based in part upon more recent data, lead to small differences between the present calculations and theirs.

Stephenson and Jones [48] have calculated the functions for BrF_5 (g); as they assumed different molecular dimensions, their values of $-(F°-H_0°)/T$ and $S°$ should differ from the present ones by a constant amount; this is nearly true. Their value for the free-energy function at 1,000° K is in error.

Murphy [121] and Zeise [122] have calculated free-energy functions for I (g); Murphy's values, corrected to the new constants, agree with the present ones. They have also calculated the free-energy function for I_2 (g); again, Murphy's calculations agree.

Cole and Elverum [115] have calculated the functions for IF (g). Their tabulated values of $-(F°-H_0°)/T$ are seriously in error for some reason; their other functions are in good agreement with the present ones.

Cole and Elverum also calculated the functions for ICl (g) and IBr (g); Zeise [120] has calculated free-energy functions for IBr (g). The calculations, corrected for constants, of Cole and Elverum agree with ours.

Gaydon has recently [128] revised many of his previous selections [63] of the values of gaseous diatomic dissociation energies. These values differ in part from those selected here. Because of a different choice of decomposition products, the values of $D_0°$ that Gaydon selects for ClF, BrF, and IF differ from ours; this is discussed under the individual compounds. The other difference is for BrCl; in this case Gaydon does not give details sufficient to locate the source of the discrepancy.

TABLE 7. *Thermodynamic properties of* F (g)

T	$(F°-H_0°)/T$	$(H°-H_0°)/T$	$S°$	$H°-H_0°$	$C_p°$	$\Delta Hf°$	$\Delta Ff°$	log Kf
°K	cal/deg mole	cal/deg mole	cal/deg mole	cal/mole	cal/deg mole	kcal/mole	kcal/mole	
0	0	0	0	0	0	18.4	18.4	
250	−31.7750	5.1834	36.9584	1295.8	5.4454	18.819	15.472	−13.5257
273.16	−32.2352	5.2057	37.4409	1422.0	5.4452	18.861	15.161	−12.1238
298.16	−32.6919	5.2254	37.9173	1558.0	5.4365	18.903	14.820	−10.8631
300	−32.7241	5.2267	37.9508	1568.0	5.4355	18.906	14.794	−10.7779
400	−34.2348	5.2703	39.5051	2108.1	5.3612	19.06	13.40	−7.322
500	−35.4123	5.2804	40.6927	2640.2	5.2819	19.19	11.97	−5.232
600	−36.3747	5.2751	41.6498	3165.1	5.2180	19.30	10.51	−3.830
700	−37.1871	5.2633	42.4504	3684.3	5.1692	19.40	9.04	−2.823
800	−37.8889	5.2491	43.1380	4199.3	5.1324	19.48	7.56	−2.065
900	−38.5063	5.2345	43.7408	4711.0	5.1043	19.55	6.06	−1.472
1,000	−39.0571	5.2204	44.2775	5220.4	5.0826	19.62	4.56	−0.997
1,100	−39.5540	5.2070	44.7610	5727.7	5.0655	19.69	3.05	−.606
1,200	−40.0065	5.1946	45.2011	6233.5	5.0519	19.75	1.53	−.280
1,300	−40.4218	5.1832	45.6050	6738.2	5.0409	19.80	0.01	−.002
1,400	−40.8056	5.1727	45.9783	7241.8	5.0319	19.86	−1.51	.235
1,500	−41.1622	5.1631	46.3253	7744.6	5.0244	19.91	−3.04	.442
1,600	−41.4951	5.1542	46.6493	8246.7	5.0182	19.96	−4.57	.624
1,700	−41.8073	5.1460	46.9533	8748.2	5.0129	20.00	−6.10	.784
1,800	−42.1012	5.1385	47.2397	9249.3	5.0084	20.05	−7.64	.927
1,900	−42.3788	5.1316	47.5104	9750.0	5.0045	20.09	−9.18	1.056
2,000	−42.6419	5.1252	47.7671	10250.4	5.0012	20.13	−10.72	1.171
2,100	−42.8918	5.1192	48.0110	10750.3	4.9983	20.17	−12.26	1.276
2,200	−43.1298	5.1136	48.2434	11249.9	4.9958	20.21	−13.81	1.372
2,300	−43.3571	5.1084	48.4655	11749.3	4.9936	20.25	−15.36	1.459
2,400	−43.5744	5.1036	48.6780	12248.6	4.9916	20.29	−16.91	1.539
2,500	−43.7826	5.0991	48.8817	12747.8	4.9898	20.32	−18.46	1.613
2,750	−44.2681	5.0890	49.3571	13994.8	4.9862	20.41	−22.34	1.775
3,000	−44.7105	5.0803	49.7908	15240.9	4.9834	20.49	−26.23	1.911
3,250	−45.1168	5.0728	50.1896	16486.6	4.9812	.....	.....	.....
3,500	−45.4925	5.0662	50.5587	17731.7	4.9794	.....	.....	.....
3,750	−45.8419	5.0604	50.9023	18976.5	4.9780	.....	.....	.....
4,000	−46.1683	5.0552	51.2235	20220.8	4.9768	.....	.....	.....
4,250	−46.4746	5.0505	51.5251	21464.6	4.9758	.....	.....	.....
4,500	−46.7632	5.0463	51.8095	22708.4	4.9750	.....	.....	.....
4,750	−47.0359	5.0426	52.0785	23952.4	4.9743	.....	.....	.....
5,000	−47.2945	5.0392	52.3337	25196.0	4.9737	.....	.....	.....

TABLE 8. *Thermodynamic properties of* F_2 (g)

T	$(F°-H_0^\circ)/T$	$(H°-H_0^\circ)/T$	$S°$	$H°-H_0^\circ$	C_p°	$\Delta Hf°$	$\Delta Ff°$	log Kf
°K	*cal/deg mole*	*cal/deg mole*	*cal/deg mole*	*cal/mole*	*cal/deg mole*	*kcal/mole*	*kcal/mole*	
0	0	0	0	0	0	0	0	----------
250	−40.129	7.017	47.146	1754.2	7.28	0	0	0
273.16	−40.755	7.033	47.788	1921.1	7.38	0	0	0
298.16	−41.371	7.076	48.447	2109.8	7.49	0	0	0
300	−41.415	7.078	48.493	2123.4	7.49	0	0	0
400	−43.472	7.233	50.705	2893.2	7.89	0	0	0
500	−45.103	7.396	52.499	3698.0	8.19	0	0	0
600	−46.464	7.547	54.011	4528.2	8.41	0	0	0
700	−47.639	7.682	55.321	5377.4	8.56	0	0	0
800	−48.672	7.800	56.472	6240.0	8.68	0	0	0
900	−49.598	7.903	57.501	7112.7	8.77	0	0	0
1,000	−50.435	7.992	58.427	7992.0	8.84	0	0	0
1,100	−51.200	8.074	59.274	8881.4	8.90	0	0	0
1,200	−51.905	8.144	60.049	9772.8	8.94	0	0	0
1,300	−52.559	8.207	60.766	10669.1	8.99	0	0	0
1,400	−53.171	8.265	61.436	11571.0	9.02	0	0	0
1,500	−53.744	8.316	62.060	12474.0	9.06	0	0	0
1,600	−54.280	8.362	62.642	13379.2	9.08	0	0	0
1,700	−54.789	8.406	63.195	14290.2	9.11	0	0	0
1,800	−55.272	8.446	63.718	15202.8	9.13	0	0	0
1,900	−55.729	8.483	64.212	16117.7	9.15	0	0	0
2,000	−56.164	8.517	64.681	17034.0	9.18	0	0	0
2,100	−56.581	8.549	65.130	17952.9	9.20	0	0	0
2,200	−56.979	8.579	65.558	18873.8	9.22	0	0	0
2,300	−57.390	8.607	65.967	19796.1	9.23	0	0	0
2,400	−57.728	8.634	66.362	20721.6	9.25	0	0	0
2,500	−58.082	8.658	66.740	21645.6	9.27	0	0	0
2,750	−58.908	8.715	67.623	23966.2	9.31	0	0	0
3,000	−59.669	8.767	68.436	26301.0	9.34	0	0	0

TABLE 9. *Thermodynamic properties of* F_2O (g)

T	$(F°-H_0^\circ)/T$	$(H°-H_0^\circ)/T$	$S°$	$H°-H_0^\circ$	C_p°	$\Delta Hf°$	$\Delta Ff°$	log Kf
°K	*cal/deg mole*	*cal/deg mole*	*cal/deg mole*	*cal/mole*	*cal/deg mole*	*kcal/mole*	*kcal/mole*	
0	0	0	0	0	0	8.14	8.14	----------
250	−48.73	8.48	57.21	2120	9.75	7.64	11.09	−9.698
273.16	−49.49	8.60	58.09	2349	10.05	7.62	11.41	−9.132
298.16	−50.25	8.74	58.99	2606	10.35	7.6	11.8	−8.65
300	−50.30	8.75	59.05	2625	10.38	7.60	11.79	−8.589
400	−52.89	9.29	62.18	3716	11.38	7.57	13.20	−7.209
500	−55.02	9.78	64.80	4890	12.06	7.57	14.60	−6.382
600	−55.84	10.20	66.04	6120	12.53	7.59	16.00	−5.830
700	−58.44	10.56	69.00	7392	12.84	7.63	17.40	−5.434
800	−59.87	10.86	70.73	8688	13.07	7.66	18.80	−5.136
900	−61.16	11.11	72.27	9999	13.23	7.69	20.19	−4.904
1,000	−62.35	11.33	73.68	11330	13.35	7.73	21.57	−4.715
1,100	−63.44	11.52	74.96	12672	13.44	7.76	22.95	−4.560
1,200	−64.44	11.68	76.12	14016	13.51	7.79	24.34	−4.432
1,300	−65.38	11.82	77.20	15366	13.57	7.82	25.72	−4.325
1,400	−66.27	11.95	78.22	16730	13.61	7.85	27.09	−4.230
1,500	−67.09	12.06	79.15	18090	13.65	7.87	28.47	−4.149

TABLE 10. *Thermodynamic properties of* Cl (g)

T	$(F°-H_0^\circ)/T$	$(H°-H_0^\circ)/T$	$S°$	$H°-H_0^\circ$	C_p°	$\Delta Hf°$	$\Delta Ff°$	log Kf
°K	cal/deg mole	cal/deg mole	cal/deg mole	cal/mole	cal/deg mole	kcal/mole	kcal/mole	
0	0	0	0	0	0	28.54	28.54	.....
250	−33.5460	4.9986	38.5456	1249.9	5.1275	28.886	25.735	−22.4968
273.16	−33.9984	5.0123	39.0107	1369.2	5.1946	28.913	25.439	−20.3531
298.16	−34.4291	5.0278	39.4569	1499.1	5.2203	28.942	25.122	−18.4144
300	−34.4600	5.0290	39.4890	1508.7	5.2237	28.943	25.099	−18.2843
400	−35.9161	5.0977	41.0138	2039.1	5.3705	29.06	23.80	−13.003
500	−37.0605	5.1601	42.2206	2580.0	5.4363	29.17	22.47	−9.822
600	−38.0058	5.2074	43.2132	3124.4	5.4448	29.28	21.12	−7.693
700	−38.8111	5.2400	44.0511	3668.0	5.4232	29.39	19.75	−6.166
800	−39.5123	5.2608	44.7731	4208.6	5.3887	29.49	18.37	−5.018
900	−40.1327	5.2729	45.4056	4745.6	5.3506	29.58	16.97	−4.121
1,000	−40.6886	5.2788	45.9674	5278.8	5.3133	29.66	15.57	−3.402
1,100	−41.1918	5.2804	46.4722	5808.4	5.2788	29.74	14.15	−2.812
1,200	−41.6512	5.2789	46.9301	6334.7	5.2477	29.82	12.73	−2.319
1,300	−42.0736	5.2754	47.3490	6858.0	5.2201	29.89	11.31	−1.901
1,400	−42.4644	5.2706	47.7350	7378.8	5.1958	29.96	9.88	−1.542
1,500	−42.8278	5.2649	48.0927	7897.4	5.1745	30.02	8.44	−1.229
1,600	−43.1674	5.2586	48.4230	8413.8	5.1557	30.09	7.00	−0.956
1,700	−43.4860	5.2521	48.7381	8928.6	5.1392	30.15	5.55	−.713
1,800	−43.7860	5.2454	49.0314	9441.7	5.1246	30.21	4.10	−.498
1,900	−44.0695	5.2387	49.3082	9953.5	5.1117	30.26	2.65	−.304
2,000	−44.3380	5.2320	49.5700	10464.0	5.1002	30.31	1.20	−.131
2,100	−44.5931	5.2255	49.8186	10973.6	5.0900	30.37	−0.25	.027
2,200	−44.8361	5.2192	50.0553	11482.2	5.0809	30.42	−1.87	.186
2,300	−45.0679	5.2130	50.2809	11989.9	5.0727	30.46	−3.18	.302
2,400	−45.2896	5.2070	50.4966	12496.8	5.0654	30.51	−4.65	.423
2,500	−45.5021	5.2012	50.7033	13003.0	5.0588	30.56	−6.12	.535
2,750	−45.9972	5.1876	51.1848	14265.9	5.0449	30.67	−9.86	.783
3,000	−46.4480	5.1752	51.6232	15525.6	5.0339	30.76	−13.47	.981
3,250	−46.8618	5.1640	52.0258	16783.0	5.0251	.....	.....	.....
3,500	−47.2441	5.1538	52.3979	18038.3	5.0179	.....	.....	.....
3,750	−47.5994	5.1445	52.7439	19291.9	5.0120	.....	.....	.....
4,000	−47.9311	5.1361	53.0672	20544.4	5.0070	.....	.....	.....
4,250	−48.2422	5.1284	53.3706	21795.7	5.0028	.....	.....	.....
4,500	−48.5352	5.1213	53.6565	23045.8	4.9993	.....	.....	.....
4,750	−48.8119	5.1148	53.9267	24295.3	4.9964	.....	.....	.....
5,000	−49.0744	5.1088	54.1832	25544.0	4.9941	.....	.....	.....

TABLE 11. *Thermodynamic properties of* Cl_2 (g)

T	$(F°-H_0^\circ)/T$	$(H°-H_0^\circ)/T$	$S°$	$H°-H_0^\circ$	C_p°	$\Delta Hf°$	$\Delta Ff°$	log Kf
°K	cal/deg mole	cal/deg mole	cal/deg mole	cal/mole	cal/deg mole	kcal/mole	kcal/mole	
0	0	0	0	0	0	0	0	.....
250	−44.649	7.233	51.882	1808.2	7.88	0	0	0
273.16	−45.292	7.293	52.585	1992.2	8.00	0	0	0
298.16	−45.934	7.357	53.291	2193.6	8.11	0	0	0
300	−45.979	7.362	53.341	2208.6	8.12	0	0	0
400	−48.130	7.595	55.725	3038.0	8.44	0	0	0
500	−49.847	7.783	57.630	3891.5	8.62	0	0	0
600	−51.278	7.935	59.213	4761.0	8.74	0	0	0
700	−52.511	8.057	60.568	5639.9	8.82	0	0	0
800	−53.594	8.156	61.750	6524.8	8.88	0	0	0
900	−54.560	8.238	62.798	7414.2	8.92	0	0	0
1,000	−55.432	8.309	63.741	8309.0	8.96	0	0	0
1,100	−56.226	8.370	64.596	9207.0	8.99	0	0	0
1,200	−56.956	8.423	65.379	10107.6	9.02	0	0	0
1,300	−57.633	8.469	66.102	11009.7	9.04	0	0	0
1,400	−58.263	8.510	66.773	11914.0	9.06	0	0	0
1,500	−58.851	8.548	67.399	12822.0	9.08	0	0	0
1,600	−59.404	8.581	67.985	13729.6	9.10	0	0	0
1,700	−59.925	8.611	68.536	14638.7	9.11	0	0	0
1,800	−60.418	8.640	69.058	15552.0	9.13	0	0	0
1,900	−60.885	8.665	69.550	16463.5	9.14	0	0	0
2,000	−61.331	8.690	70.021	17380.0	9.16	0	0	0
2,100	−61.756	8.712	70.468	18295.2	9.17	0	0	0
2,200	−62.162	8.734	70.896	19214.8	9.19	0	0	0
2,300	−62.550	8.754	71.304	20134.2	9.20	0	0	0
2,400	−62.923	8.773	71.696	21055.2	9.22	0	0	0
2,500	−63.281	8.791	72.072	21977.5	9.23	0	0	0
2,750	−64.069	8.824	72.893	24266.0	9.26	0	0	0
3,000	−64.891	8.870	73.761	26610.0	9.30	0	0	0

TABLE 12. *Thermodynamic properties of* ClO_2 (g)

T	$(F°-H°_0)/T$	$(H°-H°_0)/T$	$S°$	$H°-H°_0$	$C°_p$	$\Delta Hf°$	$\Delta Ff°$	log Kf
°K	*cal/deg mole*	*cal/deg mole*	*cal/deg mole*	*cal/mole*	*cal/deg mole*	*kcal/mole*	*kcal/mole*	
0	0	0	0	0	0	25.590	25.590	
250	−49.910	8.431	58.341	2107.8	9.50	25.061	28.902	−25.2660
273.16	−50.661	8.531	59.192	2330.3	9.74	25.025	29.258	−23.4088
298.16	−51.413	8.642	60.055	2576.7	10.00	25.0	29.6	−21.73
300	−51.467	8.651	60.118	2595.3	10.02	24.998	29.678	−21.6204
400	−54.019	9.115	63.134	3646.0	10.96	24.92	31.25	−17.076
500	−56.101	9.561	65.662	4780.5	11.69	24.90	32.84	−14.354
600	−57.881	9.963	67.844	5977.8	12.22	24.91	34.42	−12.539
700	−59.444	10.316	69.760	7221.2	12.61	24.93	36.01	−11.242
800	−60.841	10.622	71.463	8497.6	12.90	24.97	37.59	−10.269
900	−62.108	10.888	72.996	9799.2	13.12	25.01	39.16	−9.510
1,000	−63.268	11.120	74.388	11120.0	13.29	25.06	40.74	−8.902
1,100	−64.338	11.323	75.661	12455.3	13.42	25.11	42.30	−8.404
1,200	−65.331	11.502	76.833	13802.4	13.53	25.16	43.86	−7.988
1,300	−66.258	11.661	77.919	15159.3	13.61	25.20	45.42	−7.635
1,400	−67.127	11.804	78.931	16525.6	13.68	25.25	46.97	−7.332
1,500	−67.946	11.932	79.878	17898.0	13.74	25.30	48.52	−7.070

TABLE 13. *Thermodynamic properties of* Cl_2O (g)

T	$(F°-H°_0)/T$	$(H°-H°_0)/T$	$S°$	$H°-H°_0$	$C°_p$	$\Delta Hf°$	$\Delta Ff°$	log Kf
°K	*cal/deg mole*	*cal/deg mole*	*cal/deg mole*	*cal/mole*	*cal/deg mole*	*kcal/mole*	*kcal/mole*	
0	0	0	0	0	0	18.61	18.61	
250	−52.94	8.84	61.78	2210	10.3	18.15	21.64	−18.919
273.16	−53.73	8.97	62.70	2450	10.6	18.12	21.97	−17.574
298.16	−54.52	9.12	63.64	2719	10.9	18.1	22.3	−16.36
300	−54.59	9.13	63.72	2739	10.9	18.10	22.34	−16.276
400	−57.28	9.68	66.96	3872	11.7	18.05	23.77	−12.989
500	−59.49	10.16	69.65	5080	12.3	18.04	25.21	−11.018
600	−61.38	10.55	71.93	6330	12.7	18.04	26.64	−9.704
700	−63.03	0.88	73.91	7616	13.0	18.06	28.07	−8.764
800	−64.50	11.16	75.66	8928	13.2	18.09	29.50	−8.060
900	−65.83	11.39	77.22	10251	13.3	18.11	30.93	−7.510
1,000	−67.04	11.59	78.63	11590	13.4	18.14	32.35	−7.070
1,100	−68.16	11.76	79.92	12936	13.5	18.17	33.76	−6.707
1,200	−69.19	11.91	81.10	14292	13.6	18.20	35.18	−6.406
1,300	−70.14	12.04	82.18	15652	13.6	18.23	36.60	−6.153
1,400	−71.04	12.16	83.20	17024	13.7	18.27	38.01	−5.934
1,500	−71.91	12.27	84.18	18405	13.7	18.31	39.39	−5.737

TABLE 14. *Thermodynamic properties of* ClF (g)

T	$(F°-H°_0)/T$	$(H°-H°_0)/T$	$S°$	$H°-H°_0$	$C°_p$	$\Delta Hf°$	$\Delta Ff°$	log Kf
°K	*cal/deg mole*	*cal/deg mole*	*cal/deg mole*	*cal/mole*	*cal/deg mole*	*kcal/mole*	*kcal/mole*	
0	0	0	0	0	0	−13.4	−13.4	
250	−43.672	7.060	50.732	1,765.0	7.44	−13.416	−13.721	11.9945
273.16	−44.300	7.098	51.398	1,938.9	7.55	−13.418	−13.749	11.0000
298.16	−44.922	7.140	52.062	2,128.9	7.67	−13.423	−13.779	10.0095
300	−44.966	7.144	52.110	2,143.2	7.68	−13.423	−13.781	10.0391
400	−47.047	7.329	54.376	2,931.6	8.07	−13.43	−13.90	7.594
500	−48.702	7.506	56.208	3,753.0	8.33	−13.44	−14.01	6.126
600	−50.085	7.659	57.744	4,595.4	8.51	−13.45	−14.13	5.146
700	−51.275	7.790	59.065	5,453.0	8.64	−13.46	−14.24	4.446
800	−52.323	7.902	60.225	6,321.6	8.73	−13.46	−14.35	3.921
900	−53.260	7.997	61.257	7,197.3	8.80	−13.47	−14.46	3.512
1,000	−54.107	8.080	62.187	8,080.0	8.85	−13.47	−14.57	3.185
1,100	−54.880	8.153	63.033	8,968.3	8.89	−13.48	−14.68	2.917
1,200	−55.592	8.216	63.808	9,859.2	8.93	−13.48	−14.79	2.694
1,300	−56.252	8.271	64.523	10,752.3	8.96	−13.49	−14.90	2.505
1,400	−56.867	8.320	65.187	11,648.0	8.98	−13.49	−15.01	2.343
1,500	−57.442	8.366	65.808	12,549.0	9.00	−13.50	−15.12	2.203

TABLE 15. *Thermodynamic properties of* ClF_3 (g)

T	$(F°-H°_0)/T$	$(H°-H°_0)/T$	$S°$	$H°-H°_0$	$C°_p$	$\Delta Hf°$	$\Delta Ff°$	log Kf
°K	*cal/deg mole*	*cal/deg mole*	*cal/deg mole*	*cal/mole*	*cal/deg mole*	*kcal/mole*	*kcal/mole*	
0	0	0	0	0	0	−37.9	−37.9	
250	−54.81	10.59	65.40	2,647.5	14.48	−38.79	−30.97	27.076
273.16	−55.76	10.94	66.70	2,988.4	15.03	−38.79	−30.24	24.193
298.16	−56.73	11.31	68.04	3,372.2	15.55	−38.79	−29.46	21.597
300	−56.80	11.33	68.13	3,399.0	15.58	−38.79	−29.41	21.422
400	−60.24	12.59	72.83	5,036	17.05	−38.72	−25.29	14.363
500	−63.16	13.58	76.74	6,790	17.92	−38.60	−23.19	10.138
600	−65.71	14.35	80.06	8,610	18.45	−38.46	−20.13	7.340
700	−67.97	14.96	82.93	10,472	18.80	−38.31	−17.09	5.332
800	−70.00	15.45	85.45	12,360	19.03	−38.16	−14.06	3.840
900	−71.84	15.86	87.70	14,274	19.20	−38.00	−11.05	2.682
1,000	−73.52	16.20	89.72	16,200	19.32	−37.84	−8.05	1.176
1,100	−75.08	16.49	91.57	18,139	19.41	−37.69	−5.08	1.010
1,200	−76.54	16.74	93.28	20,088	19.48	−37.53	−2.14	0.391
1,300	−77.90	16.95	94.85	22,035	19.54	−37.37	0.78	−.132
1,400	−79.16	17.13	96.29	23,982	19.59	−37.22	3.71	−.581
1,500	−80.34	17.30	97.64	25,950	19.63	−37.07	6.65	−.969

TABLE 16. *Thermodynamic properties of* Br (g)

T	$(F°-H°_0)/T$	$(H°-H°_0)/T$	$S°$	$H°-H°_0$	$C°_p$	$\Delta tHf°$	$\Delta Ff°$	log Kf
°K	*cal/deg mole*	*cal/deg mole*	*cal/deg mole*	*cal/mole*	*cal/deg mole*	*kcal/mole*	*kcal/mole*	
0	0	0	0	0	0	22.73	22.73	
250	−35.9621	4.9680	40.9300	1,242.0	4.9680	23.016	19.926	−17.4189
273.16	−36.4022	4.9680	41.3702	1,357.1	4.9680	23.032	19.639	−15.7125
298.16	−36.8372	4.9680	41.8052	1,481.3	4.9680	23.049	19.327	−14.1669
300	−36.8678	4.9680	41.8358	1,490.4	4.9680	23.050	19.305	−14.0633
400	−38.2970	4.9680	43.2650	1,987.2	4.9683	23.11	18.05	−9.850
500	−39.4057	4.9682	44.3739	2,484.1	4.9708	23.17	16.77	−7.332
600	−40.3115	4.9693	45.2808	2,981.6	4.9793	23.22	15.49	−5.642
700	−41.0776	4.9718	46.0494	3,480.3	4.9973	23.27	14.20	−4.432
800	−41.7418	4.9767	46.7185	3,981.4	5.0257	23.33	12.90	−3.523
900	−42.3285	4.9841	47.3126	4,485.7	5.0631	23.38	11.59	−2.814
1,000	−42.8541	4.9942	47.8483	4,994.2	5.1065	23.44	10.28	−2.246
1,100	−43.3306	5.0065	48.3371	5,507.2	5.1528	23.50	8.96	−1.780
1,200	−43.7669	5.0206	48.7875	6,024.7	5.1991	23.57	7.63	−1.390
1,300	−44.1693	5.0361	49.2054	6,546.9	5.2433	23.64	6.30	−1.060
1,400	−44.5431	5.0523	49.5954	7,073.2	5.2838	23.71	4.97	−0.975
1,500	−44.8922	5.0690	49.9612	7,603.5	5.3198	23.79	3.62	−.528
1,600	−45.2210	5.0857	50.3057	8,137.1	5.3509	23.87	2.28	−.311
1,700	−45.5298	5.1021	50.6309	8,673.6	5.3770	23.95	0.92	−.119
1,800	−45.8218	5.1180	50.9388	9,212.4	5.3983	24.03	−.43	.052
1,900	−46.0979	5.1332	51.2311	9,753.1	5.4151	24.12	−1.79	.206
2,000	−46.3616	5.1476	51.5092	10,295.2	5.4279	24.20	−3.16	.345
2,100	−46.6131	5.1612	51.7743	10,838.5	5.4369	24.29	−4.53	.471
2,200	−46.8535	5.1739	52.0274	11,382.6	5.4427	24.37	−5.90	.586
2,300	−47.0838	5.1856	52.2694	11,925.9	5.4457	24.46	−7.28	.692
2,400	−47.3047	5.1965	52.5012	12,471.6	5.4464	24.54	−8.66	.789
2,500	−47.5170	5.2065	52.7235	13,016.3	5.4451	24.63	−10.05	.878
2,750	−48.0143	5.2277	53.2420	14,376.2	5.4348	24.84	−13.52	1.075
3,000	−48.4689	5.2443	53.7132	15,732.9	5.4178	25.04	−17.02	1.240
3,250	−48.8802	5.2569	54.1471	17,084.9	5.3972	.....	.....	.....
3,500	−49.2801	5.2661	54.5462	18,431.4	5.3748	.....	.....	.....
3,750	−49.6437	5.2726	54.9163	19,772.3	5.3519	.....	.....	.....
4,000	−49.9841	5.2769	55.2610	21,107.6	5.3293	.....	.....	.....
4,250	−50.3041	5.2793	55.5834	22,437.0	5.3075	.....	.....	.....
4,500	−50.6059	5.2803	55.8862	23,761.4	5.2868	.....	.....	.....
4,750	−50.8914	5.2801	56.1715	25,080.5	5.2673	.....	.....	.....
5,000	−51.1622	5.2790	56.4412	26,395.0	5.2490	.....	.....	.....

TABLE 17. *Thermodynamic properties of* Br_2 (g)

T	$(F°-H°_0)/T$	$(H°-H°_0)/T$	$S°$	$H°-H°_0$	$C°_p$	$\Delta Hf°$	$\Delta Ff°$	log Kf
°K	*cal/deg mole*	*cal/deg mole*	*cal/deg mole*	*cal/mole*	*cal/deg mole*	*kcal/mole*	*kcal/mole*	
0	0	0	0	0	0	0	0	
250	−49.491	7.650	57.141	1,912.5	8.48	0	0	0
273.16	−50.172	7.724	57.896	2,109.9	8.55	0	0	0
298.16	−50.851	7.796	58.647	2,324.5	8.62	0	0	0
300	−50.899	7.801	58.700	2,340.3	8.62	0	0	0
400	−53.176	8.028	61.204	3,211.2	8.78	0	0	0
500	−54.986	8.186	63.172	4,093.0	8.86	0	0	0
600	−56.489	8.303	64.792	4,981.8	8.91	0	0	0
700	−57.776	8.392	66.168	5,874.4	8.94	0	0	0
800	−58.901	8.462	67.363	6,769.6	8.97	0	0	0
900	−59.901	8.520	68.421	7,668.0	8.99	0	0	0
1,000	−60.801	8.568	69.369	8,568.0	9.01	0	0	0
1,100	−61.620	8.609	70.229	9,469.9	9.03	0	0	0
1,200	−62.371	8.644	71.015	10,372.8	9.04	0	0	0
1,300	−63.064	8.676	71.740	11,278.8	9.06	0	0	0
1,400	−63.708	8.703	72.411	12,184.2	9.07	0	0	0
1,500	−64.309	8.728	73.037	13,092.0	9.08	0	0	0
1,600	−64.873	8.750	73.623	14,000.0	9.09	0	0	0
1,700	−65.404	8.770	74.174	14,909.0	9.11	0	0	0
1,800	−65.906	8.790	74.696	15,822.0	9.12	0	0	0
1,900	−66.382	8.807	75.189	16,733.3	9.13	0	0	0
2,000	−66.834	8.824	75.658	17,648.0	9.14	0	0	0
2,100	−67.265	8.839	76.104	18,561.9	9.15	0	0	0
2,200	−67.677	8.853	76.530	19,476.6	9.16	0	0	0
2,300	−68.071	8.867	76.938	20,394.1	9.17	0	0	0
2,400	−68.448	8.880	77.328	21,312.0	9.18	0	0	0
2,500	−68.811	8.892	77.703	22,230.0	9.20	0	0	0
2,750	−69.662	8.921	78.583	24,532.8	9.22	0	0	0
3,000	−70.436	8.947	79.383	26,841.0	9.25	0	0	0

TABLE 18. *Thermodynamic properties of* BrF (g)

T	$(F°-H°_0)/T$	$(H°-H°_0)/T$	$S°$	$H°-H°_0$	$C°_p$	$\Delta Hf°$	$\Delta Ff°$	log Kf
°K	*cal/deg mole*	*cal/deg mole*	*cal/deg mole*	*cal/mole*	*cal/deg mole*	*kcal/mole*	*kcal/mole*	
0	0	0	0	0	0	−18.3	−18.3	
250	−46.206	7.128	53.334	1,782.0	7.63	−18.353	−18.649	16.3028
273.16	−46.839	7.176	54.015	1,960.2	7.76	−18.355	−18.676	14.9419
298.16	−47.470	7.230	54.700	2,155.7	7.88	−18.361	−18.705	13.7107
300	−47.514	7.234	54.748	2,170.2	7.88	−18.362	−18.707	13.6279
400	−49.625	7.446	57.071	2,978.4	8.25	−18.37	−18.82	10.283
500	−51.307	7.633	58.940	3,816.5	8.49	−18.38	−18.93	8.275
600	−52.713	7.789	60.502	4,673.4	8.64	−18.38	−19.04	6.936
700	−53.924	7.918	61.842	5,542.6	8.74	−18.38	−19.15	5.980
800	−54.989	8.027	63.016	6,421.6	8.82	−18.38	−19.26	5.262
900	−55.940	8.118	64.058	7,306.2	8.88	−18.38	−19.37	4.704
1,000	−56.700	8.196	64.995	8,196.0	8.92	−18.38	−19.48	4.258
1,100	−57.584	8.264	65.848	9,090.4	8.96	−18.39	−19.59	3.892
1,200	−58.305	8.323	66.628	9,987.6	8.99	−18.39	−19.70	3.588
1,300	−58.974	8.376	67.350	10,888.8	9.02	−18.39	−19.81	3.330
1,400	−59.596	8.423	68.019	11,792.2	9.04	−18.39	−19.92	3.109
1,500	−60.178	8.465	68.643	12,697.5	9.07	−18.39	−20.03	2.918

TABLE 19. *Thermodynamic properties of* BrF_5(g)

T	$(F°-H°_0)/T$	$(H°-H°_0)/T$	$S°$	$H°-H°_0$	$C°_p$	$\Delta Hf°$	$\Delta Ff°$	log Kf
°K	*cal/deg mole*	*cal/deg mole*	*cal/deg mole*	*cal/mole*	*cal/deg mole*	*kcal/mole*	*kcal/mole*	
0	0	0	0	0	0	−122	−122	
250	−58.93	13.48	72.41	3,370	21.78	−124.0	−105.5	92.20
273.16	−60.15	14.24	74.39	3,890	22.90	−124.0	−103.7	83.00
298.16	−61.43	15.01	76.44	4,475	23.93	−124.0	−101.9	74.69
300	−61.53	15.06	76.59	4,518	24.00	−124.0	−101.8	74.13
400	−66.23	17.68	83.91	7,072	26.82	−123.8	−94.4	51.57
500	−70.41	19.68	90.09	9,840	28.41	−123.5	−87.1	38.06
600	−74.14	21.22	95.36	12,732	29.36	−123.1	−79.8	29.08
700	−77.50	22.43	99.93	15,701	29.96	−122.7	−72.7	22.69
800	−80.56	23.40	103.96	18,720	30.37	−122.3	−65.5	17.91
900	−83.37	24.19	107.56	21,771	30.66	−121.8	−58.5	14.20
1,000	−85.95	24.85	110.80	24,850	30.87	−121.4	−51.5	11.25
1,100	−88.35	25.41	113.76	27,951	31.03	−121.0	−44.5	8.84
1,200	−90.58	25.88	116.46	31,056	31.15	−120.6	−37.6	6.84
1,300	−92.66	26.29	118.95	34,177	31.24	−120.1	−30.7	5.16
1,400	−94.62	26.64	121.26	37,296	31.31	−119.7	−23.8	3.71
1,500	−96.47	26.96	123.43	40,440	31.38	−119.3	−16.9	2.47

TABLE 20. *Thermodynamic properties of* BrCl (g)

T	$(F°-H°_0)/T$	$(H°-H°_0)/T$	$S°$	$H°-H°_0$	$C°_p$	$\Delta Hf°$	$\Delta Ff°$	log Kf
°K	*cal/deg mole*	*cal/deg mole*	*cal/deg mole*	*cal/mole*	*cal/deg mole*	*kcal/mole*	*kcal/mole*	
0	0	0	0	0	0	−0.20	−0.20	
250	−48.485	7.396	55.881	1849.0	8.17	−.213	−.554	0.4841
273.16	−49.144	7.466	56.610	2039.4	8.27	−.212	−.586	.4686
298.16	−49.800	7.538	57.338	2247.5	8.36	−.212	−.620	.4544
300	−49.847	7.543	57.390	2262.9	8.37	−.212	−.623	.4535
400	−52.051	7.783	59.834	3113.2	8.61	−.21	−.76	.415
500	−53.808	7.963	61.771	3981.5	8.74	−.21	−.90	.392
600	−55.272	8.100	63.372	4860.0	8.83	−.21	−1.03	.376
700	−56.528	8.208	64.736	5745.6	8.88	−.21	−1.17	.365
800	−57.631	8.295	65.926	6636.0	8.92	−.21	−1.31	.357
900	−58.613	8.366	66.979	7529.4	8.95	−.21	−1.44	.350
1,000	−59.498	8.426	67.924	8426.0	8.98	−.21	−1.58	.346
1,100	−60.303	8.477	68.780	9324.7	9.00	−.21	−1.72	.341
1,200	−61.043	8.521	69.564	10225.2	9.02	−.22	−1.86	.338
1,300	−61.726	8.560	70.286	11128.0	9.03	−.22	−1.99	.335
1,400	−62.362	8.594	70.956	12031.6	9.05	−.22	−2.13	.332
1,500	−62.956	8.625	71.581	12937.5	9.06	−.22	−2.26	.330

TABLE 21. *Thermodynamic properties of* I (g)

T	$(F°-H°_0)/T$	$(H°-H°_0)/T$	$S°$	$H°-H°_0$	$C°_p$	$\Delta Hf°$	$\Delta Ff°$	log Kf
°K	*cal/deg mole*	*cal/deg mole*	*cal/deg mole*	*cal/mole*	*cal/deg mole*	*kcal/mole*	*kcal/mole*	
0	0	0	0	0	0	17.77	17.77	----
250	−37.3406	4.9680	42.3086	1242.0	4.9680	18.015	15.030	−13.1386
273.16	−37.7808	4.9680	42.7488	1357.1	4.9680	18.030	14.752	−11.8029
298.16	−38.2158	4.9680	43.1838	1481.3	4.9680	18.042	14.452	−10.5932
300	−38.2464	4.9680	43.2144	1490.4	4.9680	18.043	14.430	−10.5119
400	−39.6756	4.9680	44.6436	1987.2	4.9680	18.10	13.22	−7.221
500	−40.7842	4.9680	45.7522	2484.0	4.9680	18.15	11.99	−5.241
600	−41.6899	4.9680	46.6579	2980.8	4.9680	18.20	10.76	−3.917
700	−42.4557	4.9680	47.4237	3477.6	4.9680	18.24	9.51	−2.969
800	−43.1191	4.9680	48.0871	3974.4	4.9682	18.29	8.26	−2.257
900	−43.7043	4.9681	48.6724	4471.3	4.9688	18.33	7.00	−1.700
1,000	−44.2277	4.9682	49.1959	4968.2	4.9700	18.38	5.74	−1.255
1,100	−44.7013	4.9685	49.6698	5465.4	4.9726	18.42	4.48	−0.889
1,200	−45.1336	4.9690	50.1026	5962.8	4.9770	18.47	3.21	−.584
1,300	−45.5313	4.9698	50.5011	6460.7	4.9836	18.51	1.93	−.325
1,400	−45.8997	4.9711	50.8708	6959.5	4.9925	18.55	0.66	−.103
1,500	−46.2427	4.9729	51.2156	7459.4	5.0039	18.60	−.62	.090
1,600	−46.5638	4.9753	51.5391	7960.5	5.0178	18.64	−1.90	.260
1,700	−46.8655	4.9783	51.8438	8463.1	5.0340	18.68	−3.19	.410
1,800	−47.1501	4.9818	52.1319	8967.2	5.0521	18.73	−4.48	.544
1,900	−47.4196	4.9860	52.4056	9473.4	5.0718	18.78	−5.77	.663
2,000	−47.6754	4.9908	52.6662	9981.6	5.0928	18.83	−7.06	.771
2,100	−47.9190	4.9962	52.9152	10492.0	5.1147	18.88	−8.36	.870
2,200	−48.1516	5.0021	53.1537	11004.6	5.1371	18.93	−9.66	.959
2,300	−48.3742	5.0085	53.3827	11519.6	5.1597	18.98	−10.96	1.041
2,400	−48.5874	5.0152	53.6026	12036.5	5.1822	19.03	−12.26	1.116
2,500	−48.7923	5.0224	53.8147	12556.0	5.2045	19.09	−13.56	1.185
2,750	−49.2719	5.0414	54.3133	13863.8	5.2571	19.23	−16.84	1.338
3,000	−49.7114	5.0613	54.7727	15183.9	5.3039	19.69	−20.12	1.466
3,250	−50.1173	5.0816	55.1989	16515.2	5.3437	.....	.....	.....
3,500	−50.4946	5.1015	55.5961	17855.2	5.3762	.....	.....	.....
3,750	−50.8473	5.1207	55.9680	19202.6	5.4016	.....	.....	.....
4,000	−51.1783	5.1389	56.3172	20555.6	5.4205	.....	.....	.....
4,250	−51.4904	5.1559	56.6463	21912.6	5.4337	.....	.....	.....
4,500	−51.7855	5.1716	56.9571	23272.2	5.4419	.....	.....	.....
4,750	−52.0655	5.1859	57.2514	24633.0	5.4458	.....	.....	.....
5,000	−52.3319	5.1989	57.5308	25994.5	5.4462	.....	.....	.....

TABLE 22. *Thermodynamic properties of* I_2 (g)

T	$(F°-H°_0)/T$	$(H°-H°_0)/T$	$S°$	$H°-H°_0$	$C°_p$	$\Delta Hf°$	$\Delta Ff°$	log Kf
°K	*cal/deg mole*	*cal/deg mole*	*cal/deg mole*	*cal/mole*	*cal/deg mole*	*kcal/mole*	*kcal/mole*	
0	0	0	0	0	0	0	0	.....
250	−52.757	7.980	60.737	1995.0	8.74	0	0	0
273.16	−53.467	8.032	61.499	2194.0	8.78	0	0	0
298.16	−54.175	8.109	62.284	2417.8	8.81	0	0	0
300	−54.225	8.114	62.339	2434.2	8.82	0	0	0
400	−56.586	8.301	64.887	3320.4	8.90	0	0	0
500	−58.453	8.426	66.879	4213.0	8.95	0	0	0
600	−59.998	8.516	68.514	5109.6	8.98	0	0	0
700	−61.316	8.584	69.900	6008.8	9.00	0	0	0
800	−62.465	8.638	71.103	6910.4	9.02	0	0	0
900	−63.485	8.682	72.167	7813.8	9.04	0	0	0
1,000	−64.402	8.719	73.121	8719.0	9.06	0	0	0
1,100	−65.234	8.750	73.984	9625.0	9.08	0	0	0
1,200	−65.986	8.778	74.774	10533.6	9.09	0	0	0
1,300	−66.700	8.803	75.503	11443.9	9.11	0	0	0
1,400	−67.354	8.825	76.179	12355.0	9.12	0	0	0
1,500	−67.964	8.845	76.809	13267.5	9.14	0	0	0
1,600	−68.535	8.864	77.399	14182.4	9.15	0	0	0
1,700	−69.074	8.881	77.955	15097.7	9.16	0	0	0
1,800	−69.581	8.897	78.478	16014.6	9.18	0	0	0
1,900	−70.063	8.912	78.975	16932.8	9.19	0	0	0
2,000	−70.520	8.927	79.447	17854.0	9.21	0	0	0
2,100	−70.956	8.940	79.896	18774.0	9.22	0	0	0
2,200	−71.372	8.953	80.325	19696.6	9.23	0	0	0
2,300	−71.770	8.966	80.736	20621.8	9.25	0	0	0
2,400	−72.152	8.978	81.130	21547.2	9.26	0	0	0
2,500	−72.519	8.989	81.508	22472.5	9.27	0	0	0
2,750	−73.377	9.017	82.394	24796.8	9.31	0	0	0
3,000	−74.162	9.041	83.203	27123.0	9.34	0	0	0

TABLE 23. *Thermodynamic properties of* IF (g)

T	$(F°-H°_0)/T$	$(H°-H°_0)/T$	$S°$	$H°-H°_0$	$C°_p$	$\Delta Hf°$	$\Delta Ff°$	log Kf
°K	*cal/deg mole*	*cal/deg mole*	*cal/deg mole*	*cal/mole*	*cal/deg mole*	*kcal/mole*	*kcal/mole*	
0	0	0	0	0	0	−30.0	−30.0	.....
250	−47.858	7.177	55.035	1794.2	7.76	−30.080	−30.354	26.5349
273.16	−48.496	7.234	55.730	1976.0	7.88	−30.082	−30.378	24.3047
298.16	−49.133	7.293	56.426	2174.5	8.00	−30.089	−30.405	22.2868
300	−49.177	7.297	56.474	2189.1	8.01	−30.090	−30.407	22.1514
400	−51.308	7.521	58.829	3008.4	8.35	−30.10	−30.51	16.670
500	−53.007	7.710	60.717	3855.0	8.56	−30.10	−30.61	13.381
600	−54.427	7.862	62.289	4717.2	8.69	−30.10	−30.72	11.189
700	−55.648	7.987	63.635	5590.9	8.78	−30.10	−30.82	9.622
800	−56.722	8.090	64.812	6472.0	8.84	−30.10	−30.92	8.448
900	−57.680	8.177	65.857	7359.3	8.89	−30.10	−31.03	7.534
1,000	−58.546	8.250	66.796	8250.0	8.93	−30.11	−31.13	6.803
1,100	−59.335	8.314	67.649	9145.4	8.96	−30.11	−31.23	6.205
1,200	−60.060	8.369	68.429	10042.8	8.99	−30.11	−31.33	5.706
1,300	−60.732	8.418	69.150	10943.4	9.01	−30.11	−31.43	5.284
1,400	−61.358	8.461	69.819	11845.4	9.03	−30.12	−31.53	4.923
1,500	−61.943	8.500	70.443	12750.0	9.05	−30.12	−31.63	4.609

TABLE 24. *Thermodynamic properties of* IF_5 (g)

T	$(F°-H°_0)/T$	$(H°-H°_0)/T$	$S°$	$H°-H°_0$	$C°_p$	$\Delta Hf°$	$\Delta Ff°$	log Kf
°K	*cal/deg mole*	*cal/deg mole*	*cal/deg mole*	*cal/mole*	*cal/deg mole*	*kcal/mole*	*kcal/mole*	
0	0	0	0	0	0	−200.68	−200.68	.....
250	−60.74	13.89	74.63	3472	21.65	−202.59	−184.19	161.017
273.16	−61.95	14.59	76.54	3985	22.65	−202.59	−182.47	145.987
298.16	−63.32	15.31	78.63	4565	23.70	−202.6	−180.6	132.41
300	−63.41	15.37	78.78	4611	23.77	−202.59	−180.51	131.498
400	−68.19	17.85	86.04	7140	26.57	−202.43	−173.17	94.613
500	−72.38	19.77	92.15	9885	28.19	−202.15	−165.88	72.505
600	−76.13	21.26	97.39	12756	29.18	−201.80	−158.66	57.792
700	−79.50	22.44	101.94	15708	29.82	−201.41	−151.50	47.301
800	−82.56	23.39	105.95	18712	30.26	−201.02	−144.40	39.447
900	−85.36	24.17	109.53	21753	30.57	−200.61	−137.34	33.351
1,000	−87.94	24.83	112.77	24830	30.79	−200.19	−130.33	28.483
1,100	−90.33	25.38	115.71	27918	30.96	−199.78	−123.36	24.510
1,200	−92.56	25.85	118.41	31020	31.09	−199.36	−116.44	21.206
1,300	−94.64	26.25	120.89	34125	31.19	−198.95	−109.54	18.415
1,400	−96.60	26.61	123.21	37254	31.27	−198.53	−102.67	16.028
1,500	−98.45	26.92	125.37	40380	31.34	−198.12	−95.84	13.964

TABLE 25. *Thermodynamic properties of* IF^7 (g)

T	$(F°-H_0^\circ)/T$	$(H°-H_0^\circ)/T$	$S°$	$H°-H_0^\circ$	$C_p°$	$\Delta Hf°$	$\Delta Ff°$	log Kf
°K	*cal/deg mole*	*cal/deg mole*	*cal/deg mole*	*cal/mole*	*cal/deg mole*	*kcal/mole*	*kcal/mole*	
0	0	0	0	0	0	−228.69	−228.69	.....
250	−61.14	16.40	77.54	4100	29.1	−231.73	−202.27	176.820
273.16	−62.64	17.55	80.19	4794	30.8	−231.72	−199.53	159.641
298.16	−64.23	18.96	82.73	5585	32.3	−231.7	−196.6	144.10
300	−64.34	18.81	83.15	5643	32.4	−231.70	−196.37	143.056
400	−70.32	22.77	93.09	9108	36.5	−231.37	−184.64	100.881
500	−75.74	25.77	101.51	12885	38.8	−230.85	−173.02	75.625
600	−80.66	28.07	108.73	16842	40.2	−230.25	−161.51	58.830
700	−85.12	29.87	114.99	20909	41.1	−229.61	−150.10	46.862
800	−89.21	31.31	120.52	25048	41.7	−228.94	−138.79	37.915
900	−92.96	32.48	125.44	29232	42.1	−228.26	−127.55	30.974
1,000	−96.44	33.46	129.90	33460	42.4	−227.56	−116.41	25.440

TABLE 26. *Thermodynamic properties of* ICl (g)

T	$(F°-H_0^\circ)/T$	$(H°-H_0^\circ)/T$	$S°$	$H°-H_0^\circ$	$C_p°$	$\Delta Hf°$	$\Delta Ff°$	log Kf
°K	*cal/deg mole*	*cal/deg mole*	*cal/deg mole*	*cal/mole*	*cal/deg mole*	*kcal/mole*	*kcal/mole*	
0	0	0	0	0	0	−3.33	−3.33	
250	−48.598	7.513	56.111	1878.2	8.33	−3.35	−3.30	2.885
273.16	−50.819	7.586	58.405	2072.2	8.42	−3.351	−3.723	2.9790
298.16	−51.486	7.660	59.146	2283.9	8.50	−3.352	−3.757	2.7539
300	−51.534	7.665	59.199	2299.5	8.50	−3.352	−3.760	2.7388
400	−53.773	7.902	61.675	3160.8	8.70	−3.35	−3.90	2.129
500	−55.555	8.073	63.628	4036.5	8.81	−3.35	−4.03	1.763
600	−57.039	8.201	65.240	4920.6	8.87	−3.34	−4.17	1.519
700	−58.311	8.301	66.612	5810.7	8.92	−3.34	−4.31	1.345
800	−59.425	8.380	67.805	6704.0	8.95	−3.34	−4.45	1.215
900	−60.416	8.445	68.861	7600.5	8.98	−3.34	−4.58	1.113
1,000	−61.309	8.499	69.808	8499.0	9.00	−3.34	−4.72	1.032
1,100	−62.121	8.546	70.667	9400.6	9.02	−3.35	−4.86	0.966
1,200	−62.866	8.586	71.452	10303.2	9.04	−3.35	−5.00	.910
1,300	−63.555	8.621	72.176	11207.3	9.05	−3.35	−5.14	.863
1,400	−64.195	8.652	72.847	12112.8	9.06	−3.35	−5.27	.823
1,500	−64.793	8.680	73.473	13020.0	9.08	−3.35	−5.41	.788

TABLE 27. *Thermodynamic properties of* IBr (g)

T	$(F°-H_0^\circ)/T$	$(H°-H_0^\circ)/T$	$S°$	$H°-H_0^\circ$	$C_p°$	$\Delta Hf°$	$\Delta Ff°$	log Kf
°K	*cal/deg mole*	*cal/deg mole*	*cal/deg mole*	*cal/mole*	*cal/deg mole*	*kcal/mole*	*kcal/mole*	
0	0	0	0	0	0	−1.42	−1.42	.....
250	−52.501	7.805	60.306	1951.2	8.62	−1.42	−1.76	1.538
273.16	−53.196	7.877	61.073	2151.7	8.68	−1.420	−1.796	1.4369
298.16	−53.889	7.946	61.835	2369.2	8.72	−1.422	−1.830	1.3417
300	−53.938	7.951	61.889	2385.3	8.72	−1.422	−1.833	1.3351
400	−56.256	8.161	64.417	3264.4	8.84	−1.42	−1.97	1.076
500	−58.093	8.304	66.397	4152.0	8.90	−1.42	−2.11	0.921
600	−59.617	8.407	68.024	5044.2	8.94	−1.42	−2.24	.818
700	−60.918	8.486	69.404	5940.2	8.97	−1.42	−2.38	.743
800	−62.056	8.548	70.604	6838.4	8.99	−1.42	−2.52	.688
900	−63.066	8.599	71.665	7739.1	9.01	−1.42	−2.66	.644
1,000	−63.974	8.641	72.615	8641.0	9.03	−1.42	−2.79	.610
1,100	−64.799	8.677	73.476	9544.7	9.05	−1.42	−2.93	.582
1,200	−65.556	8.708	74.264	10449.6	9.06	−1.42	−3.07	.559
1,300	−66.254	8.736	74.990	11356.8	9.07	−1.42	−3.20	.538
1,400	−66.902	8.761	75.663	12265.4	9.09	−1.42	−3.34	.521
1,500	−67.507	8.783	76.290	13174.5	9.10	−1.43	−3.48	.507

6. References

[1] F. D. Rossini, D. D. Wagman, W. H. Evans, S. Levine, and I. Jaffe, Selected values of chemical thermodynamic properties, NBS Circular 500 (U. S. Government Printing Office, Washington 25, D. C., 1952).
[2] D. D. Wagman, J. E. Kilpatrick, W. J. Taylor, K. S. Pitzer, and F. D. Rossini, J. Research NBS **34,** 143 (1945) RP1634.
[3] H. F. Stimson, J. Research NBS **42,** 209 (1949) RP1962.
[4] E. Wichers, J. Am. Chem. Soc. **76,** 2033 (1954).
[5] W. H. Evans, R. Jacobson, T. R. Munson, and D. D. Wagman, J. Research NBS **55,** 83 (1955) RP2608.
[6] C. E. Moore, Atomic energy levels **I, II, III (III,** in press), NBS Circular 467 (U. S. Government Printing Office, Washington 25, D. C., 1949–1955).
[7] L. Haar and C. W. Beckett (unpublished calculations).
[8] H. L. Johnston, L. Savedoff, and J. Belzer, Contributions to the thermodynamic functions by a Planck-Einstein oscillator in one degree of freedom, NAVEXOS **P–646** (U. S. Government Printing Office, Washington 25, D. C., 1949).
[9] T. L. Collins, A. O. Nier, and W. H. Johnson, Jr., Phys. Rev. **84,** 717 (1951).
[10] K. T. Bainbridge and A. O. Nier, Relative isotopic abundances of the elements, Preliminary Report No. 9, Nuclear Science Series, Division of Mathematical and Physical Sciences, National Research Council (1951).
[11] J. E. Mayer and M. G. Mayer, Statistical mechanics, p. 160 (John Wiley & Sons, Inc., New York, N. Y., 1940).
[12] D. Andrychuk, J. Chem. Phys. **18,** 233 (1950).
[13] D. Andrychuk, Can. J. Phys. **29,** 151 (1951).
[14] G. Herzberg, Molecular spectra and molecular structure, I. Spectra of diatomic molecules, 2d ed., p. 499 (D. Van Nostrand Co., Inc., New York, N. Y., 1950).
[15] D. A. Gilbert, A. Roberts, and P. A. Griswold, Phys. Rev. **76,** 1723 (1949).
[16] A. H. Nielsen and E. A. Jones, J. Chem. Phys. **19,** 1117 (1951).
[17] A. H. Nielsen and E. A. Jones, Phys. Rev. **83,** 485 (1951).
[18] D. F. Smith, M. Tidwell, and D. V. P. Williams, Phys. Rev. **77,** 420 (1950).
[19] R. A. Durie, Proc. Roy. Soc. (London) [A] **207,** 388 (1951).
[20] P. H. Brodersen and H. J. Schumacher, Z. Naturforsch. **2a,** 358 (1947).
[21] D. F. Smith, M. Tidwell, and D. V. P. Williams, Phys. Rev. **79,** 1007 (1951).
[22] H. C. Mattraw, C. F. Pachucki, and N. J. Hawkins, J. Chem. Phys. **22,** 1117 (1954).
[23] H. Stammreich and R. Forneris, J. Chem. Phys. **21,** 944 (1953).
[24] D. H. Rank and W. M. Baldwin, J. Chem. Phys. **19,** 1210 (1951).
[25] C. H. Townes, F. R. Merritt, and B. D. Wright, Phys. Rev. **73,** 1334 (1948).
[26] V. Schomaker and D. P. Stevenson, J. Am. Chem. Soc. **63,** 37 (1941).
[27] G. Herzberg, Molecular spectra and molecular structure, I. Spectra of diatomic molecules, 2d ed., p. 90 (D. Van Nostrand Co., Inc., New York, N. Y., 1950).
[28] H. J. Bernstein and J. Powling, J. Chem. Phys. **18,** 685 (1950).
[29] E. A. Jones, J. S. Kirby-Smith, P. J. H. Woltz, and A. H. Nielsen, J. Chem. Phys. **19,** 337 (1951).
[30] G. Hettner, R. Pohlman, and H. J. Schumacher, Z. Physik **96,** 203 (1935).
[31] G. B. B. M. Sutherland and W. G. Penney, Proc. Roy. Soc. (London) [A] **156,** 678 (1936).
[32] J. A. Ibers and V. Schomaker, J. Phys. Chem. **57,** 699 (1953).
[33] A. H. Nielsen and P. J. H. Woltz, J. Chem. Phys. **20,** 1878 (1952).
[34] C. R. Bailey and A. B. D. Cassie, Proc. Roy. Soc. (London) [A] **137,** 622 (1932).
[35] K. Hedberg, J. Chem. Phys. **19,** 509 (1951).
[36] J. B. Coon, Phys. Rev. **58,** 926 (1940).
[37] J. B. Coon, J. Chem. Phys. **14,** 665 (1946).
[38] J. B. Coon and E. Ortiz, Phys. Rev. **82,** 766 (1951).
[39] T. G. Kujumzelis, Physik. Z. **39,** 665 (1938)
[40] J. D. Dunitz and K. Hedberg, J. Am. Chem. Soc. **72,** 3108 (1950).
[41] J. B. Coon, Phys. Rev. **85,** 746 (1952) .
[42] W. H. Stockmayer, G. M. Kavanagh, and H. S. Mickley, J. Chem. Phys. **12,** 408 (1944).
[43] C. R. Bailey and A. B. D. Cassie, Proc. Roy. Soc. (London) [A] **142,** 129 (1933).
[44] R. Pohlman and H. J. Schumacher, Z. Physik **102,** 678 (1936).
[45] E. A. Jones, T. F. Parkinson, and R. B. Murray, J. Chem. Phys. **17,** 501 (1949).
[46] K. Schäfer and E. Wicke, Z. Elektrochem. **52,** 205 (1948).
[47] D. F. Smith, U. S. Atomic Energy Commission **K940,** 14 p. (October 27, 1952).
[48] C. V. Stephenson and E. A. Jones, J. Chem. Phys. **20,** 1830 (1952).
[49] T. G. Burke and E. A. Jones, J. Chem. Phys. **19,** 1611 (1951).
[50] L. Pauling, The nature of the chemical bond (Cornell University Press, Ithaca, N. Y., 1939).
[51] P. W. Allen and L. E. Sutton, Acta Cryst. **3,** 46 (1950).
[52] R. C. Lord, M. A. Lynch, Jr., W. C. Schumb, and E. J. Slowinski, Jr., J. Am. Chem. Soc. **72,** 522 (1950).
[53] L. Slutsky and S. H. Bauer, J. Am. Chem. Soc. **76,** 270 (1954).
[54] M. W. Nathans, J. Chem. Phys. **18,** 1122 (1950).
[55] M. G. Evans, E. Warhurst, and E. Whittle, J. Chem. Soc. **1950,** 1524.
[56] E. Wicke and H. Friz, Z. Elektrochem. **57,** 9 (1953).
[57] P. W. Gilles and J. L. Margrave, J. Chem. Phys. **21,** 381 (1953).
[58] R. N. Doescher, J. Chem. Phys. **20,** 330 (1952).
[59] H. Wise, J. Chem. Phys. **20,** 927 (1952).
[60] R. F. Barrow and A. D. Caunt, Proc. Roy. Soc. (London) [A] **219,** 120 (1953).
[61] H. von Wartenberg and G. Klinkhott, Z. anorg. u. allgem. Chem. **193,** 409 (1930).
[62] O. Ruff and W. Menzel, Z. anorg. u. allgem. Chem. **198,** 375 (1931).
[63] A. G. Gaydon, Dissociation energies and spectra of diatomic molecules (Chapman and Hall, Ltd., (London, 1947).
[64] H. von Wartenberg and F. A. Henglein, Ber. **55,** 1003 (1922).
[65] F. A. Henglein, Z. anorg. u. allgem. Chem. **123,** 137 (1922).
[66] K. Wohl, Z. Elektrochem. **30,** 36 (1924).
[67] M. Trautz and F. Geissler, Z. anorg. u. allgem. Chem. **140,** 116 (1924).
[68] H. von Wartenberg and D. Weigel, Z. anorg. u. allgem. Chem. **142,** 337 (1925).
[69] J. I. Wallace and C. F. Goodeve, Trans. Faraday Soc. **27,** 648 (1931).
[70] H. Booth and E. J. Bowen, J. Chem. Soc. **127,** 342 (1925).
[71] H. Mayer, Z. physik. Chem. **113,** 620 (1924).
[72] W. Finkelnburg and H. J. Schumacher, Z. physik. Chem. **Bodenstein-Festband,** 704 (1930).
[73] G. Parker and F. J. Wright, Z. Elektrochem. **56,** 782 (1952).
[74] A. A. Jakowkin, Z. physik. Chem. **29,** 613 (1899).
[75] S. Goldschmidt, Ber. **52,** 752 (1919).
[76] W. A. Roth, Z. physik. Chem. [A] **145,** 289 (1929).
[77] D. M. Yost and R. C. Felt, J. Am. Chem. Soc. **56,** 68 (1934).
[78] J. Thomsen, Thermochemische Untersuchungen [I, II, III, IV] (Verlag von J. A. Barth, Leipzig, 1882–1886).
[79] P. Günther and K. Wekua, Z. physik. Chem. [A] **154,** 193 (1931).
[80] E. Wicke and H. Friz, Naturwissenschaften **39,** 522 (1952).
[81] H. Schmitz and H. J. Schumacher, Z. Naturforsch. **2a,** 362 (1947).

[82] H. Schmitz and H. J. Schumacher, Z. Naturforsch. **2a,** 359 (1947).
[83] H. J. Schumacher, H. Schmitz, and P. H. Brodersen, Anales asoc. quím. argentina **38,** 98 (1950).
[84] A. L. Warhaftig, J. Chem. Phys. **10,** 248 (1942).
[85] O. Ruff and F. Laass, Z. anorg. u. allgem. Chem. **183,** 214 (1929).
[86] H. Schmitz and H. J. Schumacher, Z. Naturforsch. **2a,** 362 (1947).
[87] E. P. Perman and G. A. S. Atkinson, Z. physik. Chem. **33,** 215 (1900).
[88] E. P. Perman and G. A. S. Atkinson, Z. physik. Chem. **33,** 577 (1900).
[89] M. Bodenstein and F. Cramer, Z. Elektrochem. **22,** 327 (1916).
[90] T. DeVries and W. H. Rodebush, J. Am. Chem. Soc. **49,** 656 (1927).
[91] R. A. Durie and A. G. Gaydon, J. Phys. Chem. **56,** 316 (1952).
[92] G. Braune and E. Victor, Z. Elektrochem. **41,** 508 (1935).
[93] H. G. Vesper and G. K. Rollefson, J. Am. Chem. Soc. **56,** 620 (1934).
[94] L. T. M. Gray and D. W. G. Style, Proc. Roy. Soc. (London) [A] **126,** 603 (1930).
[95] C. M. Beeson and D. M. Yost, J. Am. Chem. Soc. **61,** 1432 (1939).
[96] W. Jost, Z. physik. Chem. [A] **153,** 143 (1931).
[97] H. Braune and H. Ramstetter, Z. physik. Chem. **102,** 480 (1922).
[98] G. Starck and M. Bodenstein, Z. Elektrochem. **16,** 961 (1910).
[99] M. K. Perlman and G. K. Rollefson, J. Chem. Phys. **9,** 362 (1941).
[100] A. A. Woolf, J. Chem. Soc. **1951,** 231.
[101] R. B. Bernstein and J. J. Katz, J. Phys. Chem. **56,** 885 (1952).
[102] W. G. Brown and C. E. Gibson, Phys. Rev. **40,** 529 (1932).
[103] J. McMorris and D. M. Yost, J. Am. Chem. Soc. **54,** 2247 (1932).
[104] J. McMorris and D. M. Yost, J. Am. Chem. Soc. **53,** 2625 (1931).
[105] W. G. Brown, Phys. Rev. **42,** 355 (1932).
[106] L. G. Cole, M. Farber, and G. W. Elverum, Jr., J. Chem. Phys. **20,** 586 (1952).
[107] G. M. Murphy and J. E. Vance, J. Chem. Phys. **7,** 806 (1939).
[108] K. V. Butkov and R. B. Rozenbaum, Zhur. Fiz. Khim. **24,** 706 (1950).
[109] J.-H. Hu, D. White, and H. L. Johnston, J. Am. Chem. Soc. **75,** 5642 (1953).
[110] R. L. Potter, J. Chem. Phys. **17,** 957 (1949).
[111] W. F. Giauque and R. Overstreet, J. Am. Chem. Soc. **54,** 1931 (1932).
[112] R. H. Sherman and W. F. Giauque, J. Am. Chem. Soc. **75,** 2007 (1953).
[113] J. W. M. DuMond and E. R. Cohn, Phys. Rev. **82,** 555 (1951).
[114] W. F. Giauque and T. M. Powell, J. Am. Chem. Soc. **61,** 1870 (1939).
[115] L. G. Cole and G. W. Elverum, Jr., J. Chem. Phys. **20,** 1543 (1952).
[116] M. D. Scheer, J. Chem. Phys. **20,** 924 (1952).
[117] J. W. Grisard, H. A. Bernhardt, and G. D. Oliver, J. Am. Chem. Soc. **73,** 5725 (1951).
[118] A. Weber and S. M. Ferigle, J. Chem. Phys. **20,** 1497 (1952).
[119] A. R. Gordon and C. Barnes, J. Chem. Phys. **1,** 692 (1933).
[120] H. Zeise, Z. Elektrochem. **41,** 267 (1935).
[121] G. M. Murphy, J. Chem. Phys. **4,** 344 (1936).
[122] H. Zeise, Z. Elektrochem. **40,** 662 (1934).
[123] H. Schmitz and H. J. Schumacher, Z. Naturforsch. **2a,** 363 (1947).
[124] A. A. Banks and M. J. Rudge, J. Chem. Soc. **1950,** 191.
[125] R. D. Burbank and F. N. Bensey, J. Chem. Phys. **21,** 602 (1953).
[126] M. Bodenstein and A. Schmidt, Z. physik. Chem. **123,** 28 (1926).
[127] W. Müller, Z. physik. Chem. **123,** 1 (1926).
[128] A. G. Gaydon, Dissociation energies and spectra of diatomic molecules, 2d ed., revised (Chapman and Hall, Ltd., London, 1953).

WASHINGTON, April 2, 1955.

Journal of Research of the National Bureau of Standards Vol. 55, No. 3, September 1955 Research Paper 2615

Atomic Negative-Ion-Photodetachment Cross-Section and Affinity Measurements[1]

Stephen J. Smith and Lewis M. Branscomb

The spectral distributions of the H^- and O^- cross sections for photodetachment have been measured. The H^- measurements are consistent with the theory of Chandrasekhar. A curve has been fitted to the results for O^-. The threshold of this cross section, the affinity of O^-, is found to be 1.48 ± 0.10 electron volts. No evidence is found for resonance at the threshold or for the existence of excited O^- ions. The apparatus is described in detail.

1. Introduction

The observation in this laboratory of the photodetachment of electrons from negative ions in 1953 [1][2] opened the possibility of studying the absorption spectra of negative ions. The first application of the technique was to the determination of the absolute absorption by H^-, integrated over a wide spectral range [2]. The results agreed with the theoretical predictions of Chandrasekhar and his colleagues [3]. In our H^- experiments the principal task was accurate calibration of the equipment for the absolute measurement of the integrated cross section.

This paper discusses measurements of the spectral distributions of photodetachment cross sections. These are of interest not only because of their practical applications to astrophysics and geophysics, but also because of the information that can be obtained about the electron affinities of atoms and the possible existence of excited states of negative ions. For unexcited atomic negative ions the wavelength of the threshold for photodetachment corresponds to the electron affinity of the atom. The shape of the photodetachment cross section near the threshold supplies information about the possibility of excited states of the negative ion [4, 5]. From this curve one can also determine the radiative attachment cross section from the principle of detailed balancing [6]. This is of particular interest for studies of ionospheric electron density.

A preliminary value for the oxygen affinity has been obtained [7] by this method. This paper describes the details of the procedure for determining the affinity and the shape of the detachment cross-section curve, and summarize the spectral-distribution measurements for H^- and O^-. Because the method does not uniquely determine the wavelength dependence of the cross section, sufficient data is given to permit the reader to test the compatibility of any proposed cross section and our experimental data. The first H^- paper [2] gives details of the method of calibrating the apparatus for measuring absolute cross sections.

The experimental techniques peculiar to these measurements, as contrasted with experiments on neutral atoms or positive ions, stem from two characteristics of *atomic* negative ions: (1) the low binding energies; and (2) the finite number, usually only one, of bound states. These characteristics are attributed to the weak short-range forces responsible for the stability of negative ions [8].

Because of the low binding energies it is difficult to produce useful quantities of negative ions. The atomic processes for producing them must generally compete with more probable reactions, and such ions as are produced are easily destroyed.

The practical result of the limited number of bound states is that transitions in most atomic negative ions are confined to those between the ground state and the continuum. For those negative ions that have only one bound state, for example, the negative atomic hydrogen ion, all excitations result in the complete detachment of the excess electron. In principle, these ions might be studied equivalently from the points of view of absorption spectroscopy or of ion destruction. The threshold for absorption of photons is the same as the affinity, and the study of the intensity distribution of the absorption spectrum is equivalent to a study of the energy spectrum of the detached electrons.

A few atomic negative ions may have more than one bound state. There is some experimental evidence that negative atomic oxygen is one of these [9, 10, 11]. In such a case a study of the photon absorption spectrum, if it were feasible, would give more complete information than would the photodetachment spectrum.

In practice, negative ions can be produced only in such small quantities ($\sim 10^{-7}$ amp) that the fraction of incident photons actually absorbed in a realizable experiment is difficult to observe directly; particularly as the spectrum is continuous. Negative-ion photoexcitation, therefore, is naturally studied from the point of view of ion destruction, either by observation of the neutral atoms created in an illuminated negative-ion beam or by observation of the detached electrons.

In the experiment described in this paper, the detached electrons are observed. The apparatus was designed for measurements of an absolute cross section, requiring the collection of all detached elec-

[1] Supported in part by the Office of Naval Research.
[2] Figures in brackets indicate the literature references at the end of this paper.

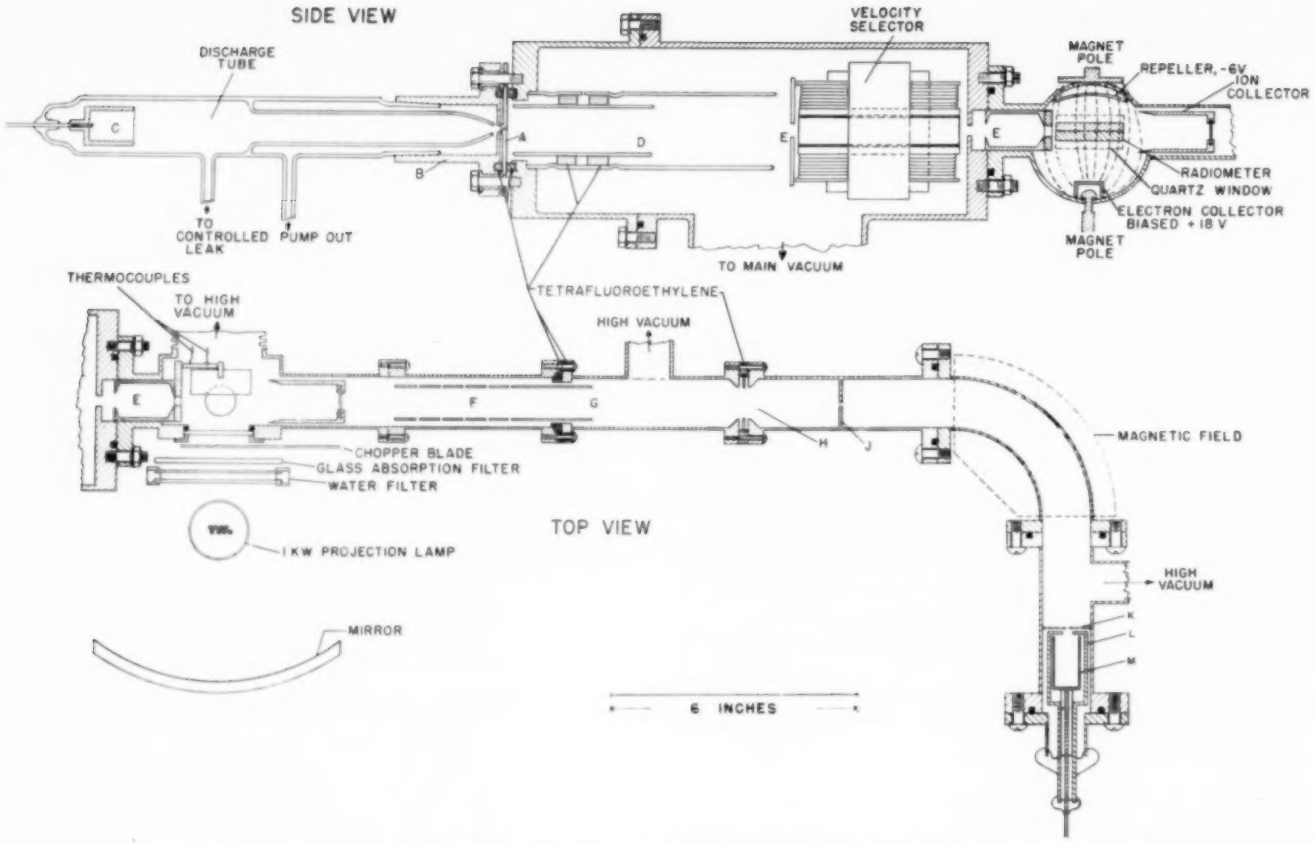

FIGURE 1. *Schematic drawing of the apparatus showing elements of the ion and photon beam optics*

The ion beam is produced in the gas discharge tube (pressure $\leq$100 Hg) by applying up to 6 kv between A, the anode, and C, the cathode. A is biased 100-200 v negative with respect to ground potential. C, the control electrode, is biased as much as 500 v negative with respect to A. D, operated about 2,500 v positive, forms an electrostatic lens with the surrounding elements; focusing the ion beam through defining apertures, E.

The ions not deflected by the velocity selector (see also fig. 4) pass through the reaction chamber into the ion collector. The back of the ion collector may be opened to allow the beam to pass into a 90° sector-field mass spectrometer. F, G, and H are an ion optical system designed to render the beam parallel at the entrance slit J, independent of mass. Lens F gradually accelerates the ions to a fixed fraction of their final energy. Lens G accelerates the ions to the proper energy to obtain a focus at the exit slit K of the mass spectrometer. The vacuum housing forms part of the lens G and that part beyond G is at high voltage. Unipotential lens H compensates for the focusing power of G. Those ions focussed on K by the magnetic field are collected in M, at ground potential. L, which shields M, is biased −67 v.

Two interchangeable magnets are used with the spectrometer. One, with a field of 3,300 gauss, is used for heavy ions; and the other, with a field of 1,100 gauss, is used for light ions. Tetrafluoroethylene resin is used where vacuum gaskets must also serve as electrical insulators. These gaskets are used where indicated and also to insulate electrically the mass spectrometer housing beyond G from the grounded high vacuum pumps and traps.

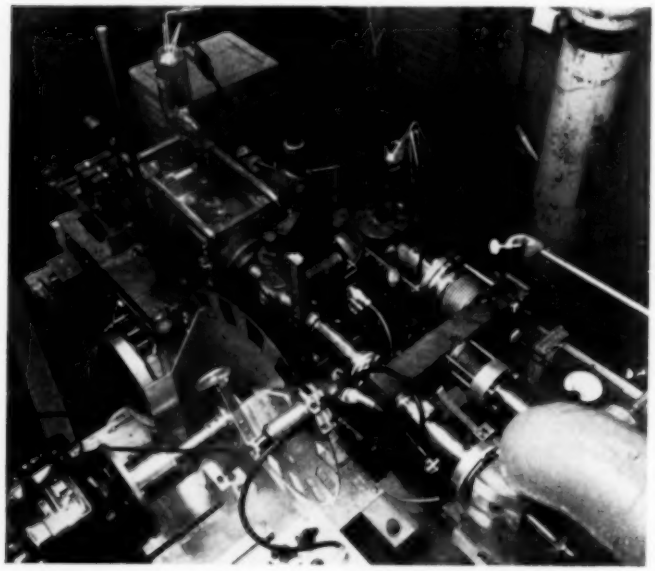

trons. For simplicity the observation of the energy spectrum of the detached electrons is not attempted, but the spectrum is deduced from the dependence of the total detached electron current on the spectral distribution of the incident photons.

The apparatus, particularly its application to integrated absolute cross sections, has been described [2]. Those features of the apparatus of particular importance for the determination of affinities and spectral distributions of cross sections are dealt with here in greater detail.

The apparatus is shown schematically in figure 1 and photographically in figure 2. A mass-separated ion beam crosses a very intense photon beam. The photon beam is chopped, and the current of detached electrons is measured with a frequency- and phase-discriminating amplifier, in order to separate the

FIGURE 2. *Over-all view of the apparatus.*

The chopper-lamp-mirror assembly is shown pulled back about 6 in. from its operating position.

photodetachment current from background currents. The average value of the chopped detachment current is compared with the direct ion current. A mass spectrometer built into the apparatus provides for analysis of the ion beam.

Monochromatic sources of radiation of adequate intensity have not been available. Therefore the radiation continuum from a hot wolfram filament is used, and changes in spectral distribution are accomplished with sharp-cutoff filters. A radiometer [2] measures the total radiant power incident on the beam.

2. Operation of the Experiment

2.1. Photon Beam

The light source is a 1-kw projection lamp [2] operating at a measured [3] color temperature of 3,420° K, corresponding to an absolute temperature of 3,300° K [12, 13]. The spectral-intensity distribution of this source was obtained by multiplying the 3,300° K Planck curve by the measured [4] transmission of the quartz envelope and by the best available values of the emissivity of the wolfram filament material, from 3000 A to 40000 A at 3,300° K [14].

Radiation from the lamp is focused by a front-aluminized spherical mirror, through a quartz window, into the negative-ion beam. A low-sensitivity platinum-blacked radiometer, located behind the ion beam measures the radiant power in the photon beam. The radiant power at the ion beam is about 30 w when no optical filtering is used.

The spectral distribution of the photon beam emitted by the projection lamp can be altered by means of optical filters. A set of polished Corning glass absorption filters and one Baird infrared multilayer reflection filter with measured transmissions [3] are used in this work. The transmissions of these filters and the spectral distribution of the lamp are illustrated in figure 3.

When the H^- cross section was measured, the water filter shown in figure 1 was not available. It is clear from figure 3 that the filters were required to absorb a large fraction of the 100 to 200 w of radiation incident on them. This resulted in severe local heating—especially in the infrared filters, which invariably broke under prolonged use with only air cooling. It is known also that the transmissions of the glass absorption filters, and their cutoff wavelengths, are temperature dependent [15]. Spectroscopic examination of transmitted light shows that the cutoff wavelengths shift toward the infrared when the filters are placed in the full photon beam. In the infrared-absorption filters the shift is about 120 A, and in the yellow filters it is of the order of 50 A.

For the O^- measurements the water filter was inserted in the photon beam in front of the filters. This reduced transmission shifts and allowed full use of the filters by absorbing the infrared beyond about 1.25 μ. Distilled water, kept at constant temperature by a heat exchanger, is circulated through the 6-mm-deep space between the two polished glass faces of the water cell. As an extra precaution the measurements with each infrared filter were made by using that filter as the back face of the water cell in place of a clear glass plate. The transmission of the water cell (see footnote 3) was found to be nearly constant (86 to 90%) and independent of moderate temperature changes over the spectral range in which O^- photodetachment occurs

[3] Measured by the NBS Photometry and Colorimetry Section.
[4] Measured by the NBS Radiometry Section.

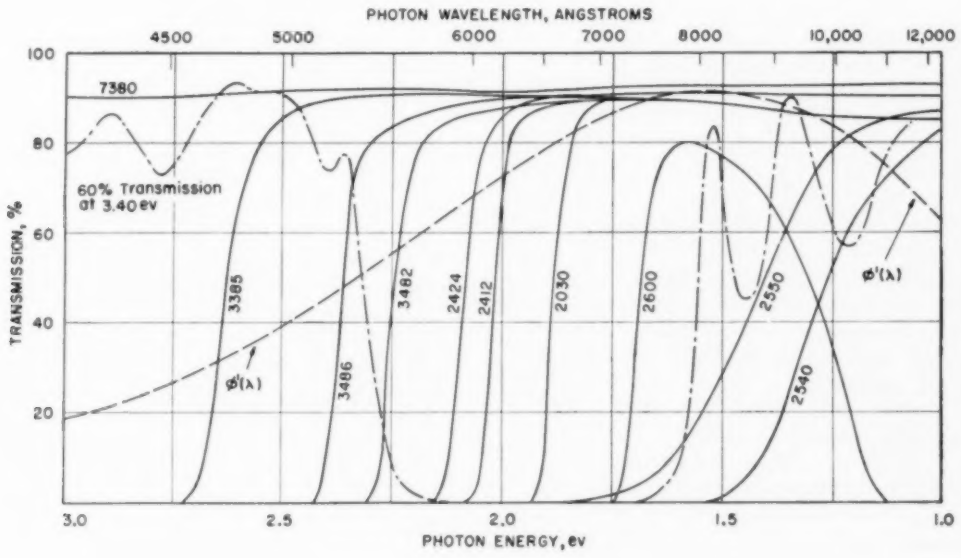

FIGURE 3. *Filter transmissions.*

The solid lines show the transmissions of the Corning glass absorption fiilters. The dot-dash line is the transmission of the Baird interference reflection filter. The dashed line gives the spectral distribution ϕ' (λ) of the radiation from the projection lamp.

2.2. Electron-Current Collection

Electrons are detached from the ions at the intersection of the ion and photon beams. A 50-gauss magnetic field in the region of intersection traps the detached electrons. These have very low energy because of the small excess of $h\nu$ over the detachment threshold energy (the affinity). (The velocity along the ion beam is negligible.) Ions of 200-v energy are deflected with a minimum radius of curvature approximately equal to 50 cm/amu, and are deflected only 1 or 2 mm at the ion collector.

The magnetic-field lines from all points of the region of the beam intersection converge onto a small electrode, where the electron current is collected for measurement (see fig. 1). This collector is biased +18 v, and a repeller plate on the opposite side of the beam is biased −6 v.

The electron collector may receive currents that are derived from the ion beam by several processes other than photodetachment: (a) collisional detachment of electrons from negative ions, (b) production of charge-exchange ions with low energy, (c) ion scattering by the residual gas in the chamber, and (d) production of secondary electrons from scattered ions. Although unmodulated by the light chopper, these undesired currents may produce large noise signals.

Collisional detachment produces low-energy electrons in the region of intersection of the beams. These will all be collected, as will charge-exchange ions in this region. Scattered ions, having higher energy, will not be trapped in the weak inhomogeneous magnetic field and should not be important, because the collector subtends a small solid angle in a direction perpendicular to the direction of the beam. Secondary electron current reaching the collector is probably considerably smaller than total scattered ion current.

The cross sections for some of these negative-ion processes have been measured in a few special cases, and these results are not directly applicable here. For an order-of-magnitude estimate of the background current to the electron collector, we use a typical collisional detachment cross section of 20 cm^{-1} (at 1-mm pressure) [10]. At normal operating pressure of 10^{-6} mm Hg and with an ion-beam current of 10^{-7} amp, the estimated background current collected from 5 cm of ion-beam path is about 10^{-11} amp. The magnitude of the photodetachment current is approximately 10^{-12} amp.

In these measurements the photodetachment current is separated from other ion-beam-dependent effects by chopping the photon beam at 450 cps and observing the photodetachment current with a frequency- and phase-discriminating narrow-band amplifier. This coherent photodetachment signal is observed against a background of noise derived from the component of ion-beam noise that lies within the pass band of the amplifier. If the ion-beam noise is a thousand times shot noise [16], the background-noise current is approximately

$$I^2 = 2\times10^3\, e\, I\Delta f,$$

where e is the electronic charge of 1.6×10^{-19} coulomb, I is the current in amperes, and Δf is the amplifier bandwidth. For a 10^{-1}-cps bandwidth the noise current would be about 10^{-14} amp, or about one hundredth of the typical observed photodetachment signal. A typical observed signal-to-noise ratio is 50 to 1.

Photoelectric effect at metal surfaces can produce a coherent 450-cps current to the electron collector. With no filters in the photon beam, the chopped photoelectric current may be several times larger than the photodetachment current. The insertion of any of the filters reduces the photoelectric effect to the magnitude of the photodetachment signal or smaller. Furthermore, with the filters, the small photoelectric current is by chance approximately 90° out of phase with the photodetachment signal. This is presumably because the rotating chopper allows the photon beam to reach a low work-function surface at the top of the reaction chamber before it reaches the ion beam. Most surfaces are nickel plated and have photoelectric thresholds beyond the cutoff wavelengths of the filters. In practice, the in-phase component of the photoelectric current is at most only a few percent of the photodetachment signal. It is easily measured by turning off the ion beam and observing the effect of the photon beam alone.

Photodetachment of those ions created by charge exchange in the reaction chamber should not produce a coherent 450-cps signal, because all charge-exchange ions or their photodetached electrons are collected. This is demonstrated by the saturation of the 450-cps current to the electron collector with an increase from zero of the electric and magnetic fields in the reaction chamber. In addition the concentration of such ions must be extremely small.

Scattered ions and other stray charges striking the inside of the quartz window would cause fluctuating potentials to build up on the glass surface, disturbing the electrostatic field used to collect the photodetached electrons. For this reason, and to eliminate capacitive pickup between the electron collector and the blades of the chopper, a fine knitted mesh of 0.001-in. wolfram wire was stretched over the quartz window.

2.3. Ion Beam

The ions are produced in the positive column of a low-pressure glow discharge. The discharge tube is an adaptation of one described by Fite [16]. A steady voltage of 2 to 8 kv is applied across the discharge. The control electrode, designed to concentrate negative ions on the axis of the tube, is biased negative with respect to the anode. The ions that pass through the anode channel to form the beam, originate at a potential about 100 v negative with respect to the anode potential. The anode potential is variable with respect to ground to afford control of the ion-beam energy.

An electrostatic lens, coaxial with the beam, accelerates the ions to about 2 kv and then decelerates them into a region of ground potential. This lens

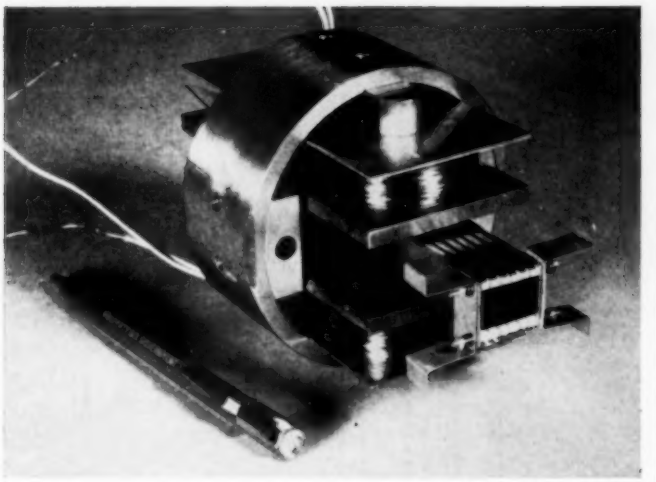

FIGURE 4. *Crossed field velocity selector used for mass separation of ions.*

The *E*-field electrodes are pulled out from the magnet pole faces to show details of the guard strips which maintain a homogeneous electric field. The potentials are distributed on these guard strips by a voltage divider made of 3,000 ohm Corning glass resistors in the vacuum.

renders the beam parallel or slightly convergent.

After being focused, the beam passes along the axis of the crossed-field velocity selector shown in figure 4. In this region weak magnetic fields can be applied from coils external to the vacuum to correct the alinement of the beam.

At the end of the velocity selector, three apertures remove the peripheral and highly divergent rays from the beam, which then passes into the detachment chamber, crosses the photon beam, and is caught in a Faraday cup. A weak transverse magnetic field and a small positive bias on the Faraday cup trap the secondary emission, so that the beam current (ordinarily from 25 mμa to nearly 1 μa) can be accurately measured. The magnitude and spread of the ion energy are determined by measuring the beam current while applying repelling potentials to the cup.

A shutter in the Faraday cup can be opened magnetically to allow part of the beam to pass into a 90°-sector-field mass spectrometer. This instrument is of conventional design, and its elements are shown in figure 1.

2.4. Ion-Beam Purity

The purity of the beam was controlled in two ways. A low-dispersion mass separator (the crossed-field velocity selector) was built into the apparatus; and for the O^- measurements spectroscopically pure gas was used in the discharge tube. In addition, the purity of the beam was subjected to repeated experimental checks.

The mass separator, shown in figure 4, is a crossed-field instrument in which a uniform electric field ($\leq$60 v/cm) opposes the deflecting force of the uniform magnetic field ($\leq$500 gauss). These fields are adjustable to allow ions having a chosen velocity to pass through undeflected. The mass-separating action depends on the experimental observation that ions of different species have approximately equal energies (see fig. 5); thus each ion has a characteristic velocity. The dispersion of this instrument depends on the length of ion path in the crossed fields and on the strength of the fields.

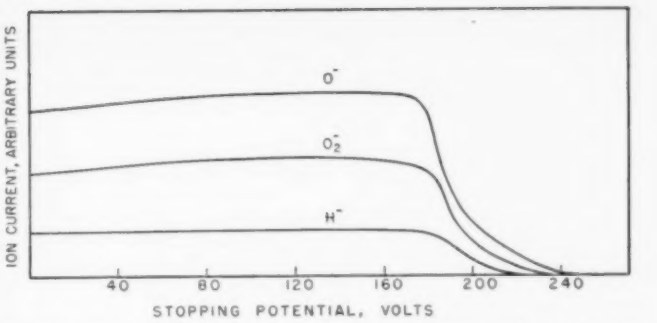

FIGURE 5. *Ion current versus stopping potential at the ion collector for several ion species from the same discharge.*

This example shows an energy spread greater than that usually obtained. All ion species appear to originate at the same potential in the plasma.

a. H^--Beam Purity

The H^- measurements were made with wet tank hydrogen or with D_2O in the discharge tube. With a 500-gauss magnetic field the velocity-selector dispersion was great enough for the separation of H^- from D^-, and D^- from O^- and heavier ions that also came from the discharge tube (fig. 6). This purity was studied by scanning the mass spectrum with the analyzing spectrometer while the velocity selector was peaked on H^- or D^-. Any impurities present were less than 0.1 percent of the ion beam.

Because ion impurities could strike the ion collector on one edge even though deflected sufficiently by the velocity selector to miss the entrance to the mass spectrometer, further verification of beam purity was necessary. The ratio of photodetachment current to ion current was independent of the dispersion of the velocity selector. Furthermore, the ratio of the photodetachment current to ion current was constant over the useful part of the H^- peak (fig. 6) obtained with the velocity selector.

b. O^--Beam Purity

Photodetachment from oxygen ions was studied in detail by using ions drawn from an oxygen discharge. After this work was completed, the oxygen affinity was redetermined, using ions from a carbon-monoxide discharge. These results are described in section 5.

For the O^- experiments, using an oxygen discharge, the velocity selector dispersion was great enough to separate O^- from O_2^-, and from H^- and D^-. However, the analyzing spectrometer showed masses 17 and 18 still present when the velocity selector was selecting O^- with largest available dispersion.

To achieve the required purity of the beam it was necessary to outgas the gas-handling system and the discharge tube carefully, and to use spectroscopically pure gas in the discharge.

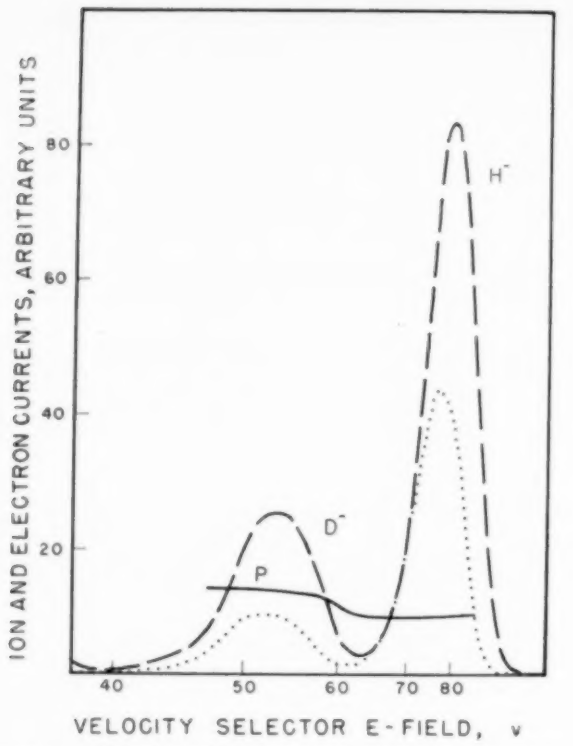

FIGURE 6. *Velocity selector scan of the ion beam from an* H_2, D_2O *discharge.*

The dashed line shows the current to the ion collector as the electrostatic *E*-field is varied, with constant magnetic field $H=150$ gauss. The horizontal scale shows the number of volts across the 1.9-cm gap between the deflector plates. The scan was run with the photon beam turned on, and the dotted line shows the photodetachment current (slightly displaced by the recording mechanism and enlarged relative to the ion current by about 10^3). The solid line is the measured ratio, *P*, of detachment current to ion current on an arbitrary scale. *P* is approximately constant over each peak, and $P_{D^-}/P_{H^-}=v_{H^-}/v_{D^-}=1.41$. Other careful measurements show *P* is accurately constant over each mass peak.

Because the gas-handling system could not be baked, outgassing was accomplished by about 20 hr of pumping, down to pressures as low as 5×10^{-6} mm Hg. The glass discharge tube was outgassed in the same way. The cathode was baked out with an induction heater. The anode and control electrode were outgassed by about 30 hr of operation of the discharge with the pure oxygen.

At the end of this time, with the velocity selector turned off, the analyzing spectrometer showed large O^-, O_2^-, and some heavier peaks. There were also traces of masses 17, 18, and 19 (fig. 7), presumably due to OH^-, OD^-, O_{18}^-, and F^-. The latter is probably from the electrically insulating tetrafluoroethylene gaskets used in the vacuum system. These trace peaks were of the order of 0.2 percent as high as the O^- and O_2^- peaks.

In the work on the O^- affinity it was particularly important to demonstrate that the O^- beam contained no O_2^-. The separation of O^- from O_2^- was checked by demonstrating that the ratio of detachment current to ion current is independent of the dispersion of the velocity selector over a reasonable range of dispersions, and constant over the useful part of the O^- mass peak (fig. 8). The O_2^- ion itself was studied. Its cross section and detachment

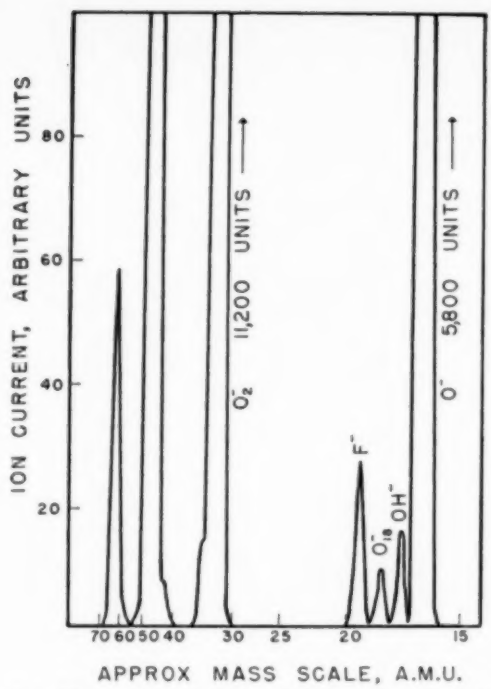

FIGURE 7. *Mass spectrum of the ion beam from an* O_2 *discharge.*

This spectrogram was taken with the 90° sector-field spectrometer. The resolution of the instrument is not high enough to allow exact determination of the mass numbers associated with the two heavy peaks. These could be NO_2^- and NO_3^- at masses 46 and 62 although no nitrogen was admitted to the spectroscopic oxygen, and nitrogen was not observable in the optical spectrum of the discharge. They could also be masses 48 and 64, although observation of O_3^- and O_4^- is not described in the literature, and the discharge pressure was less than 50 μ of Hg.

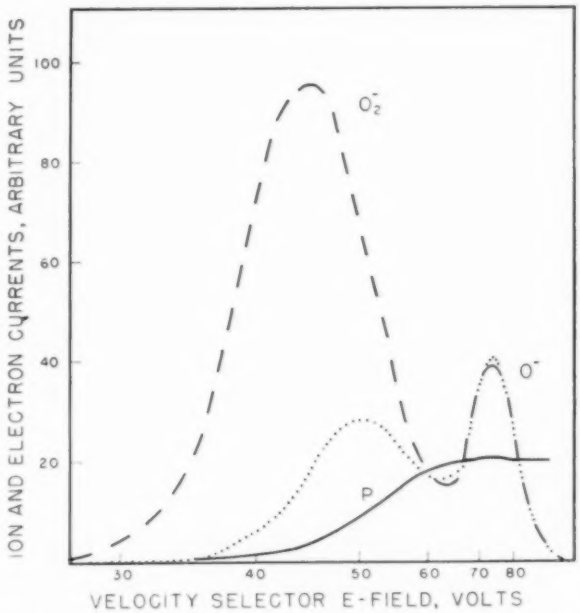

FIGURE 8. *Velocity selector scan of the ion beam from an* O_2 *discharge.*

The dashed line shows the current to the ion collector as the *E*-field is varied, with constant $H=500$ gauss. The high-field side of the large peak is O_2^-, and the low field side is composed of heavier ions (see fig. 7). The dotted line shows the corresponding photodetachment current (slightly displaced and magnified by about 10^3). The solid line is the measured ratio, *P*, of detachment current to ion current on an arbitrary scale. The constancy of *P* over the O^- peak has been verified by other measurements.

threshold were shown to be markedly different from those of O^-. The O_2^- cross section was somewhat lower and the detachment threshold lay farther into the infrared, beyond the limits of our infrared filter cutoffs.

3. Procedure for Data Analysis

The experimental probability that an ion, in passing through the photon beam, loses its extra electron is the ratio of the detached-electron current to the negative-ion current. This photodetachment probability is designated P_{exp}. It is a function of the specific geometry and conditions of the experiment.

A theoretical detachment probability, P_{theo}, that applies to our geometry has been derived [2]:

$$P_{theo}=0.317\times10^{13}W_0(M/E)^{1/2}\int\sigma(\lambda)\phi'(\lambda)T_n(\lambda)\lambda d\lambda. \quad (1)$$

Here W_0 is the power in watts of the unfiltered radiation falling on the radiometer; M is the mass of the negative ion in atomic mass units, and E is its mean energy in electron volts; $\phi'(\lambda)$ is the spectral distribution, in microns^{-1}, of the photon source, normalized to unity; $T_n(\lambda)$ is the transmission of the n^{th} filter when placed in the light beam; and λ is the wavelength, in microns. The cross section, $\sigma(\lambda)$, is in square centimeters. To test the accuracy of a proposed cross section, $\sigma(\lambda)$, the prediction of eq (1) is compared with the experimental detachment probability. We followed this procedure in the H^- work, using the theory of Chandrasekhar.

If $\sigma(\lambda)$ has not been calculated but can be presumed to be a slowly varying function of λ, $\sigma(\lambda)$ can be determined from successive differences of P_{exp} in that region of the spectrum for which sharp-cutoff filters are available. These filters must have transmission curves that maintain their maximum values to wavelengths at least as long as the threshold wavelength corresponding to the affinity. If filters a and b have sharp-cutoff characteristics and identical maximum transmissions, the difference between the experimental detachment probabilities for these filters is predicted by the equation

$$P_a-P_b=\Delta(P_{exp})=$$

$$0.317\times10^{13}W_0(M/E)^{1/2}\int\sigma(\lambda)\phi'(\lambda)(T_a-T_b)\lambda d\lambda. \quad (2)$$

Here we have assumed that the radiation power, W_0, and ion energy, E, are each the same in the two measurements. If this is not true, we must write

$$\left(P_{exp}\frac{E^{1/2}}{W_0^-}\right)_a-\left(P_{exp}\frac{E^{1/2}}{W_0^-}\right)_b=$$

$$0.317\times10^{13}M^{1/2}\int\sigma(\lambda)\phi'(\lambda)(T_a-T_b)\lambda d\lambda. \quad (3)$$

The cross section is then

$$\sigma(\lambda)\doteq\frac{\Delta(P_{exp}E^{1/2}W_0^{-1})}{0.317\times10^{13}M^{1/2}\int\phi'(\lambda)\Delta[T(\lambda)]\lambda d\lambda}\ \text{cm}^2. \quad (4)$$

If the maximum transmissions of the filters are not equal, (4) is modified as follows:

$$\sigma(\lambda)\doteq\frac{\Delta(P_{exp}T_{max}^{-1}E^{1/2}W_0^{-1})}{0.317\times10^{13}M^{1/2}\int\phi'(\lambda)\Delta\left[\frac{T(\lambda)}{T_{max}}\right]\lambda d\lambda}\ \text{cm}^2. \quad (5)$$

The difference method of determining $\sigma(\lambda)$ is not applicable in the near infrared with our absorption filters (see fig. 3). Only the selenium-glass filters with cutoff wavelengths between 4500 and 7000 A have the required transmission characteristics. For negative ions with detachment thresholds less than 1.3 ev the difference method encounters additional serious difficulties. This occurs even in the determination of the cross section in the visible spectrum, because of the slight decrease in filter transmission and the marked increase in the water-cell absorption near 0.9μ. Combined with the rapid increase with rapid increase with wavelength of the product, $\lambda\phi'(\lambda)$, this causes the difference in P_{exp}'s of two filters to arise from two widely separated regions of the cross section, introducing ambiguity in every measurement.

The affinity usually given in the literature for O^- is about 2.2 ev [17]. For this reason we used the difference method in the visible spectrum. In the near infrared region of the O^- photodetachment cross section the procedure was to adopt a reasonable monotonic trial function, $\sigma'(\lambda)$, for integration of eq (1), and to make successive adjustments of the trial function for best fit with the experimental data.

The theoretical affinity for hydrogen is 0.747 ev [3], and the detachment threshold of O_2^- is smaller than 1.3 ev. For this reason the difference method was not applied to H^- or to O_2^-.

4. Experimental Results

4.1. Results for H^-

Two sets of measurements have been made of the spectral dependence of the H^- cross section for photodetachment, using the glass absorption filters. In the preliminary set the filters were taken in random order with all measurements on a given filter taken consecutively. In the second set the filters were taken in a scrambled order. The order was rescrambled after a cycle of one measurement per filter. Eleven complete cycles were carried through.

The results are not on an absolute basis. They are given relative to the value obtained for filter 3486. We have previously described absolute measurements of the integrated cross section for H^-, using filter 3486 and filter 2412 [2]. The theory

of Chandrasekhar is used to provide a test cross section in the integration of eq (1) for the comparison with the experimental results shown in table 1. The conclusion that the trend evident in the more recent data reflects an error in the shape of Chandrasekhar's H^- cross section is not justified because of uncertainty in $\phi'(\lambda)$ and in the temperature coefficients of the filters. The experimental results are in general agreement with the theory.

4.2. Results for O^-

We have made two sets of measurements of the spectral dependence of the O^- photodetachment cross section, using the glass absorption filters and ions from an oxygen discharge. In the first set the filters were cycled 13 times in order of increasing cutoff wavelengths. In the second set the filters were rescrambled for each of 8 cycles, the order being carefully chosen to minimize the effect of long and short time drifts in the differences between probabilities for filters with adjacent cutoff wavelengths.

These measurements were made on a relative basis. Subsequently, absolute measurements were made with filter 3486 by the method described [2]. The results of the relative measurements in table 2 are therefore given on an absolute basis. The measured absolute values of the cross sections are estimated to be reliable within ± 10 percent [2].

The two sets of results are combined in table 2 because the ratios of photon-beam power, W_0, to the ion velocity ($\sim E^{\frac{1}{2}}$) were the same (see eq (1)) in both sets of measurements. Table 3 gives the transmission and photon spectral-distribution data necessary for the integration of (1) with arbitrary trial cross sections for comparison with the P_{exp}'s given in table 2.

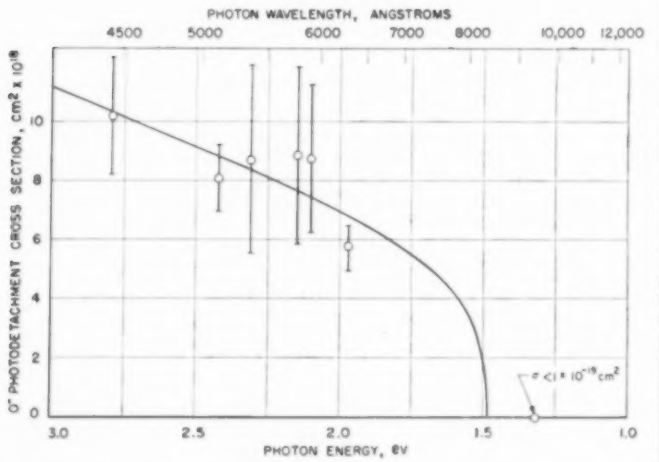

FIGURE 9. *The trial photodetachment cross section $\sigma'(\lambda)$, which is consistent with experimental results.*

Integrations of eq (1) using this cross section and the filter transmissions of figure 3 yield results which are given as P_{theo} in tables 2 and 6. Near threshold this trial cross section has the form given by eq (6) for nonresonant photodetachment.

The data given by the circles are obtained from eq (5); and are not used to determine the curve.

Where applicable, eq (5) has been used to obtain σ's associated with various ΔP_{exp}'s. This equation is used when the filters have the proper sharp cutoff and constant transmission short of cutoff, and where the P_{exp}'s seem to justify the assumption of a slowly varying cross section. The results are given in table 4 and plotted in figure 9 at the peak wavelengths associated with the differences of the filter transmissions. Note that the σ's obtained from eq (5) are not independent. An error in one P_{exp}

TABLE 1. *Comparison of the observed spectral distribution [a] of the photodetachment cross section for H^- with the theory of Chandrasekhar, relative to the results for filter 3486*

	Run A		Run B		
Corning filter No.	Number of measurements	Average relative P_{exp}/P_{theo}	Number of measurements	Average relative P_{exp}/P_{theo}	Mean deviation
3389	3	0.96	11	1.04	±0.04
3385	3	1.02	10	1.01	±.06
3486	5	(1.00)	11	(1.00)	±.03
3482	4	0.97	11	1.00	±.04
2424	3	.98	11	0.97	±.02
2412	3	1.02	10	.97	±.06
2030	2	1.00			
2550	2	0.99			
2540	4	.97			

[a] The absolute measurement of the integrated cross section for H^-, using filter 3486, is given in (2). The experimental results agree with the prediction of the theory within 2 percent and are estimated to be reliable within 10 percent.

TABLE 2. *Experimental photodetachment probability, P_{exp}, for O^- from an O_2 discharge with 10 glass filters and one interference filter; and P_{theo}, using eq (1) and the $\sigma'(\lambda)$ given in figure 9 and table 3 for a 1.48-ev affinity*

Corning filter No.	P_{exp} [a]	P_{theo}	$(P_{exp}-P_{theo})$
7380	$1.66\pm0.02\times10^{-5}$	1.69×10^{-5}	-0.03×10^{-5}
3385	1.50 ± 0.04	1.48	+.02
3486	1.35 ± 0.03	1.36	−.01
3482	1.25 ± 0.04	1.24	+.01
2424	1.08 ± 0.05	1.10	−.02
2412	0.95 ± 0.07	0.984	−.03
2030	$.82\pm0.03$	.784	+.04
2600	$.38\pm0.04$	.363	+.02
2550	$.074\pm0.016$	.089	−.015
2540	<.02	.012	<.02
Reflection filter [b]	.....	.14	.....

[a] The errors are average deviations from the mean values of the experimental data from 21 experiments.

[b] The interference filter was used with O^- from a CO discharge. See table 6 for data from CO.

TABLE 4. *Values of the O^- photodetachment cross section [a] obtained from equation (5)*

Filter combination	λ_{peak}	Denominator eq (5)	Numerator eq (5)	σ
7380-3385	4400	0.865×10^{-11}	0.118 ± 0.020 [b]	$0.102\pm0.017\times10^{-19}$
3385-3486	5120	.664	$.121\pm0.014$	$.080\pm.009$
3486-3482	5370	1.019	$.086\pm0.029$	$.088\pm0.030$
3482-2424	5770	0.540	$.162\pm0.054$	$.087\pm0.029$
3482-2412	5900	.353	$.247\pm0.068$	$.087\pm0.024$
2424-2030	6300	.268	$.216\pm0.026$	$.058\pm0.007$

[a] The values given in the fourth column are the averages of 21 independent differences of individual measurements for the indicated filter pairs.

[b] The errors are the average deviations from the mean.

TABLE 3. *Data [a] to be used in the integration of equation (1) for comparison of arbitrary cross sections σ (λ) with our experimental results*

λμ	$\mathcal{E}$ev	T_{3385}	T_{3486}	T_{3482}	T_{2412}	T_{2424}	T_{2030}	T_{2600}	T_{2550}	T_{2540}	T_r	ϕ'_λ	σ'
0.400	3.100	.....	.....	.....	.....	.....	.....	.....	.....	.....	.....	0.0588	[b] 11.77×10⁻¹⁸
.408	3.039	.....	.....	.....	.....	.....	.....	.....	.....	.....	.....	.....	.....
.416	2.981	.....	.....	.....	.....	.....	.....	.....	.....	.....	.....	.0753	11.24
.424	2.925	.....	.....	.....	.....	.....	.....	.....	.....	.....	.....	.....	.....
.432	2.870	.....	.....	.....	.....	.....	.....	.....	.....	.....	.....	.0951	10.79
.440	2.818	.....	.....	.....	.....	.....	.....	.....	.....	.....	.....	.....	.....
.448	2.768	.....	.....	.....	.....	.....	.....	.....	.....	.....	.....	.....	.....
.456	2.719	.....	.....	.....	.....	.....	.....	.....	.....	.....	.....	.1186	10.35
.464	2.672	0.000	.....	.....	.....	.....	.....	.....	.....	.....	.....	.....	.....
.472	2.627	.075	.....	.....	.....	.....	.....	.....	.....	.....	.....	.1425	9.96
.480	2.583	.375	.....	.....	.....	.....	.....	.....	.....	.....	.....	.....	.....
.488	2.541	.665	.....	.....	.....	.....	.....	.....	.....	.....	.....	.1679	9.58
.496	2.500	.790	.....	.....	.....	.....	.....	.....	.....	.....	.....	.....	.....
.504	2.460	.850	.....	.....	.....	.....	.....	.....	.....	.....	.....	.1974	9.24
.512	2.422	.875	0.015	.....	.....	.....	.....	.....	.....	.....	.....	.....	.....
.520	2.385	.890	.240	.....	.....	.....	.....	.....	.....	.....	.....	.2261	8.92
.528	2.348	.900	.640	.....	.....	.....	.....	.....	.....	.....	.....	.....	.....
.536	2.313	.904	.790	0.000	.....	.....	.....	.....	.....	.....	.....	.2610	8.62
.544	2.279	.906	.817	.125	.....	.....	.....	.....	.....	.....	.....	.....	.....
.552	2.246	.908	.835	.475	.....	.....	.....	.....	.....	.....	.....	.2902	8.33
.560	2.214	.909	.850	.725	.....	.....	.....	.....	.....	.....	.....	.....	.....
.568	2.183	.910	.858	.810	.....	.....	.....	.....	.....	.....	.....	.3235	8.04
.576	2.153	.910	.867	.835	.....	0.007	.....	.....	.....	.....	.....	.....	.....
.584	2.123	.910	.871	.847	.....	.100	.....	.....	.....	.....	.....	.3574	7.77
.592	2.095	.909	.880	.855	0.000	.375	.....	.....	.....	.....	.....	.....	.....
.600	2.067	.908	.883	.862	.015	.675	.....	.....	.....	.....	.....	.3898	7.50
.608	2.039	.907	.885	.866	.185	.800	.....	.....	.....	.....	.....	.....	.....
.616	2.013	.906	.891	.870	.550	.850	.....	.....	.....	.....	.....	.4251	7.24
.624	1.987	.905	.892	.875	.785	.865	.....	.....	.....	.....	.....	.....	.....
.632	1.962	.904	.893	.876	.845	.875	.....	.....	.....	.....	.....	.4583	7.02
.640	1.938	.903	.894	.880	.865	.883	0.000	.....	.....	.....	.....	.....	.....
.648	1.913	.902	.895	.882	.875	.888	.065	.....	0.000	.....	.....	.4897	6.72
.656	1.890	.901	.896	.885	.880	.893	.425	.....	.002	.....	.....	.....	.....
.664	1.867	.900	.897	.885	.883	.895	.650	.....	.005	.....	.....	.5211	6.44
.672	1.845	.899	.898	.886	.885	.900	.775	.....	.006	.....	.....	.....	6.32
.680	1.823	.898	.898	.887	.886	.900	.850	.....	.007	.....	.....	.5499	6.19
.688	1.802	.896	.899	.888	.888	.901	.870	.....	.010	.....	.....	.....	6.05
.696	1.781	.895	.899	.889	.889	.902	.877	.....	.014	.....	.....	.5769	5.91
.704	1.761	.894	.898	.890	.889	.905	.883	.....	.016	.....	0.000	.....	5.77
.712	1.742	.893	.897	.890	.888	.905	.885	0.015	.020	.....	.002	.6023	5.62
.720	1.722	.892	.896	.889	.887	.905	.886	.125	.030	.....	.004	.6145	5.48
.728	1.703	.891	.896	.888	.885	.905	.887	.300	.038	.....	.005	.6267	5.30
.736	1.685	.890	.895	.886	.884	.905	.889	.500	.048	.....	.008	.6406	5.20
.744	1.667	.889	.895	.883	.883	.905	.889	.635	.060	.....	.011	.6498	5.10
.752	1.649	.883	.894	.882	.879	.905	.890	.710	.067	.....	.020	.6600	4.97
.760	1.632	.882	.892	.881	.878	.905	.890	.760	.082	.....	.034	.6716	4.83
.768	1.615	.881	.892	.880	.877	.905	.890	.785	.097	.....	.055	.6823	4.68
.776	1.598	.880	.891	.880	.876	.905	.889	.795	.122	.....	.100	.6917	4.50
.784	1.582	.879	.889	.878	.876	.905	.887	.800	.140	.....	.200	.7022	4.30
.792	1.566	.878	.888	.877	.874	.905	.886	.799	.165	.....	.350	.7106	4.08
.800	1.550	.877	.888	.876	.872	.905	.886	.795	.190	.....	.600	.7188	3.82
.808	1.534	.876	.886	.875	.871	.905	.884	.790	.217	0.000	.815	.7276	3.52
.816	1.519	.874	.882	.873	.869	.905	.880	.780	.245	.005	.825	.7342	3.18
.824	1.505	.873	.881	.871	.868	.905	.879	.772	.275	.010	.725	.7418	2.74
.832	1.490	.873	.880	.870	.866	.905	.878	.764	.305	.015	.600	.7494	2.23
.840	1.476	.872	.879	.870	.864	.905	.877	.753	.337	.025	.520	.7560	1.44
.848	1.462	.871	.878	.868	.862	.905	.876	.742	.370	.035	.470	.7617	0.00
.856	1.449	.869	.877	.865	.861	.905	.875	.730	.401	.050	.450	.7680	.....
.864	1.435	.868	.876	.864	.860	.905	.874	.718	.430	.063	.....	.7740	.....
.872	1.422	.867	.875	.864	.859	.905	.873	.705	.460	.080	.....	.7796	.....
.880	1.410	.867	.874	.862	.858	.905	.872	.690	.495	.100	.....	.7858	.....
.888	1.396	.867	.873	.861	.857	.905	.871	.675	.525	.125	.....	.7916	.....
.896	1.384	.867	.871	.860	.855	.905	.869	.657	.552	.150	.....	.7945	.....
.904	1.372	.867	.868	.859	.854	.905	.866	.642	.580	.175	.....	.7985	.....
.912	1.360	.866	.867	.857	.854	.905	.865	.625	.605	.215	.....	.8022	.....
.920	1.348	.865	.866	.856	.853	.905	.864	.605	.630	.250	.....	.8062	.....
.928	1.336	.863	.865	.855	.851	.905	.863	.584	.652	.280	.....	.8105	.....
.936	1.325	.863	.864	.854	.850	.905	.862	.563	.675	.310	.....	.8112	.....
.944	1.313	.863	.863	.854	.849	.905	.861	.539	.694	.345	.....	.8136	.....
.952	1.302	.863	.862	.853	.848	.905	.860	.516	.713	.375	.....	.8159	.....
.960	1.292	.863	.861	.852	.846	.905	.859	.488	.730	.405	.....	.8192	.....
.968	1.281	.863	.860	.850	.845	.905	.858	.457	.741	.437	.....	.8217	.....
.976	1.270	.863	.859	.850	.844	.905	.857	.425	.755	.465	.....	.8223	.....
.984	1.260	.862	.858	.850	.844	.905	.856	.390	.775	.495	.....	.8242	.....
.992	1.250	.862	.858	.850	.844	.905	.856	.355	.785	.520	.....	.8261	.....

[a] Heading symbols are defined in the text of this paper. See eq (1). T_r is the transmission of the interference reflection filter.
[b] Data for integration of the trial cross section shown in figure 9.

may be reflected in the error associated with more than one ΔP_{exp}. An attempt was made, by successive approximations, to obtain the smooth monotonic cross section that most nearly fits the data of table 2. This curve is plotted in figure 9. The σ's from this curve that were used in the numerical integration of eq (1) are given in table 3, and the results of the integration are given as P_{theo} in table 2.

The cross section for radiative attachment, of interest in upper atmosphere physics, was derived [18] from this curve using the principle of detailed balancing, and is given in figure 10 and table 5.

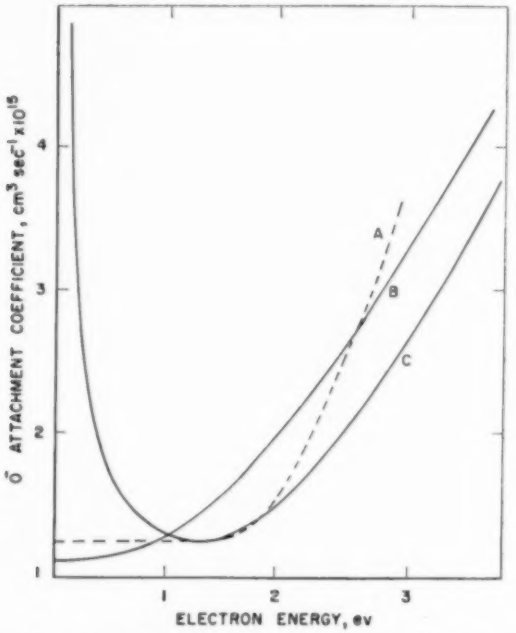

FIGURE 10. *Experimental and theoretical radiative attachment coefficients for atomic oxygen.*

The attachment coefficient is equal to the product of electron velocity and attachment cross section. Curve A is calculated from our trial cross section (see fig. 9) by the principle of detailed balancing. Curves B and C are calculated by Bates and Mass. y [4], B assuming no excited state near the continuum and C, assuming resonant capture of s electrons.

TABLE 5. *The radiative attachment coefficient α for atomic oxygen, calculated from the photodetachment "trial" cross section given in table 3*

Energy of the incident electron	α	Energy of the incident electron	α
ev	cm^3-sec^{-1}	*ev*	cm^3-sec^{-1}
1.62	3.44×10^{-11}	0.46	1.44×10^{-11}
1.50	3.15	.41	1.40
1.39	2.92	.37	1.35
1.29	2.70	.32	1.31
1.19	2.52	.28	1.27
1.10	2.35	.24	1.24
1.02	2.21	.21	1.24
0.94	2.09	.17	1.24
.87	1.98	.14	1.24
.80	1.87	.10	1.24
.73	1.78	.07	1.24
.67	1.70	.04	1.24
.62	1.62		
.56	1.55		
.51	1.50		

4.3. O^- Affinity

a. O^- from an O_2 Discharge

The threshold of the monotonic trial cross section that fits the experimental data for O^- from an O_2 discharge is about 1.48 ev. Upper and lower limits are immediately apparent if the P_{exp}'s (table 2) are compared with the filter transmission curves (fig. 3). The large detachment signal with filter 2600 shows that the threshold lies substantially below 1.75 ev. Because no signal is observed with filter 2540 [$\sigma(\lambda)<1\times10^{-19}$] cm^2], the threshold must be above 1.35 ev.

The shape of the cross section near the threshold is not uniquely determined by these experimental data. The threshold can be moved to slightly higher values on the electron-volt scale and remain in agreement with the experimental data through eq (1). This is allowable only if there is a sharp peak very near threshold, followed by a deep minimum, in order to account for the observed detachment with filter 2600.

b. O^- from a CO Discharge

After the completion of the experiments on O^- from oxygen discharges, the affinity and shape of the cross section near threshold were confirmed using ions from a discharge through carbon monoxide. The results prove that all the O_2^- ions had been eliminated from the O^- beam in the oxygen experiments. The concentration of O_2^- ions in the beam from the CO discharge was $\sim$0.1 percent of the beam current, compared to $\sim$50 percent from an O_2 discharge. Figure 11 shows the spectrum of the beam from CO, with the velocity selector turned off. The velocity selector removes the impurity peaks except for a negligible trace of C^-.

Table 6 shows the relative values of P_{exp} for a selected group of filters near the threshold, together with the corresponding P_{theo} ratios. Included with these data is a measurement with a multilayer interference reflection filter, the transmission characteristic of which is shown in figure 3. The de-

TABLE 6. *Experimental results of measurements made using O^- ions from a carbon monoxide discharge*

Filters	$\frac{P_{a_{theo}}{}^{a}}{P_{b_{theo}}}$	$\frac{P_{a_{exp}}}{P_{b_{exp}}}$
$\frac{\#1(\text{reflection})^{b}}{2424}$	0.127	0.17 ± 0.04^{c}
$\frac{2030}{2424}$	.713	$.715\pm.03$
$\frac{2600}{2030}$	.463	$.47\pm.03$
$\frac{2550}{2030}$	.114	$.16\pm.05$

[a] P_{theo}'s are calculated from the trial cross section given in table 3 and shown in figure 9.
[b] The filter transmission characteristics are shown in figure 3.
[c] The errors are the estimated reliabilities of the 2 or 3 measurements made with each filter.

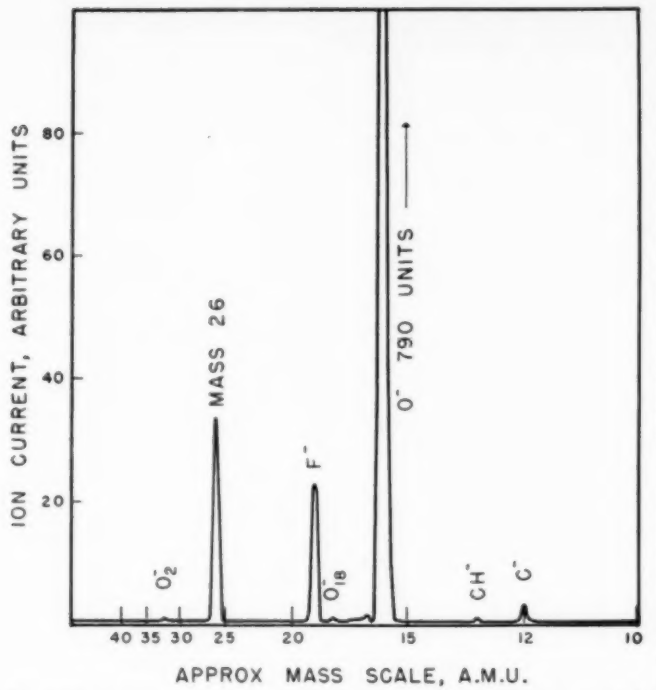

FIGURE 11. *Mass spectrum of the ion beam from a* CO *discharge.*

This spectrograph was taken with the 90° sector-field instrument. Mass 26 is not identified.

tachment signal obtained when this filter is placed behind the water cell, one face of which is filter 2424, proves that the oxygen affinity lies below 1.58 ev regardless of the shape of the curve. Within experimental error, the position of the threshold given by the ions from CO is the same as that given by the ions from O_2.

c. Discussion

The experimental results prove that the threshold lies between 1.55 and 1.35 ev. The identification of this threshold with the affinity would be taken for granted if the affinity were not in unresolved conflict with the generally accepted value of 2.2 ev [17]. The interpretation of our observed threshold as the threshold for detachment from a metastable excited state of O^- might resolve the conflict if this interpretation were not untenable. This state would necessarily lie about 0.5 ev above the ground state in order to be consistent with the 2.2 ev value of the affinity.

Bates and Massey [4], in an attempt to justify theoretically a $(2p)^4 3s$ excited configuration barely stable with respect to a 2.2-ev affinity, found that the polarization of the core of the ion "required to give a stable level was far in excess of the probable value" [19]. Bates [20] has calculated, by an empirical method, that a $(2p)^4 3s$ configuration should lie about 2 ev higher than the $(2p)^5$ configuration taken as the configuration of the ground state. Some experimental evidence has been presented in favor of a 2.2-ev affinity with an excited state lying very near to the continuum, but there is no evidence for an excited state appreciably below the continuum. The possibility that we are observing absorption from metastable ions is further reduced by the results with CO, for one would not expect CO and O_2 discharges to result in beams with equal concentrations of metastables. Use of our value of the affinity of oxygen may permit a reinterpretation of the electron impact data [21] without recourse to the assumption that negative ions are created in excited states.

For photodetachment from a $(2p)^5$ O^- ground-state configuration, in the absence of stable excited states, the shape of the cross section is restricted by the requirement [22] that near the threshold

$$\sigma(\lambda) \sim \lambda^2 (E_0 - hc/\lambda)^{1/2}. \qquad (6)$$

This requires a zero slope for the attachment coefficient (fig. 10) and an infinite slope for the cross section at the threshold. This shape was used near the threshold of the trial cross section (see fig. 9).

The measured threshold for photodetachment from the ground state of O^-, the affinity, is 1.48 ± 0.10 ev. The assigned error is derived from (a) the theoretical requirement that the cross section must intersect the wavelength abcissa with infinite slope and (b) the certainty from the observation of a finite signal with the interference filter that the threshold lies at or below 1.55 ev. Shape of the cross section must be roughly that given by σ' in figure 9, but the possibility of irregularities or fine structure is not excluded. It is quite unlikely that there exists a resonant peak at the threshold.

We are grateful to many members of the NBS staff for help in the calibration of various parts of the apparatus, particularly John Schleter, Nicholas Acquista, Russel Johnston, and Marion Belknap. Victor Grob carried out the many tedious numerical integrations and assisted with the operation of the equipment. Most of the construction of the apparatus was accomplished by Adolph Huriaux. We are indebted to the evaporation group of Baird Associates, Inc., for the development of the special interference filter. Suggestions by A. Dalgarno, D. R. Bates, Wade Fite, and Homer Hagstrum have been very helpful.

5. References

[1] L. M. Branscomb and W. L. Fite, Phys. Rev. [A] **93,** 651 (1954).
[2] L. M. Branscomb and S. J. Smith, Experimental cross section for photodetachment of electrons from H— and D—, Phys. Rev. **98,** 1028 (1955).
[3] S. Chandrasekhar, Astrophys. J. **102,** 395 (1945).
[4] D. R. Bates and H. S. W. Massey, Trans. Roy. Soc. (London) [A] **239,** 269 (1943).
[5] H. S. W. Massey, Negative ions, p. 21 (University Press, Cambridge, England, 1950).
[6] H. S. W. Massey, Negative ions, p. 36 (University Press, Cambridge, England, 1950).
[7] L. M. Branscomb and S. J. Smith, The electron affinity of atomic oxygen, Phys. Rev. (L) **98,** 1127 (1955).
[8] Massey, loc. cit., p. 3 ff.

[9] H. D. Hagstrum, Phys. Rev. **23,** 185 (1951).
[10] J. B. Hasted, Proc. Roy. Soc. (London) [A] **212,** 235 (1952).
[11] J. B. Hasted, Proc. Roy. Soc. (London) [A] **222,** 74 (1954).
[12] Handbook of Chemistry and Physics, 35th ed., p. 2466 (Rubber Publishing Co., Cleveland, 1953).
[13] D. B. Judd, J. Research NBS **44,** 1 (1950) RP2053.
[14] J. C. DeVos, The emissivity of tungsten ribbon (Dissertation, Univ. of Amsterdam 1953).
[15] K. S. Gibson, Phys. Rev. **7,** 194 (1916).
[16] W. L. Fite, Phys. Rev. **89,** 411 (1953).
[17] H. O. Pritchard, Chem. Rev. **52,** 529 (1953).
[18] L. M. Branscomb and S. J. Smith, Trans. A. G. U. to be submitted.
[19] H. S. W. Massey, Negative ions, p. 21 (University Press, Cambridge, England, 1950).
[20] D. R. Bates, Proc. Roy. Irish Acad. [A] **51,** 151 (1947).
[21] H. D. Hangstrum (private communication, 1955).
[22] H. S. W. Massey, Negative ions, p. 33 (University Press, Cambridge, England, 1950).

WASHINGTON, April 7, 1955.

Journal of Research of the National Bureau of Standards Vol. 55, No. 3, September 1955 Research Paper 2616

A Study of the Final Stages of the Austenite to Martensite Transformation in SAE 1050 Steel[1]

Melvin R. Meyerson and Samuel J. Rosenberg

The austenite-martensite transformation curves in the temperature range from M_s to −320° F have been established for two SAE 1050 steels. No significant effect of austenitizing temperature or austenite grain size on the amount of martensite formed per degree drop in transformation temperature was observed at temperatures lower than about 100° F below the M_s. Within the limits tested, cooling rate from the austenitizing temperature had no effect on the austenite-martensite transformation. The amount of martensite formed per degree drop in temperature decreased at transformation temperatures of about 350° F and below, and the transformation did not go to completion even at the lowest temperature utilized (−320° F). At this temperature the amount of retained austenite was about 1 percent.

1. Introduction

The literature contains many references to investigations of the austenite-martensite reaction, particularly the temperature at the start of the transformation, the M_s. Considerably fewer studies have been concerned with the completion of the martensite transformation, the M_f. Among these are the studies of Cohen [1][2], Averbach and Cohen [2], Averbach, Castleman, and Cohen [3], Roberts [4], Lyman and Troiano [5], Harris and Cohen [6], Howard and Cohen [7], Grange and Stewart [8], and Sadovski and Bogacheva [9]. In most of the work reported by these authors, highly alloyed materials were used. Data on effects of such heat treating variables as austenitizing temperature and grain size on the M_f of carbon steels are quite meager.

In a study [10] of the influence of austenitizing temperature, austenite grain size, and cooling rate on the martensite transformation in two SAE 1050 steels, the authors found that the M_s was raised and that the initial quantities of martensite formed below the M_s was decreased as the austenite grain size was increased. Austenitizing temperature had no effect on the M_s except insofar as it established the austenite grain size. Cooling rate, within the limits studied, also had no effect. This study has been extended to ascertain the effects of these heat treating variables on the completion of the martensite transformation (M_f).

2. Materials and Experimental Procedures

The same two steels that were used to study the effects of heat treating variables on the M_s transformation were used for the present work. Their compositions, as given in table 1, were similar except that M–182 had a greater aluminum content and was of "controlled" grain size whereas M–179 was not.

The quench-temper method as described previously [10] was used in this study. As before, the entire quench-temper cycle was limited to a maximum time interval of 11 sec in order to prevent the isothermal formation of bainite.

Specimens (0.050 in.×0.10 in.×0.10 in.) were austenitized at 1,475° and 1,600° F for 7 min and at 1,750°, 1,900°, 2,025°, and 2,150° F for 3 min. The austenite grain sizes established under these conditions are shown in table 2. Those specimens transformed above room temperature were quenched for 3 sec in 50 percent lead-50 percent bismuth alloy and then tempered for 8 sec at 625° F in another pot containing the same alloy. The remainder were quenched to room temperature in water, to 19° F in iced brine, to −105° F in a mixture of CCl_4+$CHCl_3$+solid CO_2, and to −320° F in liquid nitrogen. The approximate cooling rates of the small specimens in these media, as measured over the range 1,300° to 900° F were: Pb-Bi 5,000° F/sec, water 8,000° F/sec, iced brine 14,000° F/sec, CCl_4+$CHCl_3$+CO_2 320° F/sec, and liquid nitrogen 190° F/sec. Some of the specimens quenched directly to

TABLE 1. *Chemical composition of the steels used*

Percentage by weight

Steel	C	Mn	P	S	Si	Al_2O_3	Al		H	O	N
							Acid soluble	Total			
M–179	0.49	0.79	0.023	0.023	0.22	0.001	0.002	0.003	0.0002	0.004	0.004
M–182	0.49	0.80	0.022	0.028	0.21	0.007	0.016	0.020	0.0002	0.003	0.004

TABLE 2. *Effect of austenitizing conditions on grain size*

Austenitizing		ASTM grain size number	
Temperature	Time	M–179	M–182
°F	*min*		
1,475	7	8	8
1,600	7	5	7–8
1,750	3	4–5	5
1,900	3	4	5
2,025	3	3	5
2,150	3	2	3

[1] This work was sponsored by Watertown Arsenal, Ordnance Corps, U. S. Army.

[2] Figures in brackets indicate the literature references at the end of this paper.

−320° F in liquid nitrogen contained appreciable amounts of pearlite due to the slow cooling rate of the medium. This was particularly true of the fine-grained steel (M–182) austenitized at 1,475° F. Therefore, some specimens were quenched to −320° F indirectly, with an intermediate quench of 6 sec in either iced brine or CCl_4+$CHCl_3$+solid CO_2. This procedure also afforded an opportunity to observe any effect of the short delay in quenching on the M_f; i. e., any stabilizing effect. Specimens quenched directly to −320° F and which contained as much as one-half percent of pearlite were discarded.

An Einthoven string galvanometer, actuated by a thermocouple welded to the specimen, served to determine the temperature reached by the specimen just prior to tempering. This instrument was not used in conjunction with specimens quenched to room temperature or lower.

After mounting, all specimens were carefully ground to midpoint and given a metallographic polish. Lineal analysis was employed to determine the amount of tempered martensite up to about 90 percent. When more than this was present, the light constituents (austenite plus fresh martensite) were too finely dispersed to permit accurate lineal analysis. Typical microstructures showing advanced stages of the austenite-martensite transformation are shown in figure 1. In order to determine the amount of austenite in specimens containing more than about 90 percent of martensite, X-ray diffraction techniques, similar to the integrated intensity method reported by Averbach and Cohen [2] were used. A modification in computation described by Beu [11] was found to agree closely with the longer procedure of Averbach and Cohen and gave comparable results with less calculation. It was used throughout, with occasional verification by the longer method.

X-ray exposures were for 24 hr, using Co Kα radiation. A monochrometer equipped with a pentaerythritol crystal was employed to reduce background; this crystal had a 2θ angle of 23.60° when used with Co Kα radiation. Since X-ray methods could not be applied to specimens transformed at temperatures above ambient (subsequent cooling to room temperature would cause the transformation of some of the untransformed austenite) and since lineal analysis could not be used on specimens that had formed more than about 90 percent of martensite, no determinations could be made in this range (approximately room temperature to about 350°F). Consequently, all graphs of percent martensite versus transformation temperature plotted from experimental data have no points located in this range. The effect on the shape of the transformation curves (percent martensite versus transformation temperature) was negligible, since the quantity of austenite transformed with decreasing temperatures was extremely small both at temperatures just above and below this range.

A conventional powder camera of 57.3-mm diam was modified to accommodate the mounted specimens. The specimen holder was redesigned so as to allow the specimen to rotate slowly in the plane of its surface. By so doing the diffraction lines were uniformly free from spottiness except for specimens of steel M–179 austenitized at 2,150°F. The influence of the large grains in this steel (ASTM No. 2) in causing spottiness could not be eliminated by rotation. Details of the modified camera are shown in figures 2 and 3. The amount of light transmitted through the austenite and martensite lines on the X-ray film was determined by means of a recording microphotometer. From these data the density of the blackening curves was constructed on lineal scales and the areas under the peaks measured with a planimeter. The relative areas were used to compute the amounts of austenite and martensite. The film used was tested for linearity of blackening as a function of the amount of exposure and was found to be linear in the ranges used.

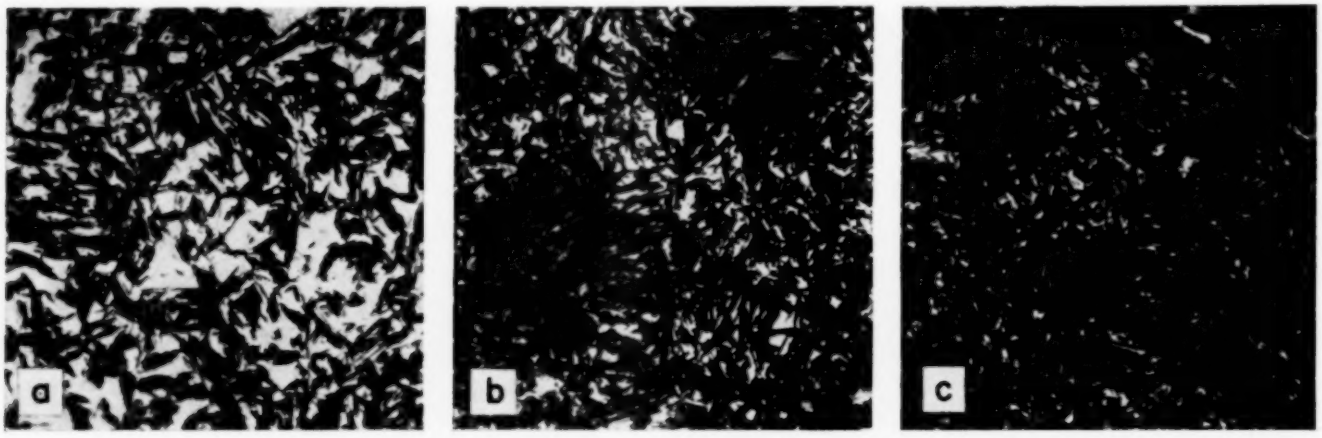

FIGURE 1. *Typical microstructures showing advanced stages of the austenite–martensite transformation.*

The martensite formed at the temperature of transformation has been darkened by subsequent tempering; the light areas are fresh (untempered) martensite plus retained austenite. Steel M–182, etched with 1 percent nital plus 1 percent zephiran chloride. ×750.
a, Transformed at 510° F, 62% martensite; b, transformed at 465° F, 81% martensite; c, transformed at 410° F, 93% martensite. Quantitative determinations by lineal analysis of structures of this type are difficult. It represents the approximate limit for which lineal analysis was used.

FIGURE 2. *Modified X-ray camera, assembled view with cover removed.*

× approx. ½.

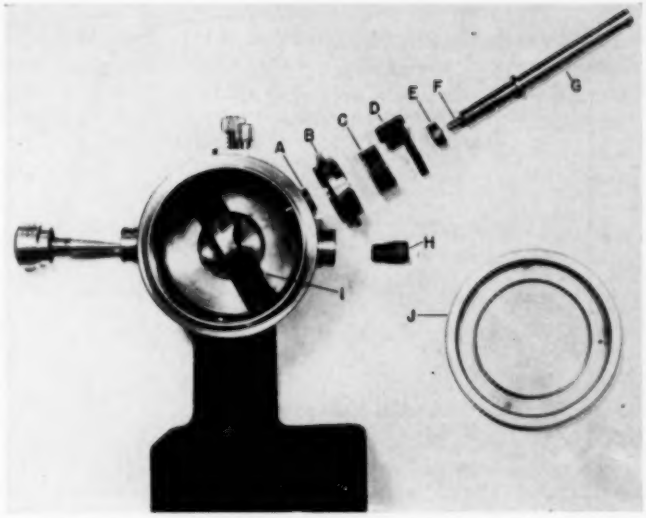

FIGURE 3. *Modified X-ray camera, exploded view.*

× ½.
A, Bearing for drive shaft; B, rotating specimen holder; C, specimen in plastic mount; D, crank; E, locking collar; F, spring-loaded plunger; G, rotating drive shaft; H, stopper; I, bearing for specimen holder; J, light-tight cover.

3. Results

The amount of martensite formed upon quenching to different temperature levels below M_s and down to −310° F was determined experimentally and then plotted to obtain transformation curves similar to the typical curves shown in figure 4. A complete curve, as illustrated, was obtained for each steel and for each austenitizing condition. It was reported previously [10], when only the initial portion of the curves was available, that those curves having lesser initial slopes (corresponding to the formation of smaller amounts of martensite per degree drop in temperature) showed tendencies to change towards increased slopes (corresponding to the formation of larger amounts of martensite per degree drop in temperature) with further decreases in transformation temperature. This trend now has been definitely established and is illustrated by the curves in figure 4. The initial slope of each curve increases to a constant value that is maintained until about 70 percent transformation has occurred.

The martensite-transformation temperature curves for each steel and for every austenitizing condition (only two of these curves are shown in fig. 4) contain values obtained on quenching directly as well as indirectly to −320° F. With one exception (steel M–179 austenitized at 1,750° F) all quantities of martensite obtained by indirect quench were within 1 percent of those obtained by direct quench.

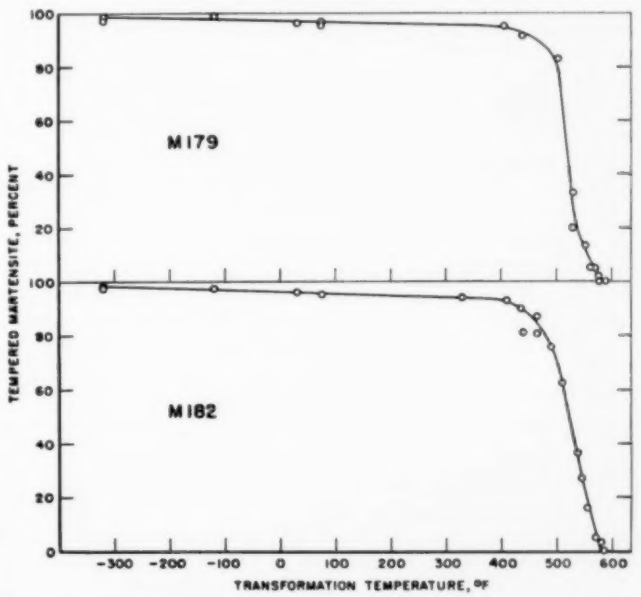

FIGURE 4. *Transformation curves for the steels austenitized at 1,475° F.*

These data indicated no effect of stabilization due to the short interruption of quench.

The amount of martensite for both steels transformed in the range of +100 to −320° F was approximately the same at any single temperature of transformation, regardless of the austenitizing temperature. The amount of martensite formed at −320° F was 98 ±1 percent. This was found to be true for both steels and for every austenitizing temperature used.

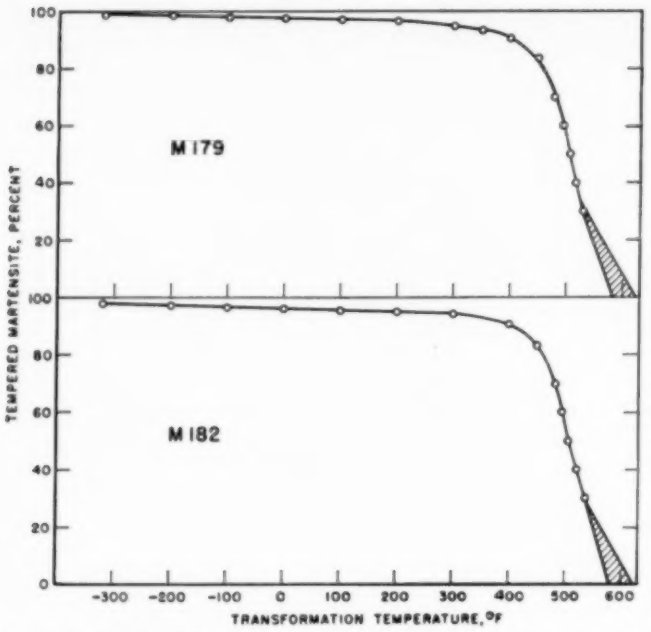

FIGURE 5. *Consolidated transformation curves for the steels austenitized at temperatures ranging from 1,475° to 2,025° F. for steel M–179 and from 1,475° to 2,150° F. for steel M–182.*

Figure 5 shows the consolidated curve for each steel under all austenitizing conditions. These curves are very similar and were derived as follows: In the range M_s to about M_s −100° F, values were taken from a previous paper [10]. The shaded area in each curve represents the spread in slope and the variations in M_s obtained in these steels with the different grain sizes established by the range of austenitizing temperatures. In the range of transformation temperatures of M_s −100° F to approximately 300° F the transformation temperatures at which regular 10 percent increases of martensite were formed were determined from the individual transformation curves and averages. The spread in values between the different curves was small enough to justify this procedure. These averages were then plotted in figure 5 as a function of martensite formed. In the range of transformation temperatures of 300° to −320° F the martensite formed at regular increments of 100° F and at −320° F was determined from the individual transformation curves (two of these curves are shown in fig. 4) for each steel and for every austenitizing condition. These data are shown in table 3 and the averages for each transformation temperature are shown in the last column of that table. The averages were then plotted in figure 5 as a function of transformation temperature.

On the basis of these curves and the data in table 3 it was concluded, that for the steels studied, variations in austenitizing temperature and grain size did not influence the quantities of austenite transformed to martensite at temperatures lower than about 100°F below the M_s. Furthermore, variations in cooling rate over the range investigated made no difference in the amount of austenite retained at −320°F.

TABLE 3. *Quantity of martensite formed as a function of transformation and austenitizing temperatures*

Transformation temperature °F	Percent of martensite at indicated transformation temperature after austenitizing at—						Average martensite, %
	1,475° F	1,600° F	1,750° F	1,900° F	2,025° F	2,150° F	
Steel M–179							
300	96.1	91.8	96.0	96.3	93.7	-----	94.8
200	96.5	94.6	96.4	97.1	95.8	-----	96.1
100	97.0	96.4	96.8	97.3	97.3	-----	97.0
0	97.3	97.7	97.1	97.4	98.6	-----	97.6
−100	97.7	98.5	97.4	97.5	99.0	-----	98.0
−200	98.1	99.0	97.8	97.6	-----	-----	98.1
−320	98.4	99.4	98.0	97.8	-----	-----	98.4
Steel M–182							
300	94.3	96.6	93.8	94.9	94.5	92.7	94.5
200	95.0	97.0	95.0	95.6	94.8	94.0	95.2
100	95.6	97.3	96.0	96.2	95.2	94.8	95.9
0	96.3	97.6	97.0	97.0	95.7	95.5	96.5
−100	97.0	97.9	97.8	97.6	96.1	96.3	97.1
−200	97.7	98.3	98.4	98.2	96.6	97.1	97.7
−320	98.3	99.0	99.0	99.0	97.0	98.0	98.4

The term M_f is generally considered as the temperature of the finish of the martensite transformation. It also has been defined as the temperature at which a certain large quantity of martensite, such as 95 or 98 percent, has formed. Neither of these definitions could be applied to the data obtained in this study to obtain a definite M_f. From the transformation curves shown in figure 4 it can be seen that transformation was not complete even at temperatures as low as −320°F, and the slopes of the curves in the region of 95 to 99 percent martensite were so low that the intersections of these curves with the abscissas (temperature scale) could not be determined with any degree of accuracy. Consequently, it was not possible to pinpoint any specific temperature as the M_f of either steel.

4. Discussion

The reaction-path theory advanced by Cohen, Machlin, and Paranjpe [12] postulates that the difference in the chemical free energy of austenite (F^A) minus that of martensite (F^M) must be greater than the resisting energies of dilatation, interfaces, and coherencies in order for the martensite reaction to proceed. Large grains lower the resisting energies because of decreased interfaces and permit the reaction to occur at lower values of $F^A - F^M$, thus accounting for the higher M_s with coarse-grained austenite.

As has been explained previously [10], the amount of martensite formed per degree drop in transformation temperature just below the M_s is less with coarse-grained than with fine-grained austenite. However, after about 30 percent of martensite has formed, at a temperature approximately 100°F below M_s, the influence of the initial grain size disappears. This was explained by the fact that the effective austenite grain size has been reduced by the martensite platelets to such an extent that the resisting energies of the interfaces have been raised to

equal those of the initially finer-grained austenite. With further reduction of transformation temperature, therefore, essentially similar amounts of transformation are obtained regardless of the initial austenite grain size.

Cohen [1] has presented an equation whereby the M_s, the quantity of martensite formed, or the temperature of transformation of the quantity of martensite (T_q) can be computed if any 2 of the 3 variables are known. This formula is: % Martensite $= 100 \times 3.05 \times 10^{-14} [820 - (M_s - T_q)]^{5.32}$, where T_q is the temperature of quench in °F. The types of steels to which this formula was said to be applicable did not include the 0.50 percent carbon steels under investigation. When applied to the steels under study, this formula gave a reasonably close approximation to the experimental transformation curves up to about 95 percent of martensite. However, the formula does not contain provision for variation of M_s with austenite grain size and any M_s obtained with it will hold only for a single grain size.

5. Summary and Conclusions

1. The austenite-martensite transformation curves in the temperature range from M_s to −320°F have been established for two SAE 1050 steels. No significant effect of austenitizing temperature or austenite grain size on the amount of martensite formed per degree drop in transformation temperature was observed at transformation temperatures lower than about 100°F below the M_s. Within the limits tested, cooling rate from the austenitizing temperature had no effect on the austenite-martensite transformation. No stabilizing effect could be determined as the result of briefly interrupting the quench to −320°F. Because of the fact that the transformation curves became asymptotic to the temperature axis and because some traces of austenite were present in the steels even after transformation at temperatures as low as −320°F, it was not possible to pinpoint the M_f temperatures.

2. The transformation curves for both steels were very similar, regardless of austenitizing temperatures, and fitted an empirical equation.

3. The reaction path theory accounts for the similarity of the austenite-martensite transformation curves of the two steels at the lower transformation temperatures as well as the differences in M_s obtained with changes in austenite grain size as previously reported [10].

The authors are grateful to Thomas G. Digges for many constructive suggestions and criticisms, to John F. Kocis for his conscientious assistance during the investigation, and to Herbert C. Vacher for his suggestions in the modification of the X-ray camera.

6. References

[1] M. Cohen, Retained austenite, Trans. ASM **41,** 35 (1949).
[2] B. L. Averbach and M. Cohen, X-ray determination of retained austinite by integrated intensities, Trans. AIME **176,** 401 (1948).
[3] B. L. Averbach, L. S. Castleman, and M. Cohen, Measurement of retained austenite in carbon steels, Trans. ASM **42,** 112 (1950).
[4] C. S. Roberts, Effect of carbon on the volume fractions and lattice parameters of retained austenite and martensite, Trans. AIME **197,** 203 (1953).
[5] T. Lyman and A. R. Troiano, Influence of carbon content upon the transformations in 3 percent chromium steel, Trans. ASM **37,** 402 (1946).
[6] W. J. Harris, Jr. and M. Cohen, Stabilization of the austenite martensite transformation, Trans. AIME **180,** 447 (1949).
[7] R. T. Howard, Jr. and M. Cohen, Austenite transformation above and within the martensite range, Trans. AIME **176,** 384 (1948).
[8] R. A. Grange and H. M. Stewart, The temperature range of the martensite formation, Trans. AIME, **167,** 467 (1946).
[9] V. D. Sadovskii and G. N. Bogacheva, On the influence of the quenching temperature upon the quantity of retained austenite in steel, Doklady Akad. Nauk SSSR [2] **83,** 221 (1952).
[10] M. R. Meyerson and S. J. Rosenberg, The influence of heat treating variables on the martensite transformation in SAE 1050 steel, Trans. ASM **46,** 1225 (1954).
[11] K. E. Beu, Modifications of an X-ray method for the measurement of retained austenite concentrations in hardened steels, J. Metals **4,** 1327 (1952).
[12] M. Cohen, E. S. Machlin, and V. G. Paranjpe, Thermodynamics of the martensite transformation, thermodynamics in physical metallurgy, ASM 242 (1950).

WASHINGTON, April 15, 1955